Dynamics of Heterogeneous Excitable Media with Pacemakers

Bartłomiej Borek

Ph.D., Physiology (Bioinformatics Option)

Department of Physiology
McGill Centre for Bioinformatics
Centre for Applied Mathematics in Bioscience and Medicine

McGill University

Montréal, Québec, Canada

March 2012

A thesis submitted to McGill University in partial fulfillment of the requirements of the degree of Doctor of Philosophy

DEDICATION

This thesis is dedicated to my dear Mom, Anna Borek, who has dedicated so much to her kids' growth and happiness.

ACKNOWLEDGEMENTS

There are many people whom I am glad to thank for enriching my experience as a graduate student. I cannot find the words, diagrams, or equations to properly express the gratitude I feel towards my doctoral advisors, Leon Glass and Alvin Shrier, for their guidance and mentorship over the years. During this time I have grown to admire their passion for scientific learning and teaching, as well as their acts of curiosity, patience, and compassion. They are my heroes.

I am also very grateful for the other members of my research advisory committee, who have greatly assisted my investigations. Thanks to Peter Swain, Michael Mackey, and especially Michael Guevara, who contributed many additional hours of discussions instrumental to the development of my understanding of the topics presented in this thesis. It has been an honour.

I am grateful to the faculty and staff in the Department of Physiology, including Christine Pamplin, Terry Kaluta, Sonia Visselli, Maria Dimas, Rosie Vasile, Ana Maria Rossi, Domnica Magrhescu, Rosmarie Siegrist-Johnstone, Kathleen Cullen, John White, Maurice Chacron, John Orlowski, Jacopo Mortola, Ursula Stochaj, Teresa Trippenbach, Gergely Lukacs, Ellis Cooper, Anne Wechsler, Monroe Cohen, Pejmun Haghighi, Mladen Glavinovic and Erik Cook for providing a professional and supportive environment for my student colleagues and I during our studies. I would then like to express my appreciation to these colleagues, especially those who served with me on the Physiology Graduate Student Association Council. It has been a privilege to interact with so many amazing people here. Also, much thanks to the

Post-Graduate Student Society for financial and logistical support, great events, and the warmth of the Thomson House! I am also grateful to the organizers and members of the Centre for Nonlinear Dynamics in Physiology and Medicine (now the Centre for Applied Mathematics in Bioscience and Medicine) who have cultivated a fertile ground for the growth of systems biology and biomathematics. Thanks to all of the people at the seminars, Angelica Todirenau, Jo-Ann Kwadzo, and the CND sys-admins who helped me discover the joy of Linux.

I have been very fortunate to work with members of Cardiac Dynamics Laboratory. I thank Alvin and Leon for introducing me to the art of tinkering with cell cultures, optical and electrophysiological devices, perfusion systems, and home-brewed codes of many flavours. Thanks to Claire Brown, Jacynthe Laliberté, and Alex Spurmanis for the lessons in bio-imaging, and Pascal Boursequin for his assistance in the physics machine shop. I am extremely grateful to Shajahan for all that he has taught me, and for his friendship in and out of the lab. I'd also like to thank Yuan Qing Zhao, Valerie Walker, Hung Lam, and Min-Young Kim for welcoming me into the laboratory, and Alex Hodge for his Yodaesque teachings, including the piloting of the Spaceship$^{\text{TM}}$(our imaging lab). I am very fortunate to have collaborated with Bart Oldeman, and I thank him for our insightful discussions and for raising the resetting pacemaker project to a higher level. I cannot forget to thank Roxana Anatasiu, who not only taught me so much about good lab practices, but was also always there to lend a happy hand to us lost students and crack a smile on my face with a little joke. ;)

I am very much obliged to Louise Taylor for her assistance in the analysis and

planning of my life trajectory during the past couple of years. Our discussions have helped me work more efficiently to improve myself. Merci beacoup Coach!

As my age increases so does my appreciation for my school teachers in undergrad, high school and elementary. Thank you Enrique Pujals, Dr. Kwan, Dr. Lim, Dr. Skinner, Sandra Raponi, my Millikan experiment lab tutor, Michael Stickings, Ms. Petrone, Mr. Klimowski, Mr. Cherwala, Mr. Annab, Mr. Roberto, Ms. McGhee, Mr. Gergely, Mr. Johnson and Mr. MacSween. Special thanks to my first teachers, my parents and grandparents (and their infectious appreciation of learning), and my first philosophy teacher, Mike Jurgaitis, for the exquisite sequence of awakenings with the light in Plato's cave.

I salute my friends, who were there through thick and thin. They have contributed to this thesis by leaving meaningful impressions on me. Thanks to Wen (my love and sweet thesis editor), Agie, Mike, Karol, Oscar, Shajahan, Piotr, Carina, Navid, Marcin, Avrum, Mario, Ana, Kate, Caitlin, Greg, George, Fred, Aliona, Dave, Cate, Therese, Lennart, Olivia, Tush, Tyler, Gavin, Alex, Raluca, Neja, Arjun, Artem, Joe, Guillaume, Vahid, Oman, Jeff, Rachel, Jonathan, Kristie, Morgan, Mike, Chris, Rich, Joanne, Jay, Steve, Stef, Agata, Loc, Eric, Roy, Val, *et al.* for these formative experiences.

Finally, I want to express my deepest appreciation to my family, for their love and support throughout my life. My heart goes out to Anna, Jacek, Agnieszka, Leszek, Ryszard, Łucja, Bożena, Andrzej, Piotrek, Richard, Janusz, Staszek, Wojtek, Zbyszek, Iwona, Bożena, Asia, Bogusia, Zosia, Jack, Peter, Adam, Angelica, Jenny, David, Elżbieta, Stefan, Karol, Jo-Wen, Hsiao-Ming and Hank. Thank you

all so much for helping me develop my vehicle of discovery, and for the fuel along this beautiful stretch of road.

CONTRIBUTIONS TO ORIGINALITY

This thesis represents my original scholarship and distinct contributions to knowledge. Chapters Two and Three are representative of my contributions to two manuscripts published in peer-reviewed scientific journals. Chapter Four is being prepared for submission as a manuscript. The following describes the contributions of the co-authors of these manuscripts.

The work presented in Chapter Two has contributed to an article in the journal Physical Review E [192]. The authors are T. K. Shajahan, Bartłomiej Borek, Alvin Shrier, and Leon Glass. For this paper I performed simulations of the FitzHugh-Nagumo (FHN) model in the presence of break and sink heterogeneities in two dimensions. T. K. Shajahan validated the results and carried out additional simulations using a cellular automaton model, and the FHN model in three dimensions (the results of which are not presented in the thesis). I wrote part of the manuscript relevant to my simulations and contributed to the introduction and discussion. T. K. Shajahan wrote the rest of the results and contributed to the introduction and discussion. He also generated the motivating experimental observations, presented in Figure 2–1. Leon Glass was the main supervisor of the project and wrote part of the introduction and conclusion. Alvin Shrier co-supervised the project and the laboratory used to make Figure 2–1 and provided much insight during the formation and revisions of the manuscript. Michael Guevara also assisted the projects with helpful questions and comments on several occassions.

The results described in Chapter Three have contributed to an article published

in the journal SIAM Journal on Applied Dynamical Systems [20]. The authors are Bartłomiej Borek, Leon Glass, and Bart Oldeman. For this work I modified and characterized the FHN equations used in the study, carried out their numerical simulations, and used the shooting approach to probe the nature of the phase transition curve at the apparent discontinuity in the FHN model. I wrote parts of the manuscript relevant to my results and contributed to the introduction and discussion. Bart Oldeman carried out the simulations on the van der Pol and Morris-Lecar equations (the results of which are not presented in the thesis), and implemented the continuation method to investigate the continuity of the resetting curve. He also implemented Dormand-Prince and Collatz "Mehrstellen" integration schemes in Fortran, and wrote parts of the manuscript relevant to these. Leon Glass guided the research strategy and generated the *Continuity Lemma*, as well as parts of the introduction and discussion.

Chapter Four is in preparation for submission. For this work I developed the data analysis programs, some of which were created by Alex Hodge who also developed the macroscopic imaging setup with Alvin Shrier. I developed the mound culturing protocol (from earlier monolayer protocols in the lab) and performed the imaging experiments regarding the effect of E-4031 on dominant central pacemakers with James Gabriels. I am responsible for all of the data analysis, modeling and writing at this stage. Throughout the work, Alvin Shrier and Leon Glass have been involved in choosing the strategies and tactics for experimentation and modeling. T. K. Shajahan and Michael Guevara have also contributed many useful discussions to this work.

ABSTRACT

The heart is a heterogeneous excitable tissue embedded with pacemakers. To understand the fundamental rules governing its behaviour it is useful to investigate the interplay between structure and dynamics in simplified experimental and mathematical models. This thesis examines FitzHugh-Nagumo type reaction-diffusion equation models motivated by experiments with engineered cardiac tissue culture. The aim is to relate how the design properties of these systems determine the underlying spatiotemporal dynamics. First, a functional relation between randomly distributed heterogeneities and conduction velocity is proposed in two dimensional heterogeneous excitable media. The transitions to wave break are studied for two types of heterogeneities related to fibroblasts and collagen deposits. The effects of pacemakers are next considered with a theoretical study of the transitions in one-dimensional wave patterns of a pacemaker reset by a stimulus pulse from a distance. Reflected wave solutions are found near the apparent discontinuity in the phase transition curve of the system, and they grow into more multi-reflected trajectories for a coarser spatial discretization of the model. Finally, the dynamical regimes arising from the interaction of two pacemakers in heterogeneous excitable media are investigated. A novel chick culture is developed to exhibit dominant pacemaker dynamics. This stable rhythm undergoes transitions to more complex reentrant patterns following induction of new pacemakers by the application of the potassium channel blocker, E-4031. The dynamics are reproduced by the FitzHugh-Nagumo model, which further demonstrates the effects of pacemaker size and heterogeneity density

on the transition to wave break and reentry. These findings may contribute to our understanding of the generic mechanisms governing the dynamics of wave propagation through heterogeneous excitable media with pacemakers, including healthy and diseased hearts.

ABRÉGÉ

Le coeur est un tissu hétérogène excitable qui contient des générateurs de rythme. Pour comprendre les règles fondamentales qui dirigent son comportement, il est utile d'étudier l'interaction entre la structure et la dynamique des modèles expérimentaux et mathématiques simplifiés. Dans cette thèse, j'utilise des modèles d'équations de FitzHugh-Nagumo. Ces modèles sont motivés par l'expérimentation avec des tissus cardiaques modifiés pour étudier comment les propriétés des conceptions influencent la dynamique d'ondes. Tout d'abord, une relation fonctionelle entre la densité des hétérogénéités distribuées au hasard et la vitesse de conduction est proposée dans un modèle numérique de deux dimensions de média hétérogènes excitables. Les transitions à l'onde rupturée sont différentes pour deux types de substrats hétérogènes. Les effets des régions automatiques sont alors considérés avec une étude théorique des transitions dans les ondes unidimensionelles des générateur de rythme réinitialisés par une seule impulsion d'une distance. Des solutions d'ondes réfléchies se trouvent près de la discontinuité apparente de la courbe de transition de phase du système et deviennent des trajectoires plus complexes pour une discrétisation spatiale plus grossière du modèle. Enfin, les modèles d'ondes résultant de l'interaction de deux générateurs de rythme dans des médias hétérogènes excitables sont étudiés. Une nouvelle culture de tissu cardiaque de poussin est développée pour présenter la dynamique dominante déterminée par un générateur de rythme. Ce rythme stable subit des transitions à des modèles d'ondes réentrants plus complexes suivant l'induction de nouveaux générateurs de rythme, par l'application du bloqueur des

canaux potassiques, E-4031. La dynamique est reproduite par le modèle FitzHugh-Nagumo, prévoyant l'effet de la taille du générateur de rythme et la densité de l'hétérogèneité sur la transition de l'onde rupturée et à la réentrée. Ces résultants contribuent à notre compréhension des mécanismes de média hétérogènes excitables avec des générateurs de rythme, dont les coeurs sains et malades.

TABLE OF CONTENTS

LIST OF TABLES

LIST OF FIGURES

Figure page

CHAPTER 1
Introduction

This chapter reviews concepts relevant to the study of the properties which influence wave dynamics in heterogeneous excitable media with pacemakers. Excitability, heterogeneity and pacemakers are defined and their properties are discussed in the context of mathematical and experimental models of cardiac tissue. These topics motivate my investigations in Chapters Two, Three, and Four using reaction-diffusion equations and engineered cardiac tissue to characterize determinants of wave dynamics in heterogeneous excitable media with pacemakers.

1.1 Excitable Media

1.1.1 Definition and Examples

Excitable media are spatially distributed systems with the ability to propagate waves of excitation. The waves travel without amplitude dissipation, but annihilate each other on contact. These properties arise because coupled elements in the media, called cells, have the property of *excitability*. Excitability is defined as the ability of a cell at rest to show a large active response to a superthreshold stimulus. This active response is called an excitation and is characterized by the spontaneous increase of the activation variable to an excited state. Stimuli below the activation threshold do not excite the system which relaxes back to the rest state. Another important feature of excitable cells is *refractoriness*. The property of refractoriness reflects the unresponsiveness of a cell to quickly repeated stimulation. For some time after

excitation there is a refractory period during which a second stimulus will not be able to elicit another excitation event.

An illustrative example of an excitable medium is a forest fire. The flame propagates by exciting trees close to it, and will continue to spread as long as there are flammable trees nearby. Once a tree has burned another wave of fire cannot pass through its location until a new tree regrows there. Nature has many other examples of excitable systems across a broad range of spatiotemporal scales. These include: star formation in some spiral galaxies [191, 157], spread of some infectious diseases through populations [19, 159], aggregation of slime mold amoebae [55, 228], sperm-induced calcium waves in amphibian eggs [54, 158], waves of electrolytes in neural [31, 97], retinal [82, 48], pancreatic [142, 214], and muscle tissue [15, 95], as well as in certain chemical reactions like the Belousov-Zhabotisky reaction [243, 227], or the catalysis of carbon monoxide oxidation on platinum [83, 84].

In this thesis I examine experimental and mathematical models of excitable media that are applicable to wave propagation in cardiac tissue. Although cardiac tissue composition is remarkably diverse in animals [224, 16], and even across different regions of the heart [188, 66], the property of excitability is inherent to cardiac muscle. Excitation is mediated through a large rapid depolarization of the cell membrane potential of cardiomyocytes. This depolarization is initiated by an influx of sodium or calcium ions into the intracellular fluid known as the cytoplasm. These cations enter the cytoplasm through ion channel proteins located in the cell membrane and sacroplasmic reticulum membrane [189]. Following this there is a repolarizing return to a rest state mediated by the exit of potassium out of the cytoplasm through the cell

membrane [203]. The sequence of large depolarization followed by hyperpolarization is known as the action potential. Action potentials can not be initiated in quick repetition because the cell membrane needs time to repolarize back to rest (a duration called the refractory period). The action potential propagates through the tissue by diffusion of electric charge from one cell to its neighbours through coupling proteins called gap junctions [233]. This is the general physical mechanism underlying spread of excitation through cardiac tissue.

1.1.2 Properties of Excitable Cells

The properties of excitability and refractoriness in an excitable cell are demonstrated in a system of ordinary differential equations called the FitzHugh-Nagumo model [69],

$$\begin{aligned} \frac{dv}{dt} &= f(v,w) = -av(v-1)(v-\alpha) + w \\ \frac{dw}{dt} &= g(v,w) = \epsilon(v - bw) \end{aligned} \tag{1.1}$$

where v is the activation variable (representing the cell membrane potential) and is w the recovery variable (representing the refractoriness of the cell). The parameter $0 < \alpha < 1/2$ sets the threshold for excitation, $a > 0$ controls the magnitude of the recovery variable, and $b > 0$ sets the relaxation rate for the recovery variable. The parameter $\epsilon << 1$ ensures fast excitation and slow recovery. The state space of this system is shown in Figure 1–1, along with the *nullclines* (relation between v and w given $\frac{dv}{dt} = \frac{dw}{dt} = 0$), and some select *trajectories* (solutions of the differential equation).

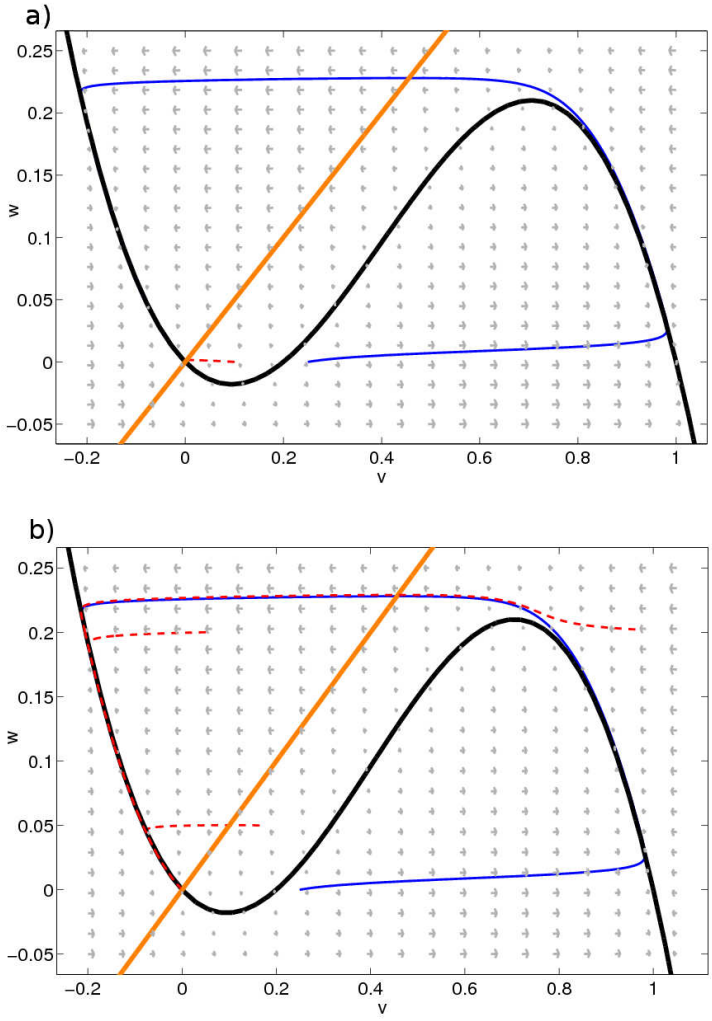

Figure 1–1: Excitability in the FitzHugh-Nagumo equations. The thick lines are the v-nullcline, $f(v, w) = 0$ (black), and the w-nullcline, $g(v, w) = 0$ (orange). The intersection of the nullclines at $(v, w) = (0, 0)$ is an attracting fixed point. (a) The effect of changing stimulus amplitude showing small stimulus relaxing back to rest (dashed trajectory) while a larger stimulus induces excitation (solid blue trajectory). (b) An initial stimulus elicit an activation (solid blue trajectory), while subsequent stimuli (dashed red trajectories) fail to do so. Vector fields are plotted using pp8.m [174] for Equation (1.1) with $a = 2, \alpha = 0.2, \epsilon = 0.01, b = 0.5$.

Figure 1–1(a) demonstrates the concept of excitability in the FitzHugh-Nagumo model. Two trajectories are shown resulting from a subthreshold perturbation to $(v, w) = (0.1, 0)$ and superthreshold perturbation to $(v, w) = (0.2, 0)$. The trajectory resulting from the small stimulus (dashed red trajectory) immediately returns to the attracting fixed point $(v, w) = (0, 0)$. The larger stimulus puts the state (v, w) in a region of phase space with $\frac{dv}{dt} > 0$ leading to an excitation to $v \approx 1.0$ followed by a return to rest (solid blue trajectory).

Figure 1–1(b) illustrates the property of refractoriness. A first stimulus of magnitude $v = 0.25$ elicits an excitation, but three subsequent stimuli (dashed red trajectories) given before the system relaxes back to rest do not elicit another excitation. Times during which a larger stimulus could put the system in a state such that $\frac{dv}{dt} > 0$ are the relative refractory period, while the period of times in which no stimulus amplitude can do this are known as the absolute refractory period.

Some excitable cells also have the ability to oscillate spontaneously - a property called *automaticity*. In dynamical systems theory automaticity manifests itself as the existence of a *stable limit cycle*. A stable limit cycle, Γ, is a periodic trajectory which attracts all states in its neighbourhood as $t \to \infty$. The FitzHugh-Nagumo equations can be induced to exhibit a limit cycle by adding a constant pacemaker current parameter, $Ip > 0$, to $f(v, w)$ in Equation (1.1). In figure 1–2a) we see that when $Ip = 0$ the system has all trajectories going towards the rest state $(v, w) = (0, 0)$, while figure 1–2b) shows that with $Ip = 0.2$ all trajectories tend to the limit cycle. Figure 1–2c) shows that the transition to oscillations in the FitzHugh-Nagumo equations is via a subcritical Hopf bifurcation. In fact, raising Ip even higher in

this case eventually terminates the limit cycle via another subcritical Hopf bifurcation. Different models of excitable media can show other types of transitions to periodic behaviour, such as: saddle node on a limit cycle, period doubling, torus, and homoclinic bifurcations [18, 109].

1.1.3 Emergent Properties of Coupled Excitable Cells

In excitable media the neighbouring cells can represent units of space which are coupled locally (to their nearest neighbours) so as to be able to excite each other. *Coupling* is an important property of excitable media because it allows for propagation of the excited state through space in the form of a wave. This leads to new properties not seen in single cells. In the following I introduce the properties of wave propagation initiation, termination, and different reentrant wave patterns.

Propagation initiation is a process more rich than the simple excitation of a single cell. First of all, in addition to stimulus amplitude, the threshold for propagation depends on the spatial extent of the stimulus. This spatial dimension to the threshold for propagation is known as the liminal length, and was first proposed by Rushton [183] and further developed by Noble [164] for strands of cardiac tissue. A parameter which captures the ability of a wave to propagate is called the safety factor. It relates how much activation a quiescent cell receives from its excited neighbours relative to how much it requires to put it over the threshold for excitation [127]. Several different formulations have been proposed [183, 144, 196, 23] for one dimensional excitable media, with the recent work of Boyle and Vigmond [23] showing improved agreement with observations in media of two spatial dimensions.

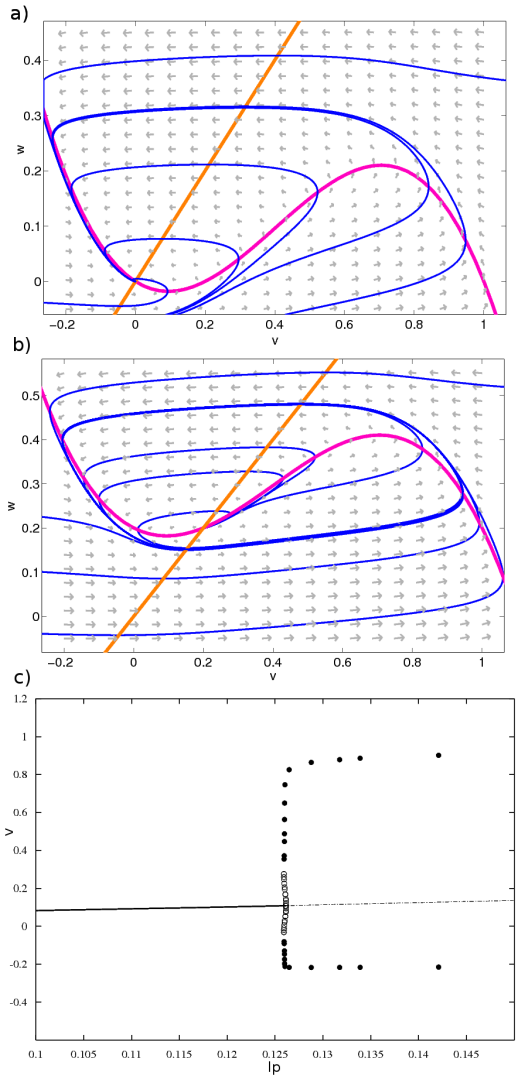

Figure 1–2: Transition to automaticity in a FitzHugh-Nagumo cell. (a) For $Ip = 0$ the trajectories are in the excitable regime. (b) For $Ip = 0.2$ the system exhibits an oscillation (bolder blue trajectory) to which all other trajectories are attracted. (c) The bifurcation diagram for the transition from the excitable dynamics to the oscillatory dynamics. As Ip increases the stable fixed point (straight line) begins to coexist with a stable oscillation (solid dots represent the minimum and maximum of oscillation) separated by an unstable oscillation (hollow dots). The unstable oscillation eventually shrinks around the stable fixed point so that it loses stability, leaving an unstable fixed point (dashed line) and a stable limit cycle. This bifurcation diagram was made using AUTO [52].

Another property that arises when excitable cells are coupled together is the ability to exhibit oscillations even though there may be no automatic cells in the medium. These spatial oscillations are generated when an excitation wave wraps around and reenters a previously excited site in a periodic fashion. These dynamics can manifest themselves in different ways depending on the geometry of the medium. For example, in one dimensional loops of excitable tissue sustained reentrant waves are quite common [74, 81, 107, 237]. When the loop is cut oscillations are more elusive, but have nevertheless been found in certain partial differential equation models [20, 47, 134, 186]. This will be further discussed in Chapter Three.

Two types of simple reentrant oscillations exist in two dimensional excitable media: circus movement reentry, and functional reentry. Circus movement reentry involves circular propagation around a fixed inexcitable region. Mayer [149] first proposed this mechanism for reentry in excitable tissue, and it has since been studied in experimental [25, 70, 154, 185] and theoretical systems [143, 170, 229, 230]. A relevant question is whether the reentrant oscillation can be sustained when the size of the obstacle is made arbitrarily small. It turns out that the answer in a number of cases is yes. Functional reentry refers to waves rotating despite the absence of an obstacle and has been demonstrated in many theoretical [143, 229, 230, 241] and experimental settings [4, 64, 104].

The reentrant wave may also have timing which is not strictly periodic. Without an obstacle to anchor itself onto, the free end (tip) of the reentrant wave can still rotate around a circular trajectory [230], or meander in a series of complicated trajectories [79, 210, 245]. The wave may also break up and spawn new rotational

centres of reentering waves [68, 245, 247]. Reentrant waves in cardiac tissue are further discussed in Section 1.3.6, and reentrant dynamics are observed in the results of Chapters Two, Three, and Four.

1.1.4 Mathematical Models of Excitable Media

Mathematical models of excitable media can be classified in terms of the continuity of their independent variables (space and time) and dependent (activation and recovery) variables. Discrete variables are mapped onto the space of integers, while continuous variables are real numbers. Models of excitable media fall into three continuity classes: cellular automata, coupled ordinary differential equations, and partial differential equations. Cellular automata are composed of a number of discrete spatial elements, called cells, which are coupled locally to each other. Each cell has a finite number of states with time-updated rules that guide the transitions between states. In contrast, coupled differential equations have a continuum of dependent variable states for each cell. Partial differential equations have these properties, but in addition treat space as a continuous variable.

Cellular automata were conceived by John von Neumann, and soon after applied to cardiac systems by Wiener and Rosenblueth [240]. These models are tempting to use because they are relatively easy to understand and implement, and computationally inexpensive. The drawback is that they tend to miss out on physically relevant properties of excitable media, such as action potential morphology, wave curvature effects, and dispersion properties [26, 173]. This is mainly due to the typically small number of variable states used which, among other things, can not faithfully reproduce excitation via diffusive coupling between adjacent cells. Furthermore, cellular

automata models in general lack the theoretical insight that we have developed from the qualitative theory of differential equations [122].

For these reasons partial differential equations are more commonly adopted for mathematical modeling of excitable media. This approach gained prominence in biomathematics following the seminal work of Hodgkin and Huxley [97], whose model accurately reproduced the dynamics of wave propagation in one dimensional squid nerve axon. A partial differential equation model of excitable media has the form,

$$\frac{\partial \mathbf{v}}{\partial t} = \mathbf{f}(\mathbf{v}) + \mathbf{D}\nabla^{\mathbf{2}}\mathbf{v} \tag{1.2}$$

where $\mathbf{f}(\mathbf{v})$ is an m-dimensional vector-valued function of m state variables, $\mathbf{v}$. The parameter $\mathbf{D}$ is a tensor of coupling strengths, and $\nabla^2 v_i = \sum_{j=1}^{n} \frac{\partial^2 v_i}{\partial {x_j}^2}$ describes the diffusion of $\mathbf{v}$. In this work we will mostly restrict our attention to the cases where $\mathbf{v} = (\mathbf{v}, \mathbf{w})$, $n = 2$, where isotropic diffusion is restricted to the activation variable such that the components of $\mathbf{D}$ are, $D_v = \begin{bmatrix} D & 0 \\ 0 & D \end{bmatrix}$ for the activation state, and $D_w = \begin{bmatrix} 0 & 0 \\ 0 & 0 \end{bmatrix}$ for the recovery state. Models of this form belong to a class of formulae know as reaction-diffusion equations. In the case of excitable media the reaction function, $\mathbf{f}(\mathbf{v})$, must exhibit the excitability properties discussed in Section 1.1.2.

Coupled ordinary differential equations offer a way of discretizing the space in Equation (1.2) on a lattice, such that the smallest interval of space becomes Δx, rather than dx. For example, on a square lattice of area $A = (L \times L)$, a

discretization into k^2 square cells with $\Delta x = L/k$ makes the m partial differential equations defined by Equation (1.2) into mk^2 coupled ordinary differential equations. A region of discretized space, represented by a cell (p, q), has its own set of m ordinary differential equations, each coupled to its neighbours. The coupling at cell (p, q) is defined by the discretized Laplacian,

$$\nabla^2 v_{(p,q)} = \Delta x^{-2}[v_{(p+1,q)} + v_{(p-1,q)} + v_{(p,q+1)} + v_{(p,q-1)} - 4v_{(p,q)}] \tag{1.3}$$

This first-order approximation of diffusional coupling on a square lattice is used in the two dimensional reaction-diffusion equations of Chapters Two and Four, inasmuch as it simplifies the definition of heterogeneities in those chapters. The one dimensional equations studied in Chapter Three are discretized according to a higher-order approximation to the Laplacian which is explained in Section 3.4.1. In general, space and time discretization is necessary when numerically solving partial differential equations on a computer, which has a finite number of states that it can hold in memory. There are a number of issues when approximating partial differential equations by discretized equations which will be discussed further in Section 1.2.3.

1.2 Mathematical Models of Cardiac Tissue

1.2.1 Biophysical and Phenomenological Models

At the biophysical level the heart is an extremely complex excitable tissue. It is composed of two main cell types (myocytes and fibroblasts) with a vast range of electrical properties, which are connected together in an irregular fashion. At the cellular scale activation is described by the depolarization of the cell membrane

caused by movement of ions in and out of the cytoplasm. Equations that explicitly model this process are called ionic models.

The simplest of these, called first-generation models, define membrane voltage as a function of changes in ion channel conductances [138]. Second-generation models incorporate changes in ion concentrations caused by ion pumps and intracellular movement of calcium through the sacroplasmic reticulum [147], while third generation models include more biophysical details, such as the effect of contraction on channel conductivity [132].

These ionic models are under continuous development so as to be able to accurately reproduce increasingly detailed experimental measurements. As such, there-Excitability is a tendency to make detailed models sometimes involving dozens of state variables [108]. The high-dimensionality of such systems makes it very difficult to obtain theoretical insight into the underlying dynamics. Furthermore these models are highly constrained to the particular circumstances under which the experiment is carried out (animal species, cell type, region of heart, environmental conditions, etc.).

These challenges are addressed by simplifying the model so as to reproduce the macroscopic characteristics of membrane potential dynamics. The first of these phenomenological models was developed by FitzHugh in the 1960's to study action potential propagation in nerve [69]. The FitzHugh-Nagumo equations of propagation take the reaction terms, $f(v, w)$ and $g(v, w)$ presented in Equation (1.1) and substitute them into the reaction-diffusion partial differential equation defined in Equation (1.2) to give,

$$\frac{\partial v}{\partial t} = -av(v-1)(v-\alpha) + w + D\nabla^2 v \tag{1.4}$$
$$\frac{\partial w}{\partial t} = \epsilon(v - bw)$$

Over time these equations have been modified to suit the particular features of the cardiac tissue experiment under consideration [94, 29, 245, 67, 2]. Although they are unable to capture mechanistic details of action potential generation, they are well suited to reproducing macroscopic characteristics of wave propagation: wave velocity, activation and refractory periods, periods of oscillations and tissue restitution properties [161]. Furthermore, these models are relatively easy to implement at the start of an investigation and can later prove useful as a reference point from which to compare different ionic models. For these reasons, in this thesis I focus on the investigation of the FitzHugh-Nagumo type propagation models.

1.2.2 Cable Theory of Cardiac Tissue

Propagation of excitation through cardiac strands can be characterized by a type of partial differential equation called the cable equation. The passive one-dimensional cable equation has the form,

$$\frac{\partial v}{\partial t} = -cv + D\frac{\partial^2 v}{\partial x^2} \tag{1.5}$$

where v represents an activation (or voltage) variable , c is a rate constant, $\frac{\partial^2 v}{\partial x^2}$ is the Laplacian of v, and D is the diffusion coefficient. The cable is passive due to the linearity of the $-cv$ term. Equation (1.5) was proposed by Lord Kelvin in 1850's to model the propagation of electrical impulses down the planned transatlantic

telegraph cable [222]. It has since been used to study current flow through nerve, muscle, and cardiac tissue [110].

Analytical solutions to Equation (1.5) have been obtained for different initial and boundary conditions [110]. One can get an idea of its properties by assuming the activation is at a steady state, $\frac{\partial v}{\partial t} = 0$, so as to reduce Equation (1.5) to a simpler linear ordinary differential equation with a solution,

$$v = v_0 e^{-x/\lambda} \tag{1.6}$$

where $\lambda = \sqrt{D/c}$ is called the space constant of the cable. The space constant characterizes the spatial scale of diffusion of subthreshold activation (electrotonus [204]) through the reaction-diffusion medium.

In general, λ can be found in more complicated partial differential equations with many state variables, including when the linear term $-cv$ in equation (1.5) is a non-linear function $f(v)$. The strategy then is to recover the passive component of the non-linear function by linearizing the equations about the stable fixed point of the system [124]. One can also numerically find λ by numerically solving the approximated partial differential equation system around its rest state, with the addition a constant (step) input stimulus of amplitude A to Equation (1.5) at $x = 0$. This ensures that A is small enough to be subthreshold to strongly non-linear responses, like the firing of an action potential. By plotting steady state v at different x on a log-log plot one obtains a linear fit with slope $-\lambda^{-1}$.

This fitting technique is also used in cardiac strand experiments where λ is typically 1-2 mm in Purkinje fiber [238] and cultured strands of chick ventricular cells

[184], and is around 0.3 mm in cultured neonatal rat cardiac monolayer [117]. In Chapter Three I investigate the effect of space constant relative to spatial discretization used in the one dimensional cable model.

In higher spatial dimensions the continuous cable theory predicts electrotonic activation spread falloffs which are sharper than Equation (1.5) [117, 110, 204, 205]. Nevertheless, propagation experiments in cardiac tissue have revealed that electrotonic properties are more comprehensively described by spatially discontinuous models of propagation than continuous partial differential equation models [204, 135, 63]. The two dimensional models used in Chapters Two and Four study the role of connective discontinuities (in the form of randomly distributed heterogeneous substrates) in modulating wave speed, and inducing propagation failure.

1.2.3 Numerical Approximation of Continuous Reaction-Diffusion Equations

When numerically solving partial differential equations, it is important to be aware of the caveats in the approximations made. One cannot make Δx and Δt infinitely small, and this invariably introduces truncation errors in the discrete approximation. To guarantee that the numerical scheme solves the underlying partial differential equation with high fidelity, one should check that: 1)the truncation errors do not grow out of control as the scheme integrates with time, and 2) they are small enough to have the numerical solution effectively approximate the solution underlying partial differential equation.

The first consideration is treated with the concept of numerical stability. A discretization of a partial differential equation is said to be stable if the truncation error, made at each time step of the iteration, does not grow as more iterations

are carried out. While it is in general very difficult to check this exactly for non-linear reaction diffusion equations, many cardiac modellers use the Neumann stability criterion for the linear diffusion equation as a general guide to stability [9, 119, 178]. When using the forward Euler finite difference scheme in n dimensions the Neumann stability criterion is defined by:

$$\frac{D\Delta t}{\Delta x^n} \leq \frac{1}{2^n} \tag{1.7}$$

Once stability is ensured, one should then check that the numerical solution is relatively close to the actual solution of the partial differential equation. Although the equations are often not analyticaly solvable, it is still possible get a an idea of the quality of the approximation by examining the numerical solutions as Δx and Δt are incrementally decreased. Figure 1–3 shows the results of such a procedure for the model used in Chapter Three. The features of the numerical solutions at small Δx seem to be converging to those of the actual partial differential equation solution ($\Delta x \to 0$, $\Delta t \to 0$).

Although there are no universal benchmarks for convergence, the space constant, λ has been used as a rough guide to ensure that the Δx chosen is small enough [9, 119, 178]. The spatial discretization is chosen so that the ratio $\Delta x/\lambda$ (known as the discretization constant) does not exceed $\approx$5 . The manuscripts published in the cardiac field that do explicitly address discretization typically have solution features varying by less than 5% as Δx and Δt are halved from the nominal values used in the simulations [9, 17, 223]. The spatial and temporal discretizations chosen to simulate the models in this thesis has been chosen to satisfy these criteria. A case in

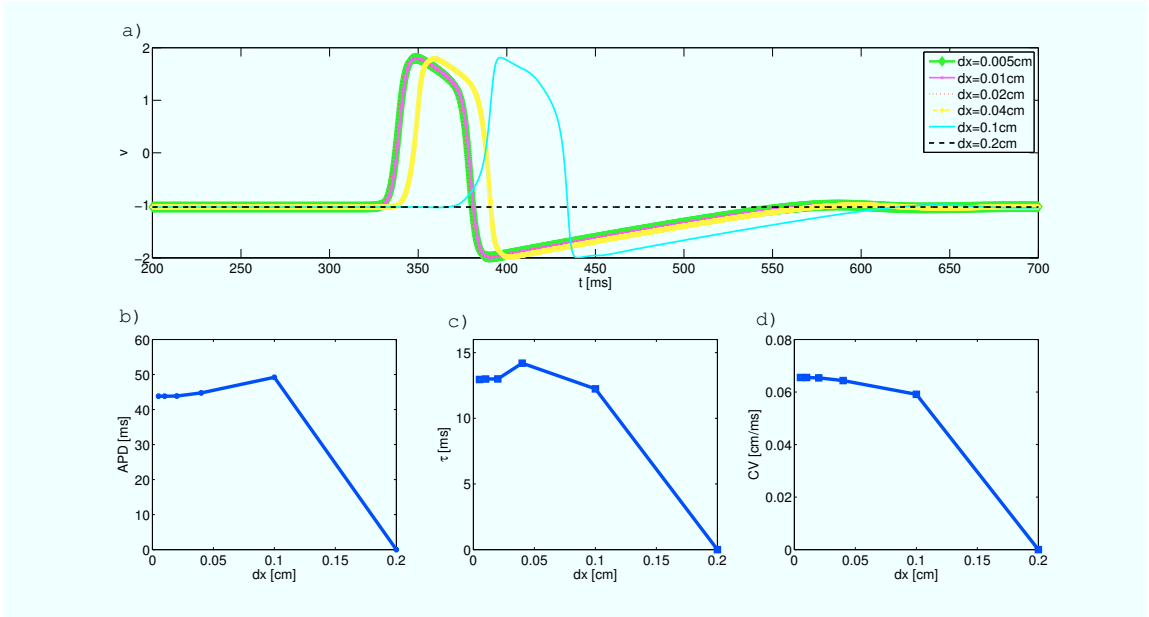

Figure 1–3: Convergence of wave features for smaller spatial discretizations of the FitzHugh-Nagumo cable model studied in Chapter Three. As spatial discretization Δx is decreased there is convergence of relevant propagation parameters: (a) activation waveform, (b) action potential duration, (c) risetime of activation, and (d) conduction velocity.

which the criteria is not met, resulting in new solutions not present in the underlying partial differential equation, is discussed in Chapter Three.

1.3 Experiments on Wave Propagation in Cardiac Tissue

1.3.1 Experimental Models

A number of experimental approaches are available to study how the structural and electrophysiological properties of cardiac tissue determine the types of activation patterns of waves which propagate through it. The experiments range from clinical research on humans *in situ* [118, 225], to highly controlled experiments in various animal cardiac preparations [4, 41, 111, 162, 185, 233].

Cardiologists use surface electrocardiograms and electrode catheters inserted into the heart to determine gross properties of electrical propagation through heart muscle [118]. The electrocardiogram records body surface potentials which give a low spatial resolution picture of wave propagation through the heart [172], while the electrode catheters can map field potentials induced by the spread of excitation on a millimeter scale [71]. These tools are essential in characterizing spatiotemporal patterns of electrical activity and their relation to known classes of cardiac arrhythmias. One example is the use of the electrodes to locate and ablate accessory pathways to propagation, which can be the source of a reentrant tachycardias [71, 118]. However, there are physical and ethical constraints on the range of experimental measurements and conditions available to study propagation in human heart.

Physiologists have used several different animal models to further our understanding of wave conduction through cardiac tissue. These studies have allowed researchers to not only elucidate the molecular basis of electrical propagation, but

also study the mechanisms of simulated arrhythmogenic situations (such as acute ischemia, volume overload, aortopulmonary shunts, fibrosis, etc.), as well as test the effects of pharmacological agents in modulating wave propagation properties (reviewed in [115, 162]). While these studies allow deeper investigation into the mechanisms underlying wave propagation, their scope is still limited by the physical peculiarities of the particular cardiac tissue used. For example, one is unable to investigate fundamental design considerations such as: how does cellular heterogeneity influence wave propagation in cardiac tissue? Questions like this are more readily tackled when one assumes control of how the tissue is built.

1.3.2 Engineered Tissue Culture Models

Cultured cardiac tissue models are composed of collections of dissociated cardiac cells subsequently reassociated into excitable tissue. There are currently many options for the type of cardiac cells to use, and for the shape that the tissue will take.

Cells have traditionally been taken from embryonic chick [50, 81, 28, 60] or neonatal rat heart [1, 34, 58, 64, 63, 104, 150, 151] as these young cells are more capable of reestablishing gap junctional connections necessary to form a functional syncytium [27]. A cell line derived form murine atrial tumors, called HL-1 cells [42] has more recently been used to study wave propagation [62, 98, 231], but these cells have proven challenging to culture into functional excitable tissue [99]. In the last few years, cardiac stem cells have become a very attractive source for tissue engineering [32, 61, ?]. These can be in the form of adult stem cells already differentiated into cardiac tissue, or embryonic stem cells which can differentiate into many types of

tissue [61]. Both cell types have direct therapeutic potential, insamuch as they can be reinserted into the host to repair unhealthy cardiac tissue [32, 61, 148, 248]. Embryonic stem derived cardiomyocyte cultures can be engineered into functional networks of connected cells which support wave propagation [125, 128, 239].

Dissociated cardiac cells can be cultured into different geometric structures, including: reaggregate spheroids, one dimensional strands, two dimensional (monolayer) sheets, or complex three dimensional shapes. Reaggregates are collections of thousands of cells rotated in liquid so as to clump into $\approx 10^{-4}$ m diameter balls [13, 50, 88, 126, 206]. They can be tuned to exhibit either rhythmic or excitable dynamics [50], but they are less amenable to monitoring of spatial activity within them. Monolayers are cells plated on a flat surface which connect up into a confluent two dimensional network of cells. The geometry of the tissue boundary can be controlled to produce shapes such as disks [1, 28, 98, 104, 259], quasi-linear strands [184, 226], annuli [81], or rectangular areas connected by a narrow isthmus [12]. Three dimensional cultures are prepared by molding cells onto polymeric scaffolds [33, 131], or by layering of preconstructed tissue sheets [198, 199]. While engineering three dimensional tissue requires more sophisticated culturing techniques than those for two dimensional sheets, the reconnected cells more closely resemble the phenotype of their counterparts *in vivo* [33, 60, 206].

Experiments on sheets of chick cardiac tissue motivate the theoretical work in Chapters Two, Three, and Four of this thesis. The experiments presented in Chapter Four were carried out using custom engineered cardiac disks of embryonic

chick ventricular cells. The properties of this preparation are discussed in detail in Section 4.3.1.

1.3.3 Mapping Wave Propagation

Tracking the evolution of excitation waves requires measurements taken at many points in space and time. In cardiac tissue culture experiments these measurements have been made using several electrodes, and various optical mapping techniques.

Microelectrode arrays are collections of extracellular electrodes, each of which detect electric potential in a region of the extracellular medium. The extracellular potential near the cells is referenced to a ground electrode in the bath. Cells are typically plated over the electrodes to reduce motion artifacts which decrease signal-to-noise ratio [56]. Custom built microelectrode arrays have been used to measure wave propagation in engineered cardiac tissue sheets [93, 106, 125, 151], and at least two [78, 101] are now commercially available. While they offer a non-invasive method of obtaining high time resolution time-series, the number of electrodes (typically < 80) in each array limits the spatial resolution of recordings [56, 247].

Optical mapping allows for higher spatial resolution measurements of wave propagation. The goal is to capture light from the surface of the excitable media. In cardiac and nerve tissue this is done by staining cells with dyes sensitive to calcium or voltage that can detect action potential generation. Voltage-sensitive dyes have the advantage of providing direct measurement of the potential across the cell membrane, which is the main activation variable diffusing in the system. Conduction experiments in monolayers have been performed by using voltage dyes like RH-237

[34, 104], di-4-ANEPPS [239] and di-8-ANEPPS [58, 259], each of which have particular excitation and emission bandwiths which required specialized light filters installed into the optical system. The drawbacks of voltage-sensitive dyes include photobleaching, phototoxicity, and a relatively poor signal-to-noise ratio [26, 239]. Calcium sensitive dyes produce a stronger fluorescence signal, and dyes like Fluo-4 and Calcium Green-1 have been utilized in cardiac propagation studies [1, 28, 239].

More recently, a method of imaging the visible light reflected by moving tissue as it contracts has provided some accurate reconstructions of wave propagation patterns [100, 247]. Despite the fact that contraction is a rather indirect measure of excitation, this dye-free method avoids the toxicity and photobleaching inherent to use of the current voltage and calcium-sensitive dyes.

Each of these methods detects electrical activation in the form of a change in the light emitted by the tissue and transduced by photoelectric sensors. These light detectors take the form of diode arrays on which the cells are cultured, or charge-coupled device chips which collect the light image through a series of lenses and filters (see [26, 239] for overview or [1, 28, 34, 58, 100, 104, 247, 259] for specific examples).

Optical mapping experiments used to motivate the studies in Chapters Two, Three and Four were performed by loading cells with Calcium Green-1 dye, and imaging using a custom-built macroscope coupled to a charge-coupled device camera. The details of this optical mapping system are described in detail in Section 4.3.2.

1.3.4 Spatial Heterogeneity

Cardiac tissue is a heterogeneous excitable medium in the sense that regions of the medium exhibit different properties. These regional differences can predispose

some parts of the medium to exhibit bursting, automatic (pacemaker), excitable, or inexcitable dynamics. How the distribution of cellular parameters affect the dynamics of coupled cells is a common theme in this thesis as well as in many other studies of cardiac tissue [30, 62, 120, 121, 169, 259].

It is not uncommon for a heart to develop heterogeneities in the form of large (millimeter-sized) inexcitable regions within the excitable tissue. These regions are composed of scar tissue formed by myocardial infarction following ischemia [57, 118]. These inexcitable zones form obstables over which waves break and wrap around to form a reentrant circuit of excitation (also known as circus movement reentry described in Section 1.1.3). Inasmuch as this situation is thought to be reason for many dangerous tachycardias, the properties of such reentrant circuits have been the focus of intense experimental [25, 70, 4, 185, 81] and theoretical research [74, 143, 170, 202, 229, 230]. In Chapter Four I investigate the role of a recovering pacemaker site acting as a large obstacle leading to wave breakup and reentry.

At the cellular level, the portion of cardiac tissue responsible for propagating waves is composed of a heterogeneous distribution of different cell types: cardiomyocytes, fibroblasts, and blood vessel endothelial cells. Cardiomyocytes are excitable cardiac muscle cells which form the bulk cardiac tissue. Despite this they are outnumbered (about 2:1) by inexcitable cells called fibroblasts [133]. Fibroblasts are thought to be primarily responsible for maintenance of the extracellular matrix of cardiac tissue, but they are also electrically coupled to myocytes via gap junctions [24, 133]. As such, they can act both as current bridges by connecting up distant myocytes, or current sinks which place an electrotonic load on surrounding myocytes

during wave propagation [72, 133]. In pathological situations like fibrosis, fibroblasts can secrete excess collagen into the extracellular matrix, which can act as small (cell sized) obstacles to propagating waves [49, 179, 221]. The influence of small structural heterogeneities like fibroblasts and collagen deposits on wave propagation has been investigated in experimental and theoretical models of cardiac tissue [35, 212, 221, 216, 259] and is the focus of the next chapter.

1.3.5 Cardiac Pacemakers

Pacemakers are regions of automaticity (defined in Section 1.1.2) which entrain the surrounding excitable tissue by emitting waves of excitation which pass through the medium with the period of the pacemaker. At the tissue scale, the heart has evolved specialized regions responsible for pacemaking. The typical rhythm of a healthy heart is set by a dominant pacemaker called the sinoatrial node. This multicellular structure is embedded in excitable right atrium muscle, where is can be distinguished histologically by the less regular distribution of cells in a relatively fibrous connective tissue matrix [156]. Sinoatrial node cells distinguish themselves from the surrounding atrial myocytes with distinct electrical properties which allow them to oscillate spontaneously. One such property is the "funny current", I_f, that is an inward current activated at hyperpolarized potentials. A heterogeneous distribution of I_f and other ion currents ($I_{Ca,L}$, I_{Na}, I_{to}) plays a functional role in pacemaking at the cellular and tissue levels [22, 156].

The distributions of cellular beat rates within cardiac pacemakers have been examined in experimental preparations of the sinoatrial node [22, 130, 166], Purkinje fibers [65, 112], as well as embryonic chick tissue [50, 51]. These studies show

that regions of cells with faster beat rates tend to set the pace of the oscillation. Nevertheless, it should be noted that, over short distances, electrotonic interactions between pacemakers can lead to synchronized beat rates slightly slower than that of the fastest uncoupled pacemaker [22, 51, 152, 166].

There are structures in the heart besides the sinoatrial node which are able to act as sites of pacemaking, including: fibers in the atria, the coronary sinus and pulmonary veins, portions of the atrioventricular junction, the His-Purkinje system, throughout ventricular muscle, right and left ventricular outflow tracts, and valves [257]. There pacemaker sites are able to drive the heart in case of sinoatrial node dysfunction (in which case they act as subsidiary pacemakers) [21, 181, 182], but can also paroxysmally compete with the sinus node for entrainment of the cardiac muscle (in which case they act as ectopic pacemakers) [38, 116, 180].

In a healthy heart the sinus node has the fastest beat rate of these pacemakers, and so resets and entrains them [113]. This follows from the property of wave annihilation in excitable media: wave trains generated by the spontaneous pacemaker (or pacing stimulator) "peel back" wave trains generated by sources of wave trains with a longer beat rate. [1, 118, 113, 140, 190, 207, 251, 256]. Once the wave train of the faster pacemaker reaches the source of slower wave trains (be it another pacemaker, or the pivot point of a reentrant wave) then that source may be reset and entrained to the period of the faster pacemaker.

A mathematical framework for describing resetting and entrainment of pacemakers is presented in Section 1.4 and the resetting properties of cardiac pacemakers are discussed in detail in Section 1.4.3. In Chapter Three I study the resetting of

a pacemaker region by stimuli delivered through an excitable cable, while in Chapter Four I investigate resetting and dynamics resulting from the interaction of two pacemaker sites embedded in a chick cardiac monolayer.

1.3.6 Reentrant Waves in Cardiac Tissue

Waves of reentry introduced in Section 1.1.3 are germane to cardiologists. Mines suggested the relevance of self-sustained rotating waves of excitation to cardiac tachycardias [153], and since then a number of dangerous cardiac arrhythmias have been associated with reentrant waves. These include: sinus node reentrant tachycardia, atrial flutter, atrial fibrillation, atrioventricular nodal reentrant tachycardia, atrioventricular reciprocating tachycardia, ventricular tachycardia, and ventricular fibrillation [257]. Experiments studying the factors influencing reentry formation and termination in excitable tissue may provide insights for effective treatment of these arrhythmias.

The determinants of reentrant wave formation have been investigated in a range of engineered cardiac tissue. These studies have shown that reentry is favoured by factors such as: premature stimuli [104], rapid pacing [1, 255], large inexcitable obstacles [146], increased fibroblast proportion [259], decreased intercellular coupling [28, 259], regions of abnormal cell density or low potassium conductance [1]. Conversely, termination of reentry can be promoted by rapid pacing [1], electrical field stimulation [104], and inhibiting sodium conductance [146]. In Chapter Four I investigate the formation of reentry in engineered chick cardiac tissue by increasing the beat rates of pacemakers through application of a potassium channel blocker.

1.4 Phase Resetting of Pacemakers

1.4.1 Perturbing a Stable Limit Cycle

Robust spontaneous oscillations of pacemakers in excitable media can be described in the language of dynamical systems theory. An oscillation is a periodic solution to a system of differential equations, represented by a simple closed trajectory in state space. Automatic and robust oscillations such as those in the heart can be thought of as a stable limit cycle defined in Section 1.1.2. A stable limit cycle, Γ, is a periodic trajectory which attracts neighbouring states. This implies there are small perturbations from a state $v \in \Gamma$ will converge back to Γ as $t \to \infty$. The *basin of attraction* of Γ, designated as $B(\Gamma)$ corresponds to all states that approach Γ in the limit $t \to \infty$. A robust heart rhythm which persists despite large perturbations, can be thought of as having a large basin of attraction.

Small perturbations from $v \in \Gamma$ to $v' \in B(\Gamma)$ can nevertheless shift the *phase* of the oscillation. A phase, $\varphi \in [0, 1)$, represents the amount of time that has elapsed in a cycle relative to the intrinsic cycle length, T_0, with $\varphi = \frac{t-t_0}{T_0} \pmod 1$ where t_0 is a time chosen to mark the start of the cycle. One can characterize the influence of a perturbation on the change of phase by performing a phase resetting experiment. A range of biological oscillations (from circadian rhythms in organims to aggregation of slime mold amoebae) have been investigated with such experiments [243].

1.4.2 Phase Transition Curve Measurements

Winfree developed a theoretical framework for analysing these phase resetting experiments. A perturbation (in the form of a brief stimulus) delivered at some phase of the oscillation, φ (also called the old phase), and causes a resultant phase,

$g(\varphi)$ (also known as the new phase). The oscillation is assumed to be a stable limit cycle, Γ, with intrinsic period, T_0. The timing of the stimulus, also known as the coupling interval, t_c is related to the old phase by $t_c = \varphi T_0$ (see Figure 1–4). The resulting cycle lengths, $(T_1, T_2, ..., T_\infty)$, after the perturbation are measured and used to calculate the phase shift, $\Delta\varphi$, given by

$$\Delta\varphi = \frac{iT_0 - T_i}{T_0} \pmod 1 \tag{1.8}$$

which holds for $i \to \infty$, but typically the limit cycle reestablishes its intrinsic period very quickly so that $T_{n+1} \approx T_n + T_0$ for $n \geq 2$. For the calculations of $\Delta\varphi$ used in this thesis I found that taking T_3 is sufficient (99.9% accurate) to approximate T_i as $i \to \infty$.

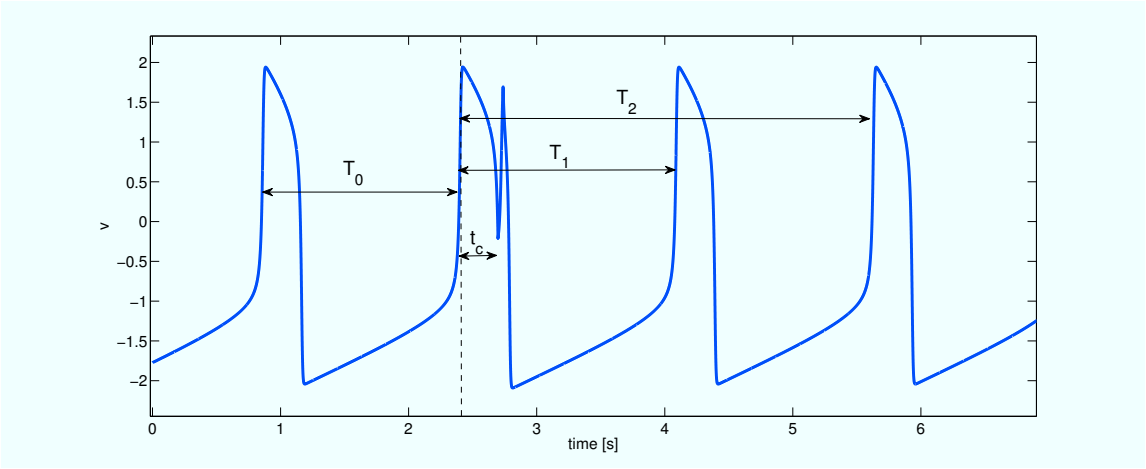

Figure 1–4: A schematic of measurements taken used to calculate the phase resetting of a pacemaker used in Chapter Three. The limit cycle oscillation is perturbed just after the second beat resulting in a slight prolongation of cycle length. The dashed vertical line represents the reference time corresponding to $\varphi = 0$ (arbitrarly set at the upward zero crossing time of v). A stimulus is delivered at a time t_c after the reference time (dashed line) leading to a perturbed cycle length, T_1.

The phase shift perturbs the old phase, φ, to the new phase, $g(\varphi) = \varphi + \Delta\varphi$, resulting in the following relationship by which the new phase is computed

$$g(\varphi) = 1 - T_3/T_0 + \varphi \pmod 1 \tag{1.9}$$

Plotting $\varphi \in [0, 1)$ against $g(\varphi) \in [0, 1)$ gives the *phase transition curve*, $g(\varphi) \in [0, 1)$, that relates the phase resetting effect of a stimulus given at any phase. In general, no resetting occurs for φ where $T_1 = T_0$ so that $\varphi = g(\varphi)$. Perturbation phases for which $T_1 < T_0$ cause phase advances. Chapters Three (Figure 3–3(a)) and Four (Figure 4–8(a)) characterize phase transition curves for partial and ordinary differential equation pacemaker models, respectively. In space, the separation time between stimulus and pacemaker, $\Delta t_{(s,p)}$, shifts φ by $\frac{-2\Delta t_{(s,p)}}{T_0}$ resulting in $\varphi = g(\varphi)$ for stimulus phases where stimulus and pacemaker waves annihilate [94]. The topological properties of phase transition curves are examined further in Chapter Three (Section 3.3.1).

1.4.3 Phase Resetting and Entraining Cardiac Pacemakers

Phase transition curves have been measured in several different cardiac pacemakers using a range of experimental preparations [8, 41, 91, 114, 111, 139, 232] and computational models [41, 45, 90, 89, 137, 176] by directly stimulating the site of pacemaking. The curves have also been investigated by stimulating a pacemaker from a distance in real cardiac tissue [74, 118] and mathematical models of excitable media [73, 74, 94, 165]. While the exact shape of the phase transition curves can be quite diverse from one experiment to the next (and for different stimulus amplitudes),

they share some interesting properties. One of these properties is the continuity of $g(\varphi)$ with respect to φ, which is further discussed in Section 3.3.1.

The phase transition curve can be used to predict the entrainment pattern when periodic stimuli with period T_s are delivered to the pacemaker [88]. Given a fast return to the limit cycle (i.e.: $T_2 - T_3 \approx T_0$), if φ_j is the phase just before jth stimulus then

$$\varphi_{j+1} = g(\varphi_j) + T_s/T_0 \pmod 1 \tag{1.10}$$

The iteration of this map with each stimulus number, j, predicts the dynamics of the pacemaker under periodic forcing. By studying the effect of different pacing periods on the dynamics of φ_j in Equation (1.10) one can find regions of M:N phase locking (where every integer M stimuli elicit N beats from the pacemaker), as well as irregular chaotic dynamics [88, 87]. I use these concepts to predict the limit of 1:1 entrainment of a pacemaker pair in Chapter Four.

1.5 Summary and Outlook

This chapter reviewed the basic concepts relevant to studying the dynamics of pacemakers in heterogenous excitable media. The properties of excitable media were introduced and it was demonstrated how they manifest themselves in many forms of cardiac tissue. This discussion was complemented by an overview of mathematical and experimental tools used for the modeling and analysis of dynamics in such systems. In the next three chapters I present results on how properties of heterogeneity, resetting, and pacemaker beat rates relate to the dynamics in heterogeneous

excitable media with pacemakers. The next chapter focuses on properties of heterogeneous media, namely the coupling between cells and distribution of two types of heterogeneous cell substrates, and their role in the dynamics of wave propagation slowing, wave break, and reentrant wave patterns.

CHAPTER 2
Dynamics of Wave Slowing and Breakup with two Heterogeneous Substrates in Excitable Media

2.1 Abstract

Waves of activity in excitable media can propagate as plane waves, or break up to form reentrant waves. In heterogeneous cardiac tissue, plane wave breakup can be associated with fatal cardiac arrhythmias. In this chapter I investigate how spatial heterogeneity can lead to wave slowing, wave break, and propagation failure in a FitzHugh-Nagumo model of two dimensional excitable media. Two types of heterogeneities are considered: *sinks* are regions in space in which the activity is held at the rest state, and *breaks* are non-conducting regions with no-flux boundary conditions. When these heterogeneities are randomly distributed through the medium they have an aggregate decremental effect on plane wave velocity, and above a critical proportion of heterogeneities the wave conduction fails. Using numerical simulations and Luther's Law I describe the functional relationship between the conduction velocity, proportion of heterogeneities, and diffusive coupling for each type of heterogeneity. The results facilitate our understanding of the properties that determine reduced propagation velocity and wave break in heterogeneous excitable cardiac tissue.

2.2 Introduction

Analysis of wave propagation through spatially heterogeneous media is a classic problem in physics [105, 253]. In this chapter I consider an excitable medium with

spatial heterogeneities related to cellular heterogeneities in cardiac tissue. However, even in a spatially homogeneous excitable medium, there may be transient spatial heterogeneities (say, in refractoriness) that in turn result in wave break and the formation of spiral waves [68, 171, 244]. A further complication arises in other natural and experimental excitable systems which invariably contain heterogeneities that lead to a variety of experimentally observed wave patterns including rotating spiral waves. Examples include heterogeneities in the form of water-in-oil microemulsions [234, 235] and experimentally generated catalyst patches in the Belousov-Zhabotinsky reaction [213], irregularities in catalytic surfaces [5, 6, 14], and variability in the spatial structure in cardiac tissue and tissue culture [28, 29, 30, 35, 216, 259].

An experimental example of wave break leading to reentrant wave formation is shown in Figure 2–1. Each panel represents a spatial map of intracellular calcium concentration in a monolayer culture of spontaneously beathing embryonic chick heart cells, further described in Sections 4.3.1 and 4.3.2. In this sequence of calcium activations, a wave starting from the top right edge of the culture propagates through the heterogeneous medium to the left boundary. The second wave attempts to take a similar trajectory but breaks up in the upper middle to form a reentrant rotating wave. The irregular propagation of the wave is thought to be influenced by heterogeneities distributed throughout the medium. The increased presence of such heterogeneities in the whole heart, such as those induced by fibrosis, may lead to serious abnormal cardiac rhythms that are associated with rhythms generated by rotating spiral waves of excitation [35, 145, 216] similar to those shown in Figure 2–1.

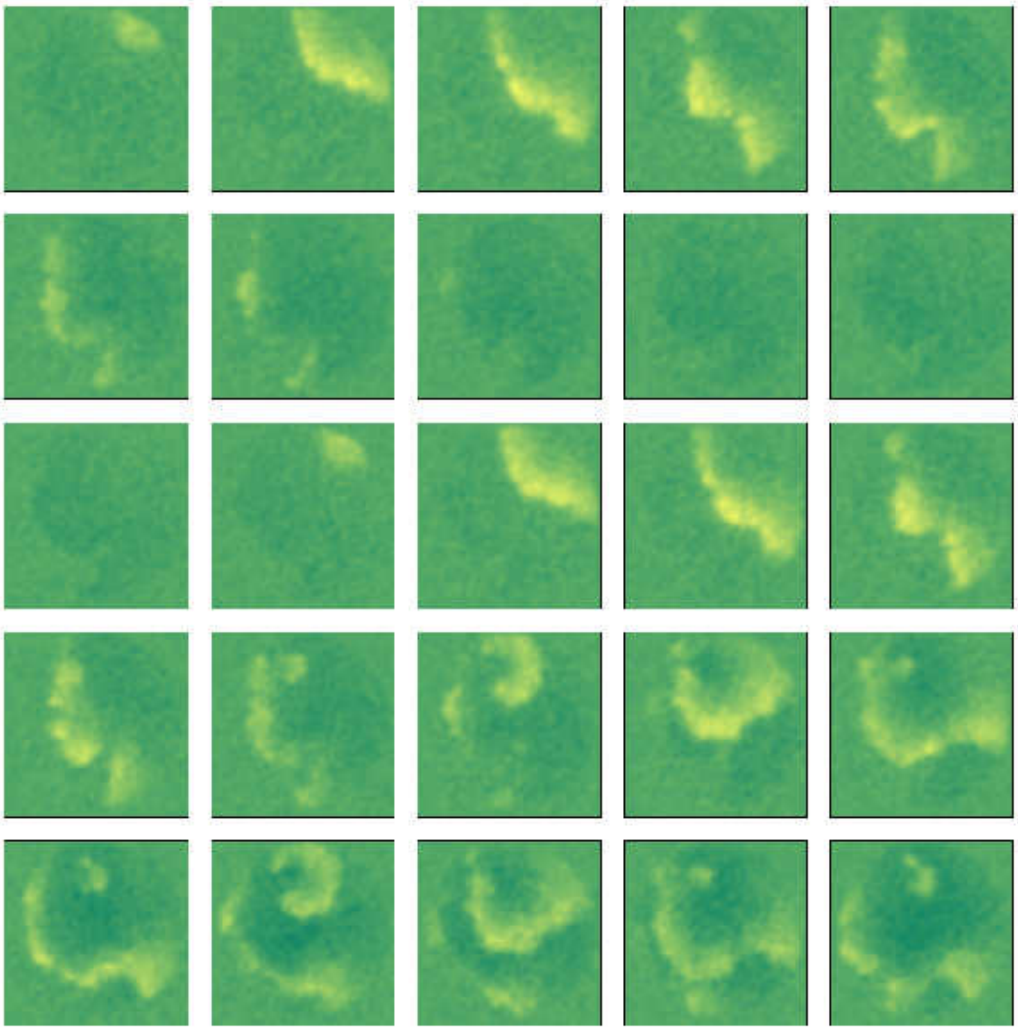

Figure 2–1: An example of wave propagation, breakup, and the formation of a reentrant wave in chick cardiac monolayer culture (courtesy of T. K. Shajahan). The activation maps have a field of view of ≈1 cm and are presented every 250 ms. The brighter colour indicates regions of higher intracellular calcium concentration.

Given the practical importance of the problem, there have been many theoretical studies of the role of heterogeneities in modulating cardiac conduction. They analyze the roles of both localized [9, 146, 175, 195, 193, 209, 249, 252] and randomly distributed heterogeneities [28, 29, 30, 212, 218, 220]. While large localized heterogeneities often act as anchoring sites for spiral waves of excitation, smaller dispersed heterogeneities have more subtle effects on the dynamics. The effects depend on the coupling and excitability properties of the medium, as well as the types of distributed heterogeneities. In this chapter I focus on two different types of heterogeneities which are relevant to cardiac tissue. *Breaks* are non-conducting regions of space with no-flux boundary conditions, and *sinks* are locations at which the activation is fixed at its rest value.

As the relative density of these randomly distributed heterogeneities increases, the conduction velocity typically decreases. This can have contrasting effects depending on the underlying properties of the medium. If the medium normally conducts plane waves without breaking up, then as the density of heterogeneities increases plane wave propagation can break leading to rotating spiral waves [29, 30, 212]. In contrast, for excitable media in which spiral wave formation is not favoured, an increase of heterogeneity can lead to a subsequent slowing of the propagating wave and paradoxical stabilization of the reentrant propagation [218, 220, 221].

Recent work has focused on understanding the decrease of propagation velocity as a function of the density of the heterogeneities. Steinberg and others proposed a dimensionless number to characterize media at the point where plane waves break

up [212]. Alonso *et al.* developed an effective medium theory in which effective diffusion coefficients and reaction rates characterize the decrease of conduction velocity with heterogeneity density [5, 6, 14].

The present findings extend these earlier studies by juxtaposing the factors which modulate conduction velocity in model cardiac systems with breaks or sinks. Specifically, for each type of heterogeneity I propose a functional form for the relationship between conduction velocity, coupling, and the density of the heterogeneities.

2.3 Methods

2.3.1 Model of Excitable Medium with Heterogeneities

The excitable medium is simulated using the FitzHugh-Nagumo model defined by Equations (1.4)

$$\frac{\partial v}{\partial t} = -av(v-1)(v-\alpha) + w + D\nabla^2 v$$
$$\frac{\partial w}{\partial t} = \epsilon(v - bw)$$

with $\alpha = 0.02$, $\epsilon = 0.01$, $\beta = 0.5$ and D is varied in the range $(0.5 - 1) \times 10^{-3}$. These equations are solved numerically using forward Euler integration with space step $\Delta x = 0.01$ and time step $\Delta t = 0.01$. The spatial unit is defined as 1 cm and time unit is 1 ms, so that D is expressed in $\mathrm{cm}^2/\mathrm{ms}$. With this choice of parameters the velocity in the homogeneous system changes by $\approx$0.1% when $\Delta x = 0.005$ and $\Delta t = 0.0025$.

The partial differential equations are spatially discretized in two spatial dimensions on a 200×200 square lattice. To generate the distribution of heterogeneities

for each cell, a probability of being a heterogeneity, P_H, is chosen . This generates a mean proportion of cells marked as a heterogeneity averaged over all possible distributions, $< \phi > \approx P_H$. The actual proportion of heterogeneities in most realizations is typically very close to $< \phi >$ on such a large lattice. Examples of distributions of heterogeneities at different ϕ are presented in the first column of Figure 2–2, with heterogeneities in black and excitable cells in white.

A *sink* heterogeneity is defined as a discretized cell, held at their rest state $(v = 0, w = 0)$ (i.e. Dirichlet boundary conditions), and a *break* cell has no-flux (i.e. Neumann) boundary conditions, $\frac{\partial v}{\partial x} = 0$, for all time. A sink is related to an inexcitable yet coupled fibroblast cell, while a break represents extracellular collagen deposits between cells that act as non-interactive obstacles to wave propagation.

Plane waves are initiated by setting the initial conditions of the first three columns of cells on the left side at $(v = 1.0, w = 0.0)$. The conduction velocity of the waves, CV, is estimated by interpolating activation times (zero crossings with $\frac{\partial v}{\partial t} = 0$) across a line perpendicular to the direction of propagation, at $N/4$ th and $3N/4$th sites in the medium, where N is the length of the simulation domain. This gives the a distribution of times taken for the wave to travel that distance. Velocities are measured by subtracting crossing times along the wavefront. The median of these velocities is taken to represent the wave speed for that system. Wave speeds are averaged over ten spatial realizations of different random spatial distributions of heterogeneities to produce the average conduction velocity, CV, presented in Figures 2–3 and 2–5.

For both heterogeneity types, $\Delta x = 0.01$ and $\Delta t = 0.01$ were chosen small enough so as not to appreciably influence the measured conduction velocity. Redoing the simulations for a smaller $\Delta x = 0.005$ and $\Delta t = 0.0025$ (at $D = 0.0007$ cm^2/ms in the the homogeneous case, $\phi = 0$) shows a 0.1% increase in conduction velocity relative to the nominal values of $\Delta x = 0.01$ and $\Delta t = 0.01$. For ensembles of equivalent spatial distributions of break heterogeneities at $\phi = 0.05$ and $\phi = 0.10$, the estimate of CV increases by 1.5% and 2.7% respectively relative to the nominal Δx and Δt. For equivalent distributions of sink heterogeneities at $\phi = 0.0005$ and $\phi = 0.001$, the estimate of CV decreases by 0.5% and 1.4% respectively when $\Delta x = 0.005$ and $\Delta t = 0.0025$.

2.4 Results

2.4.1 Effects of Breaks on Conduction Velocity

Figure 2–2 shows examples of distributions of breaks at different proportions and their effect on wave propagation when $D = 0.0007$ cm^2/ms. For ϕ=0 the medium is homogeneous and the excitation propagates as a plane wave. For $0< \phi <0.3$ the plane wave is roughened by the presence of breaks, but still propagates through the medium in one piece. For ϕ=0.40 the plane wave breaks up in several places and the resultant wavelets meander through the medium along complex trajectories. For ϕ=0.45 the wavelets are unable to propagate to the other side of the medium.

The proportion of breaks, ϕ, has a decremental effect on propagation velocity (Figure 2–3). Previous studies of randomly distributed break-type heterogeneities have noted similar findings [30, 219, 5]. For low proportion of breaks, Tusscher *et al.* [219, 221] found that the conduction velocity of the waves of excitation decreases

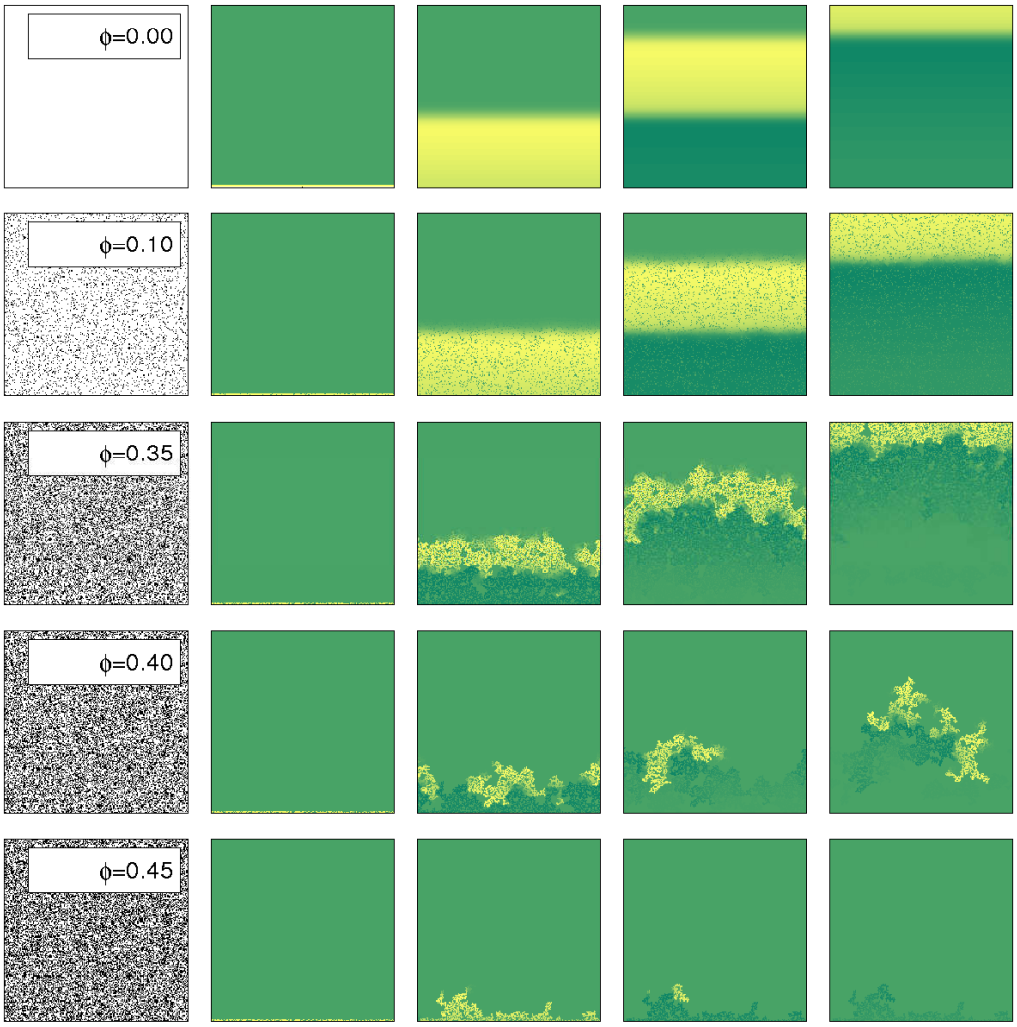

Figure 2–2: Examples of activation maps for different proportions of break sites in the FHN model. The rows correspond to different proportion of breaks with, the spatial distribution shown in the first column, followed by a sequence of snapshots of the activation variable, v, in space, for that distribution of breaks. The brighter color represents regions with high activation.

linearly with the number of breaks in accordance with Figure 2–3. These studies are extended to look at how coupling in the medium affects velocity in the presence of breaks. According to Luther's law, velocity in the homogeneous medium, CV_0, is proportional to $\sqrt{D/\tau}$, where D is the diffusion coefficient and τ is the risetime of excitation [200, 246]. In the model considered, the risetime (calculated as the time between 10% and 90% maximal activation) is τ =15.3 ms, and $CV_0 \approx 2.5\sqrt{D/\tau}$ in accordance with Luther's Law.

The effect of break proportion on conduction velocity for different D is shown in figure 2–3(a). In the heterogeneous medium with low break numbers, conduction velocity decreases linearly with ϕ (Figure 2–3(a)). The slope of CV *vs* ϕ curve depends on CV_0, as shown in Figure 2–3(b) where CV/CV_0 is plotted as a function of ϕ. Thus, the conduction velocity in the linear regime decreases with break proportion as

$$CV = CV_0(1 - k\phi) \tag{2.1}$$

where k is a parameter independent of diffusional coupling strength, D. Figure 2–3(b) shows that a linear fit of the data at D=0.0007 cm^2/ms for low ϕ (between 0 and 0.05) estimates $k = 1.28$. Integrating ensembles of identical spatial distributions at $dx = 0.005$ and $dt = 0.0025$, between $\phi = 0$ and 0.05, estimates $k = 1.21$.

Further increase in the proportion of breaks leads to deviation from the linear relation of Equation (2.1), and eventually leads conduction failure for $\phi = \phi_c \approx 0.41$, independent of D (Figure 2–3(a)). The value of ϕ_c=0.41 for conduction failure is the site percolation threshold for the square lattice [211, 163, 141]. This implies that,

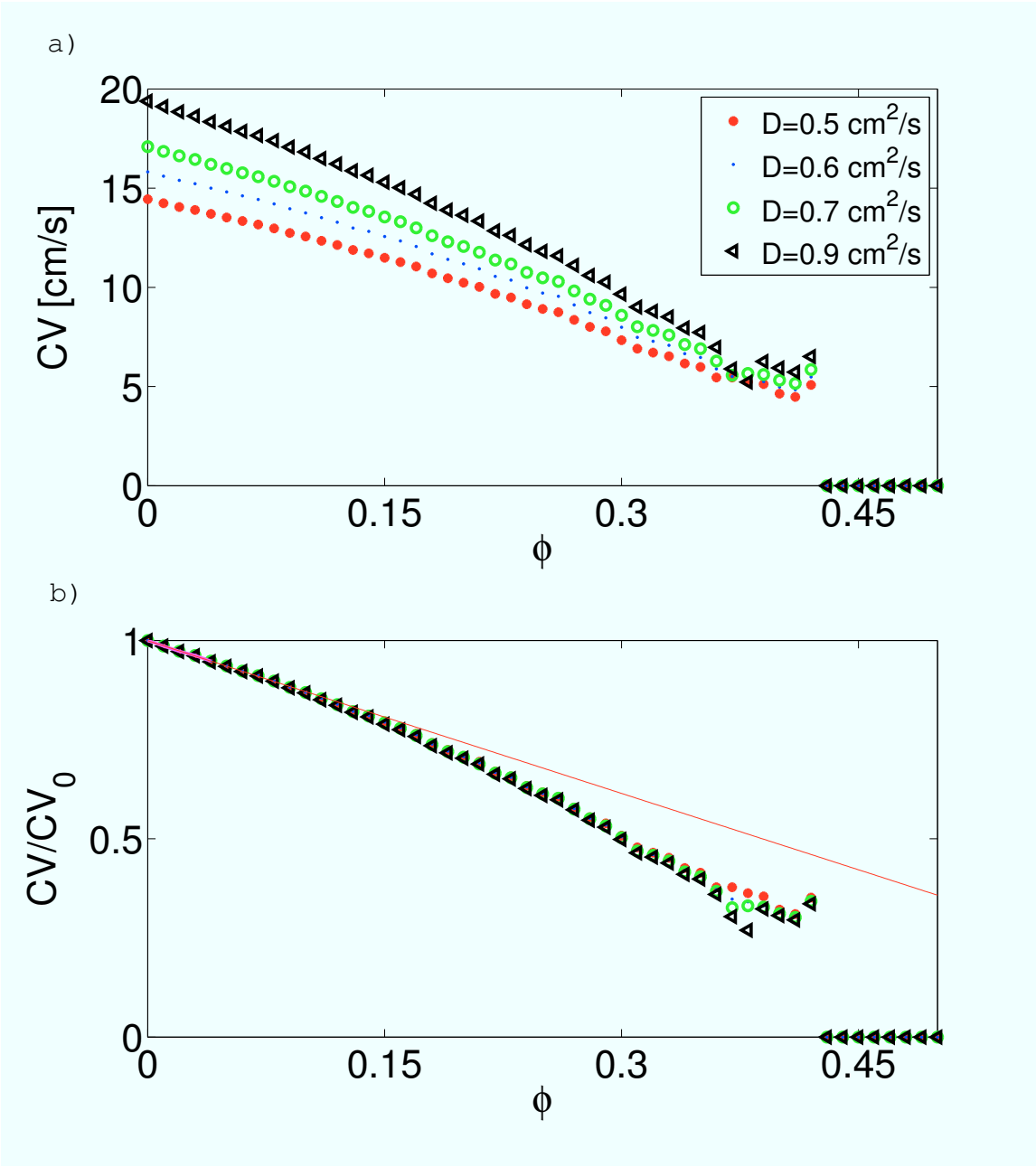

Figure 2–3: The dependence of conduction velocity on break proportion and coupling strength. (a) Conduction velocity decreases as a function of percentage of breaks eventually leading to propagation failure at a ϕ which is independent of D (b) The velocities are rescaled by CV_0 to demonstrate the functional relationship between CV, ϕ and CV_0. A linear fit between ϕ =0 and 0.05 is shown for D=0.0007 cm^2/ms.

for the range of D investigated, the wave can propagate between breaks as long as it can find a connected path in the medium.

Alonso *et al.* [5] proposed a functional relationship for the conduction velocity for all $0 \leq \phi \leq 1$

$$CV = CV_0\sqrt{1 - \phi/\phi_c} \tag{2.2}$$

where ϕ_c is the critical proportion of breaks at which propagation fails. For low ϕ equating the linear term from Equation (2.2) with Equation (2.1), one finds that ϕ_c, is related to k by

$$\phi_c = 1/(2k). \tag{2.3}$$

With $\phi_c = 0.41$, Equation (2.3) overestimates the value of $k = 1.28$ found in the propagation model by about 4%, while the $k = 1.21$ found at smaller dx and dt is underestimates by 2

2.4.2 Effects of Sinks on Conduction Velocity

Sinks, like breaks also have a slowing effect on plane wave propagation through the medium, although each sink has a much stronger effect on velocity compared to each break. When sinks are very sparse in the medium ($\phi < 0.0030$ for $D = 0.0007$ cm^2/ms), the wave travels as a roughened plane wave, and the velocity decreases approximately linearly. For $0.003 < \phi < 0.004$, the plane wave breaks in several places, but soon reforms generating a quasi-planar wave front. This is coincident with the linear decrease in velocity at these sink proportions (Figure 2–5). With higher numbers of heterogeneities in the medium ($0.006 < \phi < 0.008$, when

$D = 0.0007$ cm^2/ms), the wave breaks up forming curved wave fronts leading to sustained reentrant wave activations in the medium (Figure 2–4). With an even higher percentage of sinks ($\phi > 0.0088$, when $D = 0.0007$ cm^2/ms) the wave is unable to propagate through the medium, and the conduction fails. This is a 500-fold decrease relative to the number of equally sized breaks required to cause propagation failure.

The effect of sink proportion on conduction velocity at different diffusional coupling strengths is presented in Figure 2–5(a). For each value of D, conduction velocity decreases linearly with the number of sinks at low ϕ, but then quickly drops to zero. In addition, the ϕ_c at which propagation fails is smaller for higher coupling, in accordance with the findings of Steinberg *et al.* [212]

In the linear regime of $CV(\phi)$, the conduction velocity with sinks depends on CV_0, as in the case of breaks. In contrast, k of equation (2.1) varies with D. This is evident for the plot of CV/CV_0 against a ϕD in Figure 2–5(b), and suggests the following relation between propagation velocity, proportion of sinks, and diffusional coupling to be

$$CV = CV_0(1 - k_S D\phi) \tag{2.4}$$

where k_S is a parameter that is constant with respect to D. Figure 2–5(b) shows that a linear fit for D=0.0007 cm^2/ms at low ϕ (between 0 and 6×10^{-4}) estimates $k_S = 67.9$ s/cm^2. Integrating ensembles of identical spatial distributions of sinks at $dx = 0.005$ and $dt = 0.0025$, estimates $k_S = 67.1$ s/cm^2. In comparison to Equation (2.1), the additional slowing of the wave with sink proportion is explained by the

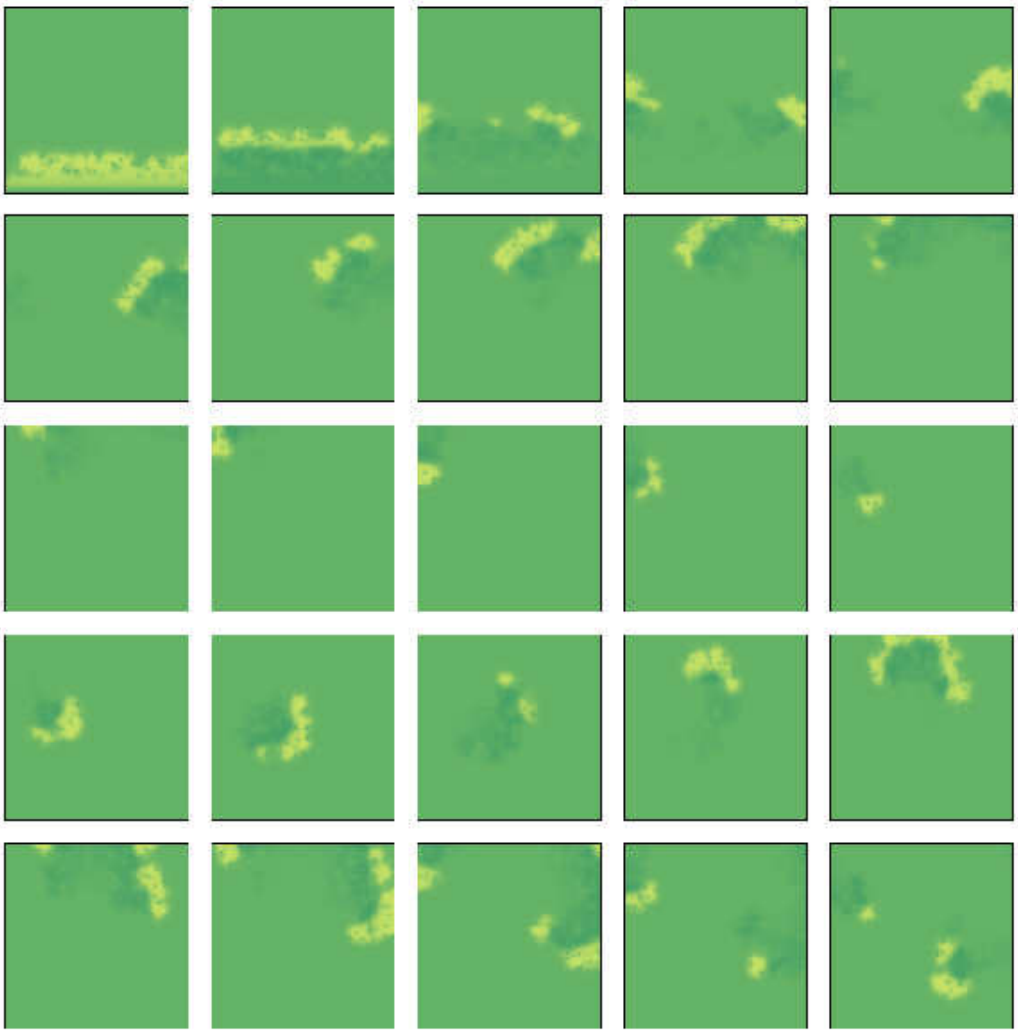

Figure 2–4: Snapshots of wave breakup and reentry in the presence of sinks. The panels are separated by 5 ms. For the parameters D=0.0007 cm^2/ms, and $\phi = 0.0052$ the plane wave breaks up and forms reentrant circuits of excitation.

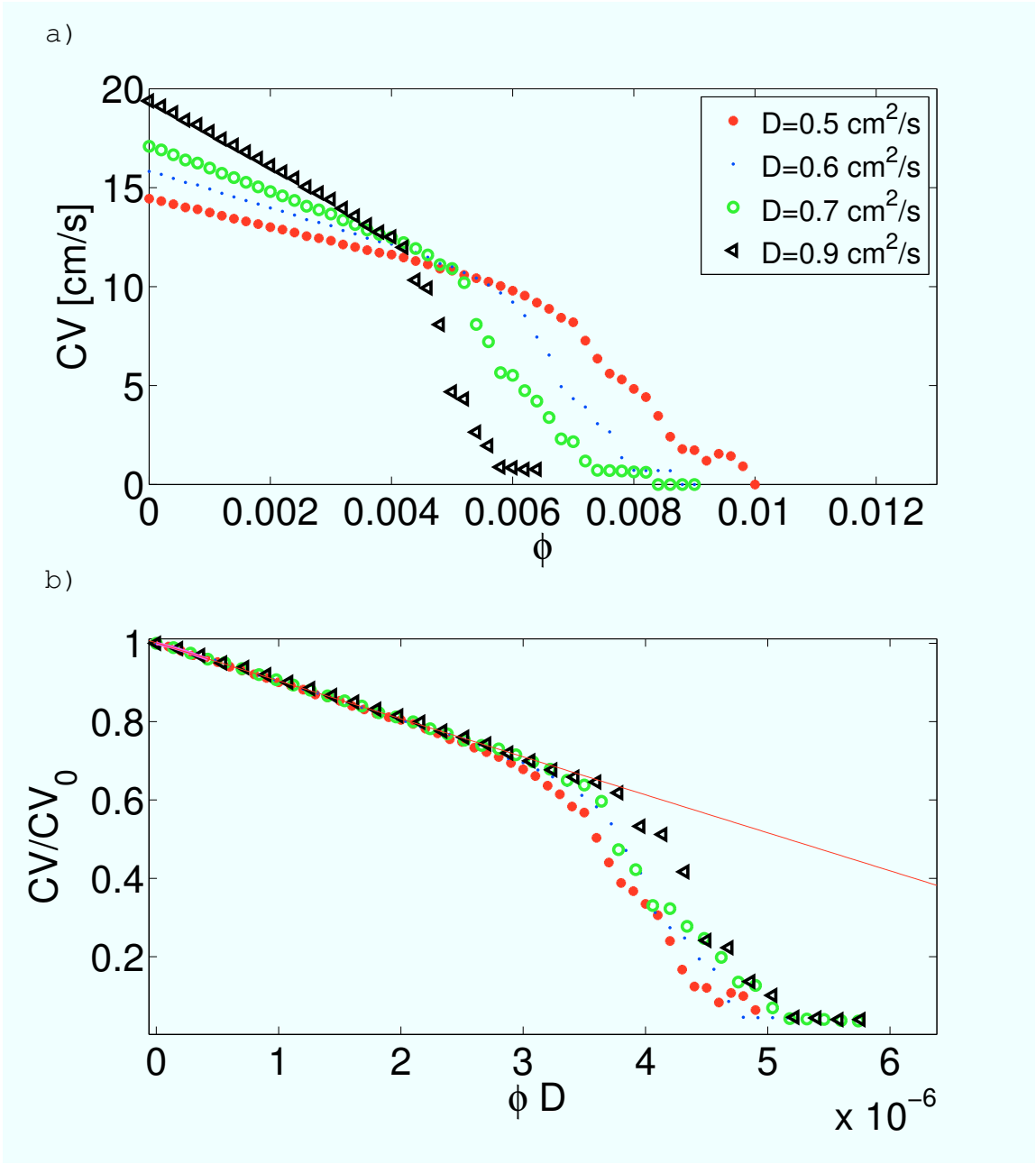

Figure 2–5: Dependence of conduction velocity on sink proportion and coupling strength (a) Conduction velocity decreases with percentage of sinks and the effect is stronger for higher diffusion. (b) Both the velocity and ϕ are rescaled as shown in the respective axes showing that the velocity decreases with D and ϕ as predicted by Equation (2.4). A linear fit between ϕ =0 and 0.006 is shown for D=0.0007 cm^2/ms.

fact that each sink draws activation from the wavefront which delays propagation in proportion to coupling strength.

Steinberg *et al.* predicted the functional dependence of ϕ_c at which propagation fails, and other parameters in the presence of sinks [212]. Figure 2–5(b) confirms their finding that propagation fails for a constant ϕD for the range of D investigated. Despite this, one would expect this observation to breakdown for very low D, because ϕ_c should not exceed 0.41 (at which point the lattice is disconnected). In fact, one would expect $\phi_c \to 0.41$ for very low coupling strength in sinks, inasmuch as decoupled sink cells are essentially breaks.

2.5 Discussion

In this Chapter I have investigated the relationships that relate the decrease of the conduction velocity to the proportion of randomly dispersed heterogeneities in an excitable medium. The results are in general agreement with several earlier numerical simulations that noted a linear decrease in conduction velocity and subsequent wave breaks and conduction failure in both simple and more complex models of excitable media [219, 212, 221, 5, 6].

Steinberg and others have shown that the linearity of the velocity with respect to sink site proportion is the additive influence of each heterogeneity [212]. Conduction velocity in the linear regime is described by Equation (2.1) for breaks and Equation (2.4) for sinks. With breaks the slope of the velocity against ϕ is independent of D as predicted by the homogenization theory of Alonso *et al.* [5, 6].

For sinks, the rate of decline of CV with ϕ depends on $k_S D$. A further examination of this system using a single sink [192] predicts that k_S should be dependent

on the length of the wavefront and the risetime of activation, but these predictions have yet to be fully verified. The slowing effect of sinks is modulated by D, because diffusional coupling influences the amount of activation sinks draw from the wave. In that sense, sinks have a similar role to fibroblasts in cardiac tissue. However, there are certain important differences between sinks and fibroblasts. For simplicity we considered the sinks to be clamped at the resting potential of the normal tissue, but the resting potentials of fibroblasts are more positive than the myocytes around them [259]. This means that while during propagation they act as sinks, they act as sources at all other times. Another limitation is that we assume homogeneous coupling in our simulation domain. In real tissue, myocyte-fibroblast coupling is smaller than myocyte-myocyte coupling [259].

For both sinks and breaks the range of ϕ where conduction velocity decreases sharply correspond to the formation of multiple wavebreaks in the plane wave. Interestingly, these wave breaks lead to sustained reentry for the case of sinks, but not breaks (compare Figures 2–2 and 2–4). This is in accordance to earlier observations of sinks [212], and breaks [218, 220, 221]. The homogeneous medium used is able to support reentrant waves, so the fundamental question is: why do breaks destabilize sustained reentry? The answer is likely related to the fact that for the diffuse spatial distributions of heterogeneities we generate, the waves can break the plane wave only in such high numbers that it is quite unlikely that a continous excitable pathway along which reentry can travel will be formed. More work is needed to put such a statement in a quantitative context, but a way to test the statement could be

to make the wave in the homogeneous medium thinner (by decreasing D or duration of activation), which should break the wave at lower ϕ.

With breaks the propagation fails at the percolation threshold, ϕ_c, in accordance with earlier studies [5, 6]. For sinks I am unable to derive the form of ϕ_c, but find that it is proportional to diffusional coupling in the medium in the range inverstigated. The main limitation of the propagation failure estimations by Equation (2.3) is that they depend on both model and discretization lattice. Real cardiac cells are not squares, and arranged in a more complicated pattern than those generated by discretizing on a square lattice [259, 35]. Possible extensions of this work include investigating the the role of mixtures of sinks and breaks using more sophisticated lattices, and non-uniformly random distributions of heterogeneities. These modifications would more accurately resemble the connective distributions seen in fibrotic cardiac tissue [35].

Furthermore, due to the connections with percolation theory [211], it may be worthwhile to consider fitting the propagation velocity to the more general functional form of Equation (2.2), namely $CV = CV_0(1 - \phi/\phi_c)^\alpha$, where α is a parameter characterizing the nature of the heterogeneities and the medium. While this is of theoretical interest, it may be less relevant to cardiac tissue where $\phi < \phi_c$ even in cases of extreme diffuse fibrosis [221].

In the intact heart, structural abnormalities are often associated with an increased risk of serious and in some cases potentially fatal cardiac rhythms. In recent years, experimental observations have manipulated the degree of heterogeneities and the strength of coupling between cells in cardiac tissue using a variety of techniques

including: the application drugs that impair conduction between cells [29, 30], growing mixtures of cells of different types [259], and inducing the growth of fibrous tissue with different conduction and coupling properties from normal cardiac muscle tissue [35, 216]. Our findings are consistent with the general observation that decreased coupling between excitable cells and increased heterogeneity of cardiac tissue facilitates the initiation of blocked conduction and reentrant waves. The results herein presented highlight properties of media which are predisposed to these types of dynamics, and show the need to further combine theoretical and experimental analysis of heterogeneous excitable systems.

2.6 Conclusions

This Chapter presented the dynamical consequences of two types of randomly distributed heterogeneities in a simplified model of cardiac tissue. At low heterogeneity numbers, both sink and break heterogeneities slowed the wave in linear proportion to ϕ. Randomly distributed breaks need to appear at high proportions to cause breakup of plane waves in the parameter range studied. Wave break up occurs at approximately the percolation threshold of the lattice used to discretize the partial differential equation. Wave breakup does not lead to sustained wave reentry in the case of breaks. In contrast, sinks cause breakup and reentry at lower numbers. The number of sinks causing wave breakup varies in proportion to the diffusion coefficient. Moreover, the linear dependence of propagation velocity proportion on heterogeneities is modulated by an additional factor of D in the case of sinks.

This study provides insights on the role of heterogeneity in wave propagation and acts as a base to study the role of repeated activation, such as in the case

of the dynamics in Figure 2–1. The repeated activations come from foci known as pacemakers, and the next Chapter is the beginning of an examination of the properties of a reset pacemaker embedded in an excitable medium.

CHAPTER 3
Dynamics of Phase Resetting a Pacemaker on an Excitable Cable

3.1 Abstract

A pacemaker in an excitable medium can have its oscillation reset by a wave generated at a distant site which propagates towards the pacemaker. The relation between the wave timing and resultant resetting of the pacemaker is captured by the phase transition curve at any spatial location in the excitable system. In this chapter I discuss conditions for the continuity of phase transition curves of an excitable medium with a pacemaker. I then use shooting and continuation methods to analyze the continuity of these curves in a FitzHugh-Nagumo model of a pacemaker in a one-dimensional excitable medium. Under continuous changes of stimulus parameters resetting curves are continuous unless a stimulus leads to dynamics that fall outside the basin of attraction of the pacemaker-driven excitable medium. An interesting sequence of dynamics is found around the apparent discontinuity in the phase transition curve. This includes unidirectional slow waves which split into bidirectional fast waves at various distances from the pacemaker. The wave patterns found near the apparent phase discontinuity of this system may be relevant to the study of pacemaker-mediated wave dynamics in cardiac tissue.

3.2 Introduction

Pacemakers in excitable media, like the heart, can be reset by waves of excitation generated by a stimulus or an ectopic pacemaker site. Figure 3–1 shows a central

pacemaker in cultures of chick ventricular cells being reset by a wave emitted at a distance. There have been several experiments which explicitly vary the timing of such an event to see how they determine resultant timing of the pacemaker in other types of cardiac tissue [8, 41, 91, 114, 111, 139, 232].

In order to discuss the properties of phase resetting I build on the theoretical framework introduced in Section 1.4.2. Winfree used these ideas to make conjectures about the properties of phase resetting [242, 243] that were subsequently examined from a topological perspective by Guckenheimer [86]. The phase transition curve relates the phase of an oscillation subsequent to a perturbation delivered at a phase, φ. Provided that the state point following the perturbation remains in the basin of attraction of the limit cycle for a stimulus delivered at any phase of the cycle, the phase transition curve is a continuous function that maps the unit circle onto itself. This *Continuity Theorem* is true for limit cycles in ordinary differential equations [86] and partial differential equations [73].

Although examination of the Continuity Theorem has not been a focus of experimental studies, apparent discontinuities in phase resetting curves of oscillating systems have been observed [243, 92]. There are at least two theoretical mechanisms that may lead to apparent discontinuities in phase transition curves [77]:

- phase transition curves can be continuous, but very steep due to large changes in dynamics over a small parameter range
- for some φ, a perturbation may displace the state point outside of the basin of attraction of the limit cycle, so that the Continuity Theorem no longer holds.

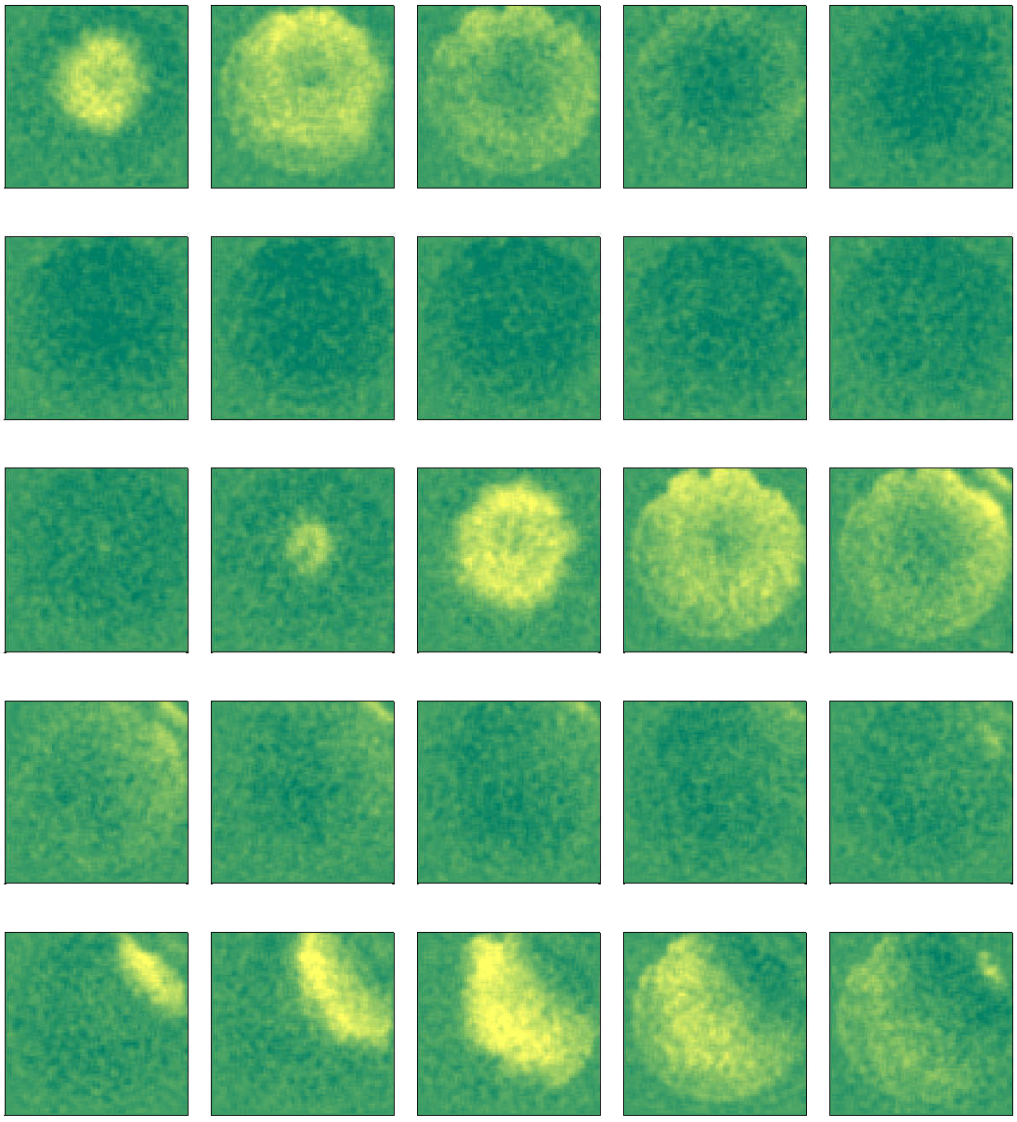

Figure 3–1: An example of a site of pacemaking being perturbed by a wave from a distance. The activation maps, are taken every 150 ms, with the brightness proportional to intercellular calcium concentration. The central pacemaker sends out two waves, but is then reset by a wave from the top right corner of the dish.

Krogh-Madsen and colleagues found an example of an apparent discontinuity, in a numerical study of resetting in an ionic ordinary differential equation model of cardiac cells [137]. By using continuation methods with AUTO [52] for stimulus phase and amplitude parameters close to those for which there is a sharp change in the phase transition curve, they showed that all perturbed trajectories stay in the basin of attraction of the limit cycle implying that the resetting curve was steep, but not discontinuous. In a real biological system, the phase transition curve would be so steep that to resolve the continuity might demand voltage resolutions smaller than the voltage changes induced by the opening or closing of a single channel. This could provide a mechanism for experimental observations of discontinuous phase resetting [92].

Glass and Josephson carried out a numerical study of resetting a circulating pulse in a one-dimensional ring and provided an example in which the system was shifted outside its basin of attraction by appropriately timed stimuli [74]. In this example, carrying out resetting with a single stimulus at low temporal resolution gives rise to discontinuous phase transition curves. However, by probing the phases finely near the discontinuous resetting, in a range of phases called the vulnerable period [208], stimuli were identified which led to a single retrograde wave. When this retrograde wave collided with the anterograde wave, both waves annihilated, thereby shifting the dynamics outside of the basin of attraction of the original anterograde propagation dynamics. However, additional studies of resetting in a related model, in which reentry occurs on a one dimensional ring with a tail showed discontinuous resetting even though there was no evidence for stimuli which would lead to annihilation of the

reentry [202, 76, 136]. Similarly, numerical results on the resetting of a pacemaker embedded in a two dimensional excitable medium appeared to lead to discontinuous resetting curves [94], even though no stimuli led to dynamics lying outside the basin of attraction of the pacemaker. These findings are in apparent contradiction to the theory.

In the following I demonstrate that examination of continuity of resetting curves using shooting methods may be inadequate due to very steep changes in resetting behaviour as a function of stimulus parameters. Complex wave dynamics are found in parameter regions containing the steep change in resetting, including cases of multi-reflected waves similar to one-dimensional spiral waves previously found [134, 59, 47]. The presence of such solutions may depend sensitively on parameters of the underlying equations as well as the discretization of the domain. Although dynamics occurring over such small regions of parameter space would normally not be considered to be important for the understanding of real physical or biological systems, the strong analogy between these dynamics and echo waves observed experimentally in biological preparations of Purkinje fiber from mammalian heart [7] suggest a possible implication of these behaviours in situations of reduced cardiac conductivity such as might occur as a result of heart disease.

3.3 Mathematical Framework

3.3.1 Continuity of Phase Transition Curves in Excitable Media

The following technical material is required for establishing continuity properties of phase resetting a pacemaker in space. The basic formulation is adopted from earlier papers [73, 76, 86, 94, 165].

Assume a dynamical system with a stable limit cycle Γ defined in Section 1.4.2 with period T_0, and define a marker event at phase $\varphi = 0$ and a point Γ as the *reference point*. Say that a marker event occurs at time $t = t_0$. Then, in the absence of perturbations, the phase of the oscillation as $\varphi = (t - t_0)/T_0 \pmod 1$. The phase $\varphi(t)$ is the phase at the reference point, and every state in Γ is identified by a phase.

The basin of attraction of Γ, $B(\Gamma)$, is foliated by hyper-surfaces called *isochrons*. In the asymptotic limit $t \to \infty$, all states on an isochron asymptotically approach the same state on Γ. Consequently, each isochron is identified by a phase defining the unique state in Γ lying on the isochron. To help fix ideas, consider a two-dimensional ordinary differential equation with a single unstable steady state and stable limit cycle that is globally attracting for all points except the steady state. The isochrons are curve segments that cut transversely across the limit cycle. All isochrons approach the neighbourhood of the steady state as shown in Figure 3–2. A point $P \in B(\Gamma)$, $P \notin \Gamma$ has the *resultant phase*, $g(\varphi(P))$ defined as the phase of the isochron containing P. If $P \in \Gamma$ then $g(\varphi(P)) = \varphi(P)$. For partial differential equations, all definitions extend naturally except that a point P on an isochron represents a function defining the values of all variables in space.

Now consider a state $X_0 \in B(\Gamma)$ and a continuous perturbation, $\Psi(\mu)$, depending on a variable μ. In traditional studies of phase resetting, $X_0 + \Psi(\mu)$ represents the locus of states in phase space generated by delivering a perturbation for all points on (at all phases of) the cycle. However, $X_0 + \Psi(\mu)$ could equally be generated by other perturbations including changing the amplitude and the location of the stimulus.

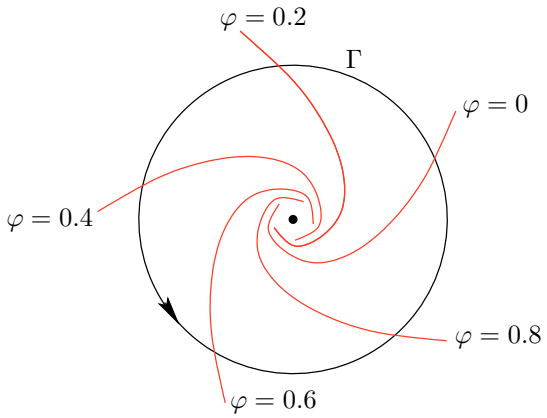

Figure 3–2: A schematic of states associated with the phases of a limit cycle in two dimensions. The isochrons are the red line segments that transversally intersect the attracting limit cycle, Γ, for different phases, φ. The velocity of the trajectory along the limit cycle is assumed to be uniform, so the phases are uniformly distributed.

As long as the stimulation parameters are changed continuously, the following lemma holds:

Lemma 1 (Continuity Lemma)**.** *If* $X_0 + \Psi(\mu) \in B(\Gamma)\ \forall \mu$*, then* $\varphi_l(X_0 + \Psi(\mu))$ *is continuous.*

In the particular case where $X_0 + \Psi(\mu)$ is generated by delivering a stimulus at all phases to a limit cycle , we have the *Continuity Theorem* and the phase transition curve, $g(X_0 + \Psi(\mu))$, is a continuous map of the circle into itself [86, 73]. In this case, the states defined by $X_0 + \Psi(\mu)$ for all μ define the image of the original limit cycle Γ following a perturbation delivered at all phases of the cycle. This is often called the *shifted cycle*.

In the current context, if a limit cycle oscillation is perturbed by delivering stimuli of varying amplitudes (rather than of varying phases) then the Continuity Lemma is required to assert continuity of the phase transition curve delivered as a

function of amplitude, and provided the stimulus does not lead to a transition outside of the basin of attraction of the limit cycle.

3.4 Methods

3.4.1 Model of Pacemaker on an Excitable Cable

The FitzHugh-Nagumo equations are adapted (as in Hall and Glass [94]) to represent a line of excitable medium with an embedded pacemaker. These take the form,

$$\begin{aligned} \frac{\partial v}{\partial t} &= \frac{1}{\varepsilon}(v - v^3 - w) + I_s + I_P + D\frac{\partial^2 v}{\partial x^2}, \\ \frac{\partial w}{\partial t} &= \varepsilon(v + \beta - \gamma w)\left(\frac{w_h - w_L}{1 + e^{-4v}} + w_L\right) \end{aligned} \tag{3.1}$$

where $\beta = 0.7$ s^{-1}, $\gamma = 0.5$ s^{-1}, $\varepsilon = 0.3$, $D = 1$ cm^2/s, I_s is a stimulation current, and I_P is a bias current (introduced in Section 1.1.2) used to establish a limit cycle pacemaker. The constants $w_L = 0.4$ and $w_h = 0.6$ control the duration of the recovery and active phases in the oscillation. The pacemaker region is induced by changing I_p and w_L in a range of space so that,

$$\begin{cases} \text{pacemaker region} : x \in [0.72, 0.76] & : I_p = 1, w_L = 0.13 \\ \text{excitable region} : x[0, 0.72) \cup (0.76, 0.84] & : I_p = 0, w_L = 0.4. \end{cases}$$

This configuration makes the region $0.72 \leq x \leq 0.76$ periodically send out waves through the rest of the excitable medium with a period $T_0 \approx 0.5735376$ s.

To perturb the pacemaker with a wave from a distance, a stimulus, I_s, is applied. The stimulus is of the form

$$I_s = A(\tanh(10(t - t_s)) - \tanh(10(t - t_e)))/2,$$

is applied at $x \leq 0.02$ cm for a duration $t_e - t_s = 1$ time unit $= 10$ ms. The start time t_s is varied to control the phase of stimulation $\varphi = t_s/T_0$, and the stimulus amplitude A is initially fixed at the nominal value $A = 1.0$.

The resulting phase $g(\varphi)$ is measured at the pacemaker at $x = 0.74$ cm as the time at which the first regular maximum of v occurs, divided by T_0, and then shifted so that $\varphi_l = 0$ for $\varphi = 0$.

The boundary conditions consist of Neumann conditions at $x = 0$ and $x = L = 0.84$ cm. The system is space discretized with $\Delta x = 0.02$ cm on a 43 cell lattice using a fourth-order compact Collatz "Mehrstellen" scheme [43] to estimate the Laplacian of Equation (3.1). This scheme is more accurate than the one presented in Equation (1.3) by estimating the Laplacian $\nu_i = (\frac{\partial^2 v}{\partial x^2})_i$ at cell i as:

$$\begin{aligned}
(2\nu_2 + 10\nu_1)/12 &= 2(v_2 - v_1)/\Delta x^2 \quad \text{for } i = 1, \\
(\nu_{i+1} + 10\nu_i + \nu_{i-1})/12 &= (v_{i+1} - 2v_i + v_{i-1})/\Delta x^2 \quad \text{for } 2 \leq i \leq 42, \\
(10\nu_{43} + 2\nu_{42})/12 &= -2(v_{43} - v_{42})/\Delta x^2 \quad \text{for } i = 43.
\end{aligned} \tag{3.2}$$

This system is solved numerically using the 4th-order Dormand-Prince method [53] to minimize numerical artifact associated with discretization. The method uses explicit Runge-Kutta fourth and fifth-order estimates to adjust the time step size Δt, but in this case the step size was kept fixed at Δt=5 μs.

In the resetting experiments a state (v, w) that lies very close to the limit cycle oscillation is used as an initial condition for each phase resetting run.

3.4.2 Shooting and Continuation Methods

Shooting and continuation are iterative numerical methods used to track solutions (orbits) of differential equations over some parameter range. We adapt these methods to generate the phase transition curve of the Equations 3.1 and dissect the stimulation phases at which $g(\varphi)$ changes rapidly. The shooting algorithm involves:

1. choosing a parameter range over which the behaviour of solutions changes,
2. integrating the equations for some guesses (shots) in that parameter range,
3. finding two contiguous parameter shots over which the solutions change, and use those as endpoints of a new parameter interval,
4. repeating step (1) for this new parameter interval.

In the implementation of shooting used here, the parameter investigated is stimulus phase, ϕ and stimulus amplitude, A. At the first iteration we compute $g(\varphi)$ for 100 equally spaced phases on the interval $\varphi \in [0, 0.99]$. At each subsequent iteration step we take ten equally spaced shots over a decimal place range, and look for solutions which change from a non-propagating (non-resetting) response to a propagating (resetting) response.

Continuation methods provide an alternative to shooting to investigate resetting curves [45, 137, 168], as they are suited for investigating resetting in continuous ordinary or partial differential equations in settings where there are strong divergences between trajectories arising from neighboring initial conditions.

To be more specific, given the trajectory $\mathbf{u}$ at parameter values $\mathbf{p}$, and a continuation direction $(\mathbf{u}', \mathbf{p}')$, the next orbit, for step size Δs in the continuation is predicted to be at $(\mathbf{u}, \mathbf{p})_{\text{new}} = (\mathbf{u}, \mathbf{p}) + \Delta s(\mathbf{u}', \mathbf{p}')$, and then corrected using Newton iterations in a process called pseudo-arclength continuation [52]. A new value for the continuation direction is then computed by subtracting the corrected new and old orbits.

In the mathematical model under consideration continuation is implemented using fixed integration time in AUTO [52], defining a boundary value problem with the integration time fixed at $T = 2.5$ s. This amounts to solving the 87-dimensional ordinary differential equation discretized using Equation 3.2 with $\dot{t} = 1$, subject to 87 no-flux boundary conditions, plus $t(0) = 0$.

3.5 Results

3.5.1 Phase Resetting from a Distance

The phase transition curve of the FitzHugh-Nagumo system stimulated from a distance of 0.74 cm is shown in Figure 3–3(a). The gross features of this curve are three intervals of phase with distinct resetting features:

1. $0 \leq \varphi \leq \varphi^* \approx 0.50$. The stimulus generates a large amplitude fast pulse, F, which collides with a wave generated by the pacemaker (Figure 3–5(a)) or falls in the refractory period of the tissue and fails to elicit a wave that propagates to the pacemaker (Figure 3–5(b)). In either case the stimulus has no effect on the pacemaker, so $g(\varphi) = \varphi$.
2. $\varphi^* < \varphi < 0.82$: The stimulus generates a fast pulse, F, that propagates to the pacemaker and resets it (Figure 3–5(e-f)). The first instance of resetting

around φ causes an apparent jump discontinuity in the phase transition curve. In this range $g(\varphi) \approx 0.82$.

3. $0.82 < \varphi < 1.0$; see Figure 3–5(g). For all stimulus phases in this range the induced fast pulse collides with a wave emitted by the pacemaker, so that there is no resetting. In this range $g(\varphi) = \varphi$.

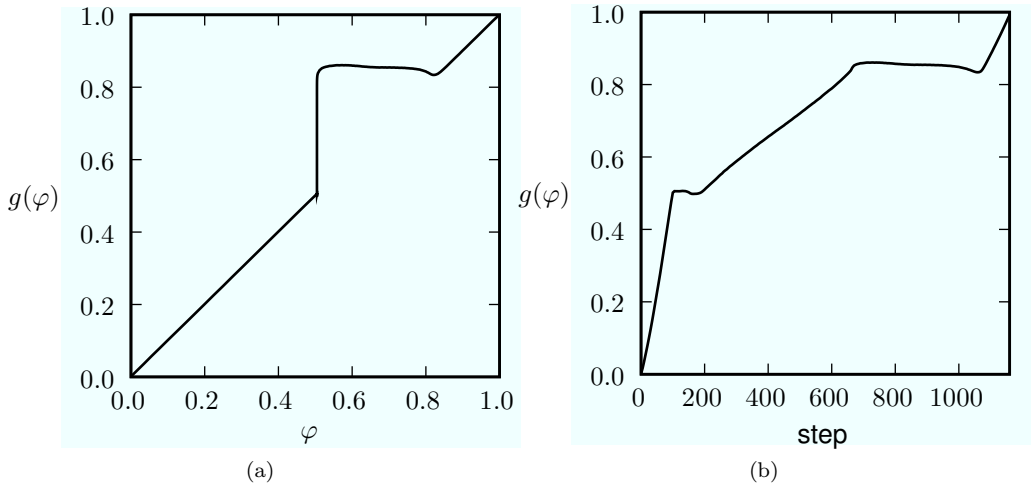

Figure 3–3: Phase resetting of the FitzHugh-Nagumo system using continuation in stimulus phase. (a) The phase transition curve found using a stimulus at a distance of 0.74 cm. (b) The new phase, $g(\varphi)$, shown for each continuation step.

These ranges can be compared to predictions of a general model of an excitable medium with refractory period, R, wave conduction velocity, CV, pacemaker period, T_0, and the stimulus is at a distance, d, from the pacemaker. In this model a stimulus at a distance $d > CV(T_0 - R)/2$ will fail to reset the pacemaker at any phase. The general model also predicts that the first phase to lead to propagation and cause resetting is $\varphi^* = (R + \frac{d}{CV})/T_0$, and the resultant phase during resetting is $g(\varphi) = (T_0 - \frac{d}{CV})/T_0$. In the FitzHugh-Nagumo model considered the relevant

parameters are $R = 0.186$ s, $d = 0.74$ cm, $CV = 6.7$ cm/s, and $T_0 = 0.574$ s, giving predictions of $\varphi^* \approx 0.51$ and $g(\varphi) \approx 0.81$. The small discrepancies between these values and those found in the resetting experiment arise from nonlinear effects such as variable wave propagation velocity through a medium recovering from an excitation.

3.5.2 Resolving the Apparent Discontinuity in the Phase Transition Curve

The apparent jump in $g(\varphi)$ just beyond φ^* is unable to be resolved using the shooting method. Figure 3–4 demonstrates that the transition to propagation is still a jump somewhere in the interval $\varphi = [0.506378, 0.506379]$. The shooting in phase cannot give a more precise phase, as the numerical solution of T_0 fluctuatates in the sixth significant figure. The issue is resolved, by invoking the Continuity Lemma, and measuring the effect of stimulus amplitude at $\varphi = 0.506378$. As A is increased from the nominal value, $A = 1.0$, the shooting method identifies the transition to propagation at between $A = 1.000025$ s^{-1} and $A = 1.000026$ s^{-1}. In this region the stimulus generates a slow wave, S, which splits into two counter-propagating fast waves, f and F (Figure 3–4(e)). This type of solution, labeled SfF, is similar to reflected pulse solutions seen by others using different excitable models [11, 36, 47, 59]. The F wave at $A = 1.000026$ s^{-1} resets the pacemaker and causes a jump in the phase transition curve from $g(\varphi) = 0.506$ to $g(\varphi) = 0.861$. Unless higher precision numerical integration is performed, the shooting approach is not able to resolve the continuity of $g(\varphi)$ in the system defined by Equations (3.1).

Fortunately, using the continuation method does resolve the jump around $g(\varphi^*)$. The phase φ^* is encountered around step 130 of the continuation, at which point the

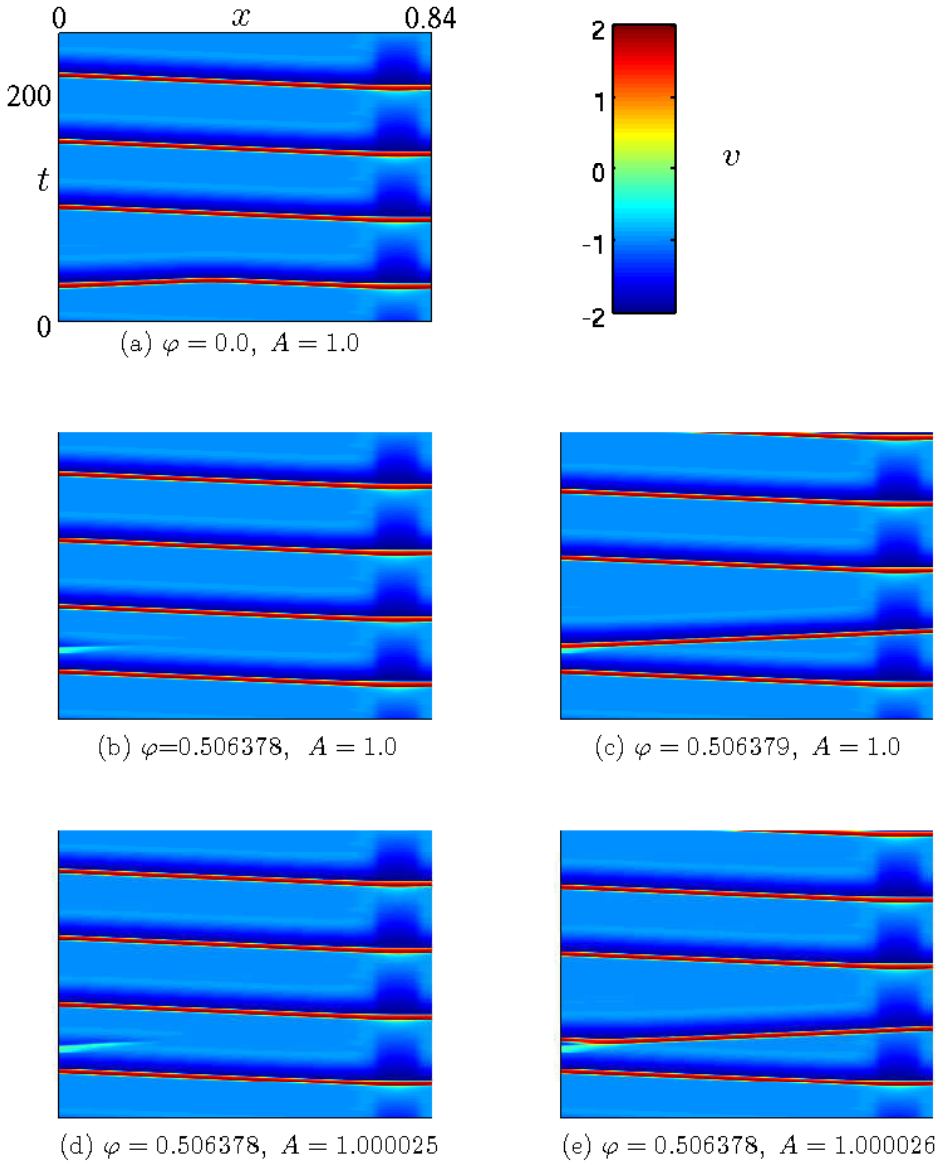

(a) $\varphi = 0.0,\ A = 1.0$

(b) φ=0.506378, $A = 1.0$

(c) $\varphi = 0.506379,\ A = 1.0$

(d) $\varphi = 0.506378,\ A = 1.000025$

(e) $\varphi = 0.506378,\ A = 1.000026$

Figure 3–4: Space-time plots of v in the for different stimulation phases and amplitudes using shooting. Stimulus at phase (a) $\varphi = 0.506378$ does not propagate, while (b) $\varphi = 0.506379$ does. Raising stimulus amplitude to (c) $A = 1.000025\ \mathrm{s}^{-1}$ still does not lead to resetting, but (d) $A = 1.000026\ \mathrm{s}^{-1}$ does, and corresponds to a reflected wave solution, SfF.

slow low-amplitude wave S is generated at the stimulus site and propagates farther to the right with each continuation step until it almost reaches the pacemaker site in Figure 3–5(b). Just beyond this point the pacemaker begins to experience a small delay in its firing due to the influence of the slow wave S, which corresponds to the small decrease in the phase transition curve between steps 130 and 165; see Figure 3–5(c). When the slow pulse S propagates sufficiently close to the pacemaker the SfF solution appears, with the split from S to fF occurring at the pacemaker site. At around step 170 the SfF split site begins to move left towards the stimulus site, as shown in Figure 3–5(d), incrementally advancing the resultant phase of the pacemaker. When the SfF split site reaches the stimulus site, around step 730, the S and f pulses disappear and what is left is the fast pulse F resetting the pacemaker as shown in Figure 3–5(e).

To complement these observations, the phase resetting caused by varying the stimulus amplitude A is examined using continuation at $\varphi \approx 0.509$. Figure 3–6(a) shows a sharp transition to resetting following a stimulus of amplitude $A \approx 0.502$.At the transition to propagation the jump in $g(\varphi)$ from 0.509 to 0.845 is similar to what is seen around φ^* in the phase resetting experiment. The transition from no propagation, to S, to SfF, to F is also observed in this amplitude continuation. The main difference between using the phase and amplitude for resetting is that the slow wave generated at the stimulus site is not able to reach the pacemaker site and cause the small phase advances seen during steps 130–165 of the stimulus phase continuation. This is due to the fact that the slow wave begins to propagate from the stimulus site slightly later relative to the time in the phase resetting experiment,

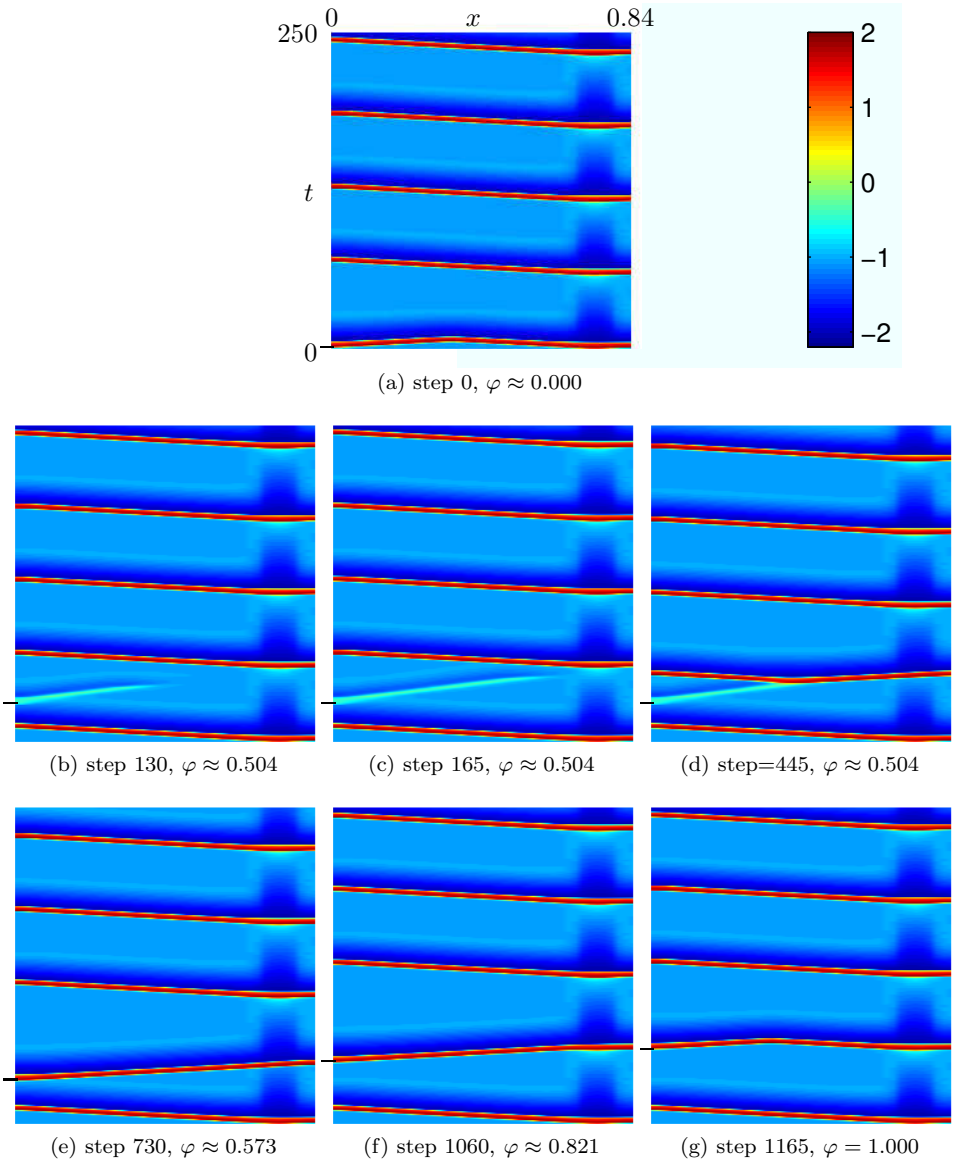

(a) step 0, $\varphi \approx 0.000$

(b) step 130, $\varphi \approx 0.504$ (c) step 165, $\varphi \approx 0.504$ (d) step=445, $\varphi \approx 0.504$

(e) step 730, $\varphi \approx 0.573$ (f) step 1060, $\varphi \approx 0.821$ (g) step 1165, $\varphi = 1.000$

Figure 3–5: Space-time plots of the activation solutions found during stimulus phase continuation. The "step" denotes the continuation step number). Panels (b), (c), (e), and (f) correspond to extrema in Figure 3–3(b). Intermediate panel (d) shows the pattern SfF most clearly.

which happens because the stimulus is applied for a non-zero duration. Nevertheless, the continuity of the phase transition curve is preserved under amplitude continuation at $\varphi \approx 0.509$, in concordance with the Continuity Lemma.

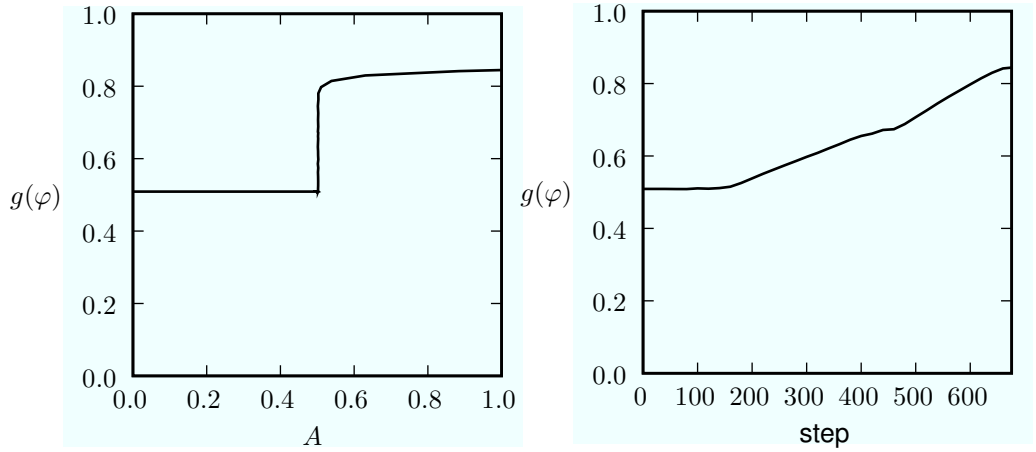

Figure 3–6: Phase resetting caused by varying the stimulus amplitude A using the continuation method. Note how $g(\varphi)$ changes from 0.509 to 0.845, corresponding to a the point $(\varphi, g(\varphi)) \approx (0.509, 0.845)$ in Figure 3–3(b) The new phase $g(\varphi)$ is tracked with the continuation step for the amplitude resetting experiment.

3.5.3 Effects of a Coarser Spatial Discretization

A different resetting scenario occurs when varying the amplitude for a coarser discretization of space ($\Delta x = 0.04$ cm). Analysis of the propagation parameters at different mesh discretizations showed appreciable change of action potential duration, maximal rate of activation, and propagation velocity between the discretizations $\Delta x = 0.02$ cm and 0.04 cm (see Figure 1–3). In contrast, comparing $\Delta x = 0.02$ cm with the even finer discretization $\Delta x = 0.01$ cm showed much smaller variations ($<$ 2% for propagation velocity, activation duration, and risetime of activation). These observations corroborate the possibility that the coarser discretization $\Delta x = 0.04$ cm

may have different wave patterns from the continuous partial differential equation defined by Equation (3.1).

The gross features of the phase transition curve for the coarse case are very similar to those of the finely discretized case shown in Figure 3–6(a). However, looking closely around the apparent jump discontinuity at $A \approx 0.502$ s^{-1} using continuation we find differences in the fine structure of the phase transition curve at $\Delta x = 0.04$ cm.

Continuation begins to track solutions which are not present in the $\Delta x = 0.02$ cm case, including trajectories consisting of a slow wave S which in general:

- reflect from the no-flux boundary as the slow wave s, or
- split into a anterograde fast wave F and a retrograde slow wave s, or
- the slow wave s can reflect or split another S multiple times

These cases are demostrated in the complex solution Figure 3–7. The sequence of slow pulse reflections $(SsF, sfS, SsF, \ldots)$, begins to look like a solution where the pacemaker never reestablishes entrainment of the medium, and so the system is taken out of $B(\Gamma)$.

In Figure 3–7(a) the initial range of times show the slow wave S hitting the fast wave around $t = 0.9$ s at cell 15 ($x = 0.56$ cm), much like in Figure 3–5(b). However, the wave now splits into an anterograde fast pulse F and retrograde slow wave s at a point distant from the pacemaker site. The continuation shows a complex recursive interaction of fast wave stubs with slow waves, where fast waves grow or shrink one cell at a time. Eventually the fast wave around $t = 0.9$ s grows to cell 14 ($x = 0.52$ cm), then to cell 13 ($x = 0.48$ cm), and so on, up to cell 5 ($x = 0.16$ cm).

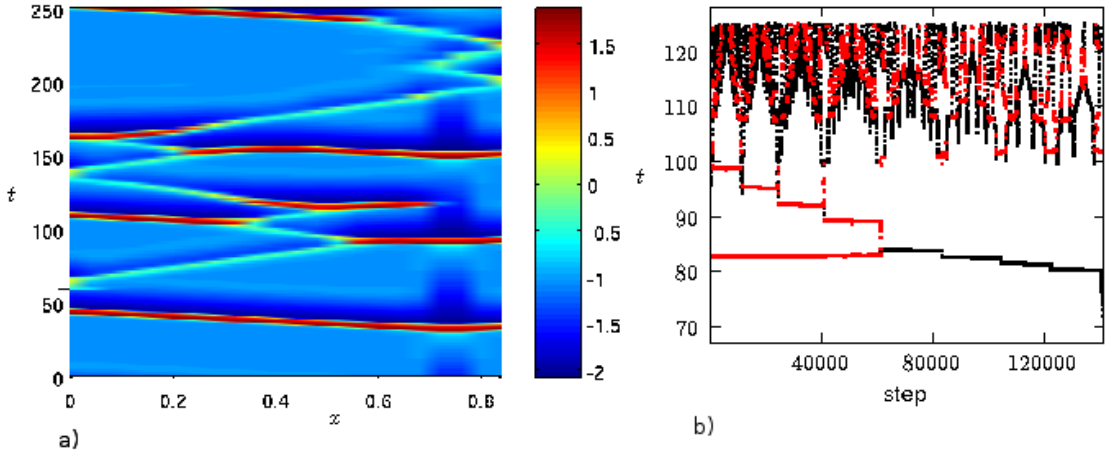

Figure 3–7: Complex reentrant waves for the discretization $\Delta x = 0.04$ cm.(a) The space-time plot for a solution of v encounetered during the continuation in phase. This situation corresponds to the first time that the waves caused by the stimulus reach $t = 250$ time units (2.5 s) in the continuation method using phase. The phase is at $\varphi \approx 0.509$; the amplitude is at the critical value $A \approx 0.502$ s^{-1}. (b) Tracking time values of the maxima of v at cell 11 ($x = 0.4$ cm) versus continuation step on. Black points denote maxima of fast waves and red points maxima of slow waves.

Beyond cell 5 the procedure arrives at a situation similar to Figure 3–5(d) and then continues to Figure 3–5(e) in a straightforward fashion. The time values of the maxima at cell 11 ($x = 0.4$ cm) for a continuation up to $t = 1.25$ s are tracked in Figure 3–7(b). Before continuation step 60000, there exist two slow waves, one starting around $t = 0.1$ s and one starting around $t = 0.083$ s. The wave for $t = 0.1$ s moves a little each time as the fast wave grows one cell. Around continuation step 60000, that is, at the fourth bump, the fast wave has grown to cell 11 and the two reflected slow waves are merged into the fast wave.

The main problem with dissecting the full sequence of phase transitions in the $\Delta x = 0.04$ cm case is the extremely long computation time required to make it through the continuation, as evidenced by the number of steps in Figure 3–7(b). Continuing up to $t = 1.25$ s took around a week of computation; higher values quickly become prohibitively expensive because of the recursive nature of the structure. Nevertheless, the fact that the multi-reflected unstable slow wave disappears at finer Δx implies that the solution is inherent to the discretized system of coupled ordinary differential equations rather than the continuous partial differential equations.

3.6 Discussion

This chapter analyzes the resetting of oscillators that are localized to some region of excitable space. For neural and cardiac systems, stimuli will typically have to travel through excitable tissue before resetting is elicited. Consider for example, an intact heart in which an excitation from the normal (sinus) pacemaker resets a pacemaker at an abnormal (ectopic) location, or in which an inserted artificial pacemaker interacts with sinus or ectopic rhythms. Resetting from a distance is also observed during

competition between pacemakers in cardiac tissue culture demonstrated in Figure 3–1.

Previous work has indicated that the threshold for excitation and propagation can have a very sensitive dependence on stimuli parameters for stimuli delivered during the transition of tissue from a refractory to an excitable state (often called the vulnerable period) [47, 74, 94, 136, 137, 208]. This sensitivite dependence can manifest itself as an apparent jump discontinuity in the phase transition curve. In the present work continuation methods [52] are developed for the case of the FitzHugh-Nagumo cable in order to tease out the fine structure of the resetting around the jump in the phase transition curve. For the cases analyzed, the continuity properties of the phase transition curve are consistent with mathematical results which indicate that unless stimuli lead to a transition outside the basin of attraction of an oscillator, the transition curves will be continuous.

For situations in which a stimulus leads to transitions outside the basin of attraction of an oscillator, the continuation methods fail to resolve the continuity of $g(\varphi)$. This is true for the $\Delta x = 0.04$ cm case presented here, and also by using the phase and amplitude continuation method to track a one-dimensional spiral solution in the Morris-Lecar equations of propagation [20]. The fact that continuation is unable to connect the curve can therefore provide an operational method to detect the existence of transitions outside the basin of attraction of the oscillation. This is true regardless of whether the discontinuous transitions originate from the pacemaker itself, or from a spatially periodic solution in the excitable medium away from the pacemaker site.

Although the focus of this study was restricted to systems in one spatial dimension, the continuation and shooting methods used here are easily adaptable to analysis of resetting in excitable media of higher dimensions. A limit cycle oscillation associated with a pacemaker in higher spatial dimensions can be perturbed to obtain solutions outside of the basin of attraction, such as spiral waves in two spatial dimensions (Figure 3–1) and scroll waves in three dimensions [243]. Modulating these new wave behaviours are new system properties associated with the higher spatial dimensions. In two dimensions, this includes the properties of heterogeneities studied in Chapter Two, and this is considered further in Chapter Four.

This chapter primarily deals with theoretical questions and methodologies that do not appear related to practical situations, since they occur over such small ranges of the stimulus parameter space. However, experimental studies of propagation of cardiac excitation in one dimensional cardiac Purkinje fibers show some strikingly similar behaviours in which echo waves are generated *in vitro* [7, 177]. These findings imply that these types of wave dynamics may represent generic (rather than unusual) dynamics as parameters are systematically varied. For the FitzhHugh-Nagumo model considered, but the extent of phase space in which these echo waves occur appears to be very small, there may well be circumstances in which the ranges are larger than those found here. Furthermore, since there are important transitions of heart dynamics that can only happen once (like those leading to sudden cardiac death [258]), studying the appearance of complex reentrant wave patterns over limited regions of parameter space in a mathematical model may still be a practically important direction for analysis.

3.7 Conclusions

In this chapter a mathematical framework is presented to express the Continuity Lemma, which implies that stimulus parameters should reset the pacemaker continuously unless there are trajectories visited which fall outside the basin of attraction of the pacemaker wave train. The FitzHugh-Nagumo cable model is numerically investigated using shooting and continuation in both stimulus phase and amplitude. The continuation method demonstrates that the jump in the phase resetting curve is caused by a slow wave being formed at the stimulus site, which splits into an echo starting near the pacemaker and that moves back towards the stimulus location. For coarser spatial discretization, new multi-reflected solutions are found, and become too computationally difficult to track to resolve the continuity of the resetting curve.

The results characterize how stimulus parameters can affect the wave dynamics in a discretized one-dimensional FitzHugh-Nagumo cable model. The motivating cardiac monolayer dynamics shown in Figure 3–1 demonstrate the need to extend the pacemaker model to two dimensions. This is the direction of the next chapter, which investigates the interaction between two pacemakers in a two-dimensional heterogeneous excitable medium.

CHAPTER 4
Dynamics of Two Pacemakers in Heterogeneous Excitable Tissue

4.1 Abstract

Wave breakup and reentry around a pacemaker have been observed in certain types of cardiac arrhythmias. In this chapter I use experimental and mathematical cardiac tissue models of pacemakers in heterogeneous excitable media to investigate system properties that determine wave break and reentrant wave dynamics. Chick ventricular cells are cultured *in vitro* to exhibit a dominant central pacemaker site that entrains other pacemakers in the medium. Application of a rapid delayed rectifier potassium channel blocker, E-4031, leads to an increase in the beat rates of pacemakers. This induces competition between pacemakers in the medium, and leads to situations in which waves emitted by faster pacemakers break up over the slower pacemaker and form reentrant waves. This scenario is simulated with a two dimensional FitzHugh-Nagumo model of a heterogeneous excitable medium with two distinct sites of pacemaking. When the intrinsic beat rates of pacemakers are similar, the faster pacemaker entrains the slower one, along with the rest of the excitable medium. To induce wave breakup the side pacemaker must emit waves at a rate faster than the one-to-one entrainment limit of the central pacemaker. The entrainment limit is predicted by the phase transition curve of the pacemaker, and is dependent on the diameter of the pacemaker as well as the proportion of randomly distributed inexcitable break sites in the excitable medium. Reentrant waves are formed on the side

of the central pacemaker that is farthest from the side pacemaker, and can in some instances be sustained by being shielded by the central pacemaker from resetting by the faster side pacemaker. These findings elucidate some features of a mechanism of pacemaker-induced reentry in excitable media that should be applicable to more realistic cardiac tissue models.

4.2 Introduction

The sinus node is the dominant pacemaker in the heart [156]. It rhythmically initiates wave trains of depolarization that propagate through the excitable cardiac tissue and entrain secondary pacemakers [21, 181]. There are instances where these secondary sites of pacemaking break out of entrainment by the sinus node and initiate ectopic beats [257]. The interaction of the sinus wave with waves emitted from other pacemakers has been experimentally shown to lead to wave reentry around either the dominant or ectopic site [167, 215]. Reentrant waves associated with the sinus pacemaker have been seen in both experimental [3] and clinical settings [80, 160, 201], where it is known as sinus node reentrant tachycardia.

In conjunction with these studies there have been theoretical investigations of the sequences of activation times possible during competition between a dominant and an ectopic pacemaker. The dynamics of successive activations can be studied by iterating difference equations (like Equation (1.10)), which can describe the phase resetting effect of the dominant pacemaker [76]. These resetting maps have been iterated to produce a variety of rhythms that are similar to those seen clinically [44, 155]. Despite this, the mathematical models considered to date do not present

the phase resetting map results in the context of the underlying spatiotemporal wave propagation dynamics.

In this chapter, I investigate the wave dynamics during competition between pacemakers in excitable medium using the FitzHugh-Nagumo model. While I am not aware of other propagation modeling studies concerning the interaction between two pacemakers leading to reentrant wave formation around a site of pacemaking, a closely related phenomenon is wave reentry due to paced wave train breakup over a region of tissue with heterogeneous excitability properties. There are several computational studies where the heterogeneity is an ischemic zone with compromised excitability. Bernus *et al.* show that in the Luo-Rudy model, a 2:1 conduction block through the ischemic border zone can give rise to reentry at high pacing frequencies [17]. Using a similar Luo-Rudy model Xu and Guevara report that depending on the potassium concentration in the ischemic zone, reentrant waves can form either inside the ischemic zone or outside of it [254]. Using a three-dimensional and anatomically-realistic mathematical model, Heidenreich and others found instances of both regular and figure eight reentrant waves initiated by an ectopic activation breaking over the ischemic zone [96]. These simulation studies show that rapid pacing and excitability properties of the ischemic zone are able to initiate several types of reentrant wave patterns.

n of of spiral waves [221], while Shajahan *et al.* demonstrated that spiral wave dynamics depend sensitively on the size and position of the obstacle [194].

To study pacemaker induced reentry experimentally, I construct excitable cardiac tissue containing sites of pacemaking. Chick ventricular aggregates are known

to act as pacemakers that, when coupled to monolayer tissue, can entrain each other through the connecting monolayer [85]. In the present context, a disk of concentrated cells is placed in the center of the tissue such that it paces and entrains the surrounding pacemakers and tissue. This situation of a single dominant pacemaker simplifies and standardizes the spontaneous wave dynamics seen in the cardiac tissue preparations. On the dominant pacemaker preparations I apply a rapid delayed rectifier potassium channel blocker, E-4031, to increase the rate of side pacemakers such that they eventually outpace the central pacemaker. This drug is known to increase the beat rate of chick ventricular aggregates [126], but decrease it in rabbit [129, 236] and mouse [40] sinus node. The agent has been shown to prolong action potential duration [39, 236], but has a negligible effect on wave conduction velocity during pacing [123, 129, 197]. Although the effect of E-4031 on wave break and reentry has not previously been published for chick ventricular tissue, in other experimental preparations the drug has been been shown to decrease [103, 123, 197], not change [129] or increase [10], the incidence of reentrant waves. In humans, mutations in the gene coding for the delayed rectifier potassium channel (HERG) cause polymorphic ventricular tachycardias associated with wave break and reentry [46, 187].

I focus my attention on cases where a side pacemaker resets the central pacemaker leading to the formation of reentrant waves. A simple mathematical model of wave propagation is used to demonstrate that a side pacemaker with a period shorter than the one-to-one entrainment limit of the central pacemaker leads to wave break and formation of reentrant waves. This one-to-one entrainment limit is predicted by the phase transition curve of the ordinary differential equation describing the

pacemaker. Discrepancies in the prediction are due to the spatial nature of the pacemaker, including the pacemaker diameter and the density of break heterogeneities in surrounding excitable medium. Near the entrainment limit there is a situation where a spiral wave is sustained despite rotating at a period longer than the driving period of the side pacemaker. These studies suggest a potential role of pacemakers in the formation and maintenace of reentrant wave patterns in cardiac tissue.

4.3 Methods

4.3.1 Culturing Cardiac Cells

Cardiac cells were collected from 7 to 8-day-old embryonic chick ventricles, and were dissociated with trypsin using methods similar to those described by Bub *et al* [28, 26]. The culturing procedure involves dissecting the heart from chick embryos and isolating the lower ventricles. The ventricles were minced and treated with four dissociation medium washes over a period of 30 minutes. The dissociation medium, called DM1+2, contains 24.7 U/mL of trypsin (Worthingtion) and 3.63×10^4 U/mL of DNAase 1 (Sigma) in solution with 120 mM NaCl, 5.1 mM KCl, 0.44 mM NaH_2P0_4, 0.95 mM $NaHP0_4$, and 5.6 mM dextrose. All culturing and imaging solutions were sterilized through a 0.22 μm pore filter (Millipore) and titrated to pH 7.3 using HCl or NaOH.

The dissociated cells were transferred into an inactivating medium, called Ti, which stops the trypsin digestion. Ti medium is composed of 20% medium 199 (GIBCO) and 10% horse serum (GIBCO), as well as, 120 mM NaCl, 1.3 mM KCl, 1.8 mM $CaCl_22H_2O$, 0.80 mM $MgS0_47H_2O$, 0.90 mM NaH_2P0_4, 20 mM $NaHC0_3$,

and 5.5 mM dextrose. The dissociated cells were isolated using a polycarbonate membrane filter (Canadian Life Science) with 12 μm diameter pore size.

The isolated cells then were centrifuged at approximately 170 g for 30 minutes. The centrifuge pellet was transferred into 1 mL maintenance medium called 818a. The 818a medium is like the Ti medium except it contains: 5% horse serum, 10% fetal bovine serum (GIBCO), 5.14 mM KCl, and 5×10^{-5} g/mL of the antibiotic gentamicin sulfate (GIBCO).

Cell plating density was set by counting a sample of intact cells inside a haematocytometer well, and diluting the stock with 818a solution to normalize the cell seeding density. For monolayer studies the target confluent cell seeding density was 10^4 cells/cm^2. The cells are plated on the central disk region of 32 mm diameter CellBind$^{\text{TM}}$-coated dishes (GIBCO).

Engineering of a dominant pacemaker was achieved by plating the cells in a stacked disk configuration shown in Figure 4–2. First, a small central inner disk of variable diameter, d_i, was plated by pipetting cells inside a small glass ring in the center of the dish. The cell plating density in the inner disk, ρ_i, was varied in the range of (1-3)$\times10^4$ cells/cm^2. Six hours later a larger disk of diameter d_o=9 mm was plated on top of the small disk with a seeding density of ρ_o=10^4 cells/cm^2.

The plated cells were kept in an incubator at 36 °C in 5% CO_2 in 2 mL 818a solution for two days. After the first day the outer glass ring was removed and cells were washed with fresh 818a. The tissue was imaged in Hank's solution containing: 130 mM NaCl, 1.3 mM KCl, 1.8 mM $CaCl_2 2H_2O$, 0.80 mM $MgS0_4 7H_2O$, 0.80 mM

$MgCl_26H_2O$, 0.40 mM Na_2HP0_4, 3.6 mM $NaHC0_3$, 0.40 mM KH_2SO_4, 10 mM dextrose, 2.9 mM sucrose, as well as 9.9 mM HEPES buffer (Calbiochem). The calcium dye was loaded into each dish using 2 mL Hank's solution containing 10 μg Calcium Green-1 fluorescent dye (Invitrogen) and 10 μL of 20% Pluronic acid in DMSO (Invitrogen) for 25 minutes. The dye solution was then discarded, and the tissue washed three times and transferred for imaging in 2 mL of regular Hank's solution.

4.3.2 Imaging of Calcium Dynamics

Recording of the intercellular calcium fluorescence was performed using a custom-built macroscopic imaging system outlined in Figure 4–1. The KL2500 light source (Zeiss) projects light through an excitation filter with 500 nm center wavelength and 50 nm bandwidth (Chroma Optical). The filtered light passes through a fiber optic guide containing an annular diaphragm mounted over the macroscope objective lens, L1. The fluorescent and reflected light emitted by the tissue is passed through the L1 lens which is a 50 mm Super-Takumar 1:1.4 (Asahi Optical) photographic F-mount lens. The focus is set to infinity so that this lens effectively collimates the light from the object to lens L2. The L2 lens is an 80 mm Nikor 1:2 (Nikon) F-mount photography lens that projects the image to the focal plane of lens L3. The L3 lens is composed of an emission filter (545 nm center wavelength with 70 nm bandwidth) and a 10× reducer (Redshirt Imaging). The reducer projects the image onto the charged-coupled diode chip of camera C1. The field of view used for macroscopic activity mapping is approximately 10 mm.

In the experiments reported, the tissue was imaged under no perfusion in a closed chamber with humidity and temperature control. The temperature controller (Zeiss

Tempcontrol 37-2) was set to 36 °C which maintained the medium at 35±1 °C during the experiments reported. The gas and humidity controler (Zeiss CTI-Controller 3700), was set to 0.1%CO_2 with fan speed set at level two to help maintain temperature and minimize evaporation.

4.3.3 Mapping Excitation in Space and Time

The data collection was carried out using CardioPlex software (Redshirt), with a spatial resolution of 0.15 μm^2 (80 × 80 pixels) and time resolution of 25 ms (40 Hz sampling). The raw data was then imported into Matlab [102] where it was zero-meaned for each pixel, spatially averaged over bins of 2×2 pixels and band-pass filtered over the frequency range of 0.1 Hz to 3.0 Hz using a third-order Butterworth filter.

To compute crossing times and interbeat intervals (IBIs), a threshold is set for the light intensity such that when a time series crosses that threshold with a positive slope, it registers that as the start of an excitation. The threshold was manually set between 10 and 80 filtered pixel intensity units to properly distinguish activation events. The exact activation crossing time at each pixel was calculated by interpolating the light intesity time series. The interbeat intervals were found by subtracting two contiguous crossing times. Crossing times which were too close to eachother (<200 ms) were typically caused by extra detections during one actual activation (see the event at 38 s in the pixel activation time series of Figure 4–4 for an example), and were discarded in the calculation of the interbeat intervals .

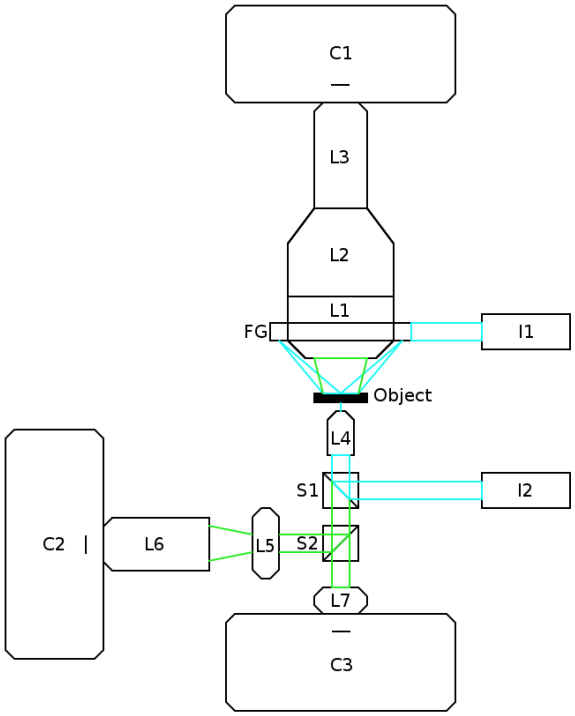

Figure 4–1: Schematic of the imaging system used to observe the chick cardiac tissue preparation and its intracellular calcium dynamics (courtesy of Alex Hodge). I1 and I2 are light sources for the macroscope and microscope, respectively. The light is projected through the calcium emission filter via fiber optic guide and emitted from a ring mounted over the macroscope lens (labeled FG). Blue lines represent light which excites the calcium dye and green lines are the light which the dye emits. L1-L7 represent the various lenses, and S1-S2 the light splitters detailed in Section 4.3.2. C1 and C2 are both Redshirt Imaging CardioCCD-SM cameras, with C1 used to macroscopic calcium imaging, and C2 used for microscopic calcium imaging. C3 is a Zeiss Axiocam HRM used for collecting higher spatial resolution still images.

4.3.4 Model of Excitable Tissue with Pacemakers

The calcium wave dynamics observed in the experiments are modeled using the FitzHugh-Nagumo equations in two spatial dimensions.

$$\begin{aligned} \frac{\partial v}{\partial t} &= \frac{1}{\varepsilon}(v - v^3 - w) + I_P + D\frac{\partial^2 v}{\partial x^2}, \\ \frac{\partial w}{\partial t} &= \varepsilon(v + \beta - \gamma w)\left(\frac{w_h - w_L}{1 + e^{-4v}} + w_L\right) \end{aligned} \tag{4.1}$$

The coupling strength D=0.2 cm^2/s is used to obtain excitable dynamics with propagation velocity like that seen in experiments (≈1-3 cm/s). The parameters ϵ=0.9, β=0.7 were tuned to obtain an excitable medium with stably rotating spiral waves similar to those seen in experiments (≈0.7-1.4 s). The pacemaker current $I_P = 1$ was added to regions of pacemaking sites (a central disk with a nominal radius of 1.75 mm and a half-disk of radius 0.5 mm at the center-left edge of the medium), and $I_P = 0$ in all other regions where the medium is excitable. The equations for the excitable media included diffuse break heterogeneities at $\phi = 0.1$ (as described in Section 2.3.1) unless otherwise stated. The system was integrated using the forward Euler method with Δt=0.5 μs on a 200×200 grid with Δx=50 μm.

4.4 Results

4.4.1 Engineering a Dominant Central Pacemaker

Standard monolayers of chick ventricular cells (like the one that generates the dynamics in Figure 2–1) exhibit a wide spectrum of wave patterns, including irregular switching between sites of pacemaking and formation of reentrant waves. In order to standardize the spontaneous dynamics of the experimental preparation, one can

exploit the fact that aggregates of cells in monolayers can entrain surrounding tissue [85]. I found that growing monolayer cultures with a concentrated disk of cells in the middle, the thicker regions (shown in Figure 4–2) tend to act as sites of pacemaking. The central mound rhythmically emits waves that propagate outward and entrain all other pacemakers in the medium. The calcium wave dynamics of a representative culture is shown in Figure 4–3, and the interbeat intervals of many cultures are summarized in Table 4–1.

To investigate how central pacemaker diameter and thickness influence spontaneous activity, tissue cultures were engineered at variable inner disk diameters and cell plating densities as shown in Figure 4–2. The smaller (d_i=1.8 mm) and denser (ρ_i=4×10^4 cells/cm^2) inner disk configurations had a dominant central pacemaker in 7/12 preparations, as summarized in Table 4–1. An example of the dominant central pacemaker dynamics of Dish 3 is shown in Figure 4–3. Culture configurations with a larger (3 mm or 5 mm) and less dense (10^4 cells/cm^2) inner disk failed to generate dominant central pacemakers in any of the nine dishes that were imaged. The wave dynamics of these dishes included pacing from various regions of the tissue as well as reentrant waves.

4.4.2 Effects of E-4031 on Pacemaker Beat Rate and Switching

The dishes with a dominant central pacemaker were treated by changing the medium to one with 0.75-1.5 μM E-4031 (Sigma-Aldrich) which almost immediately led to the emergence of pacemakers from the outer perimeter of the cultured disk. These side pacemakers had a period shorter than that of the central pacemaker and would thus eventually reset and entrain it. An example is shown in Figure 4–4 in

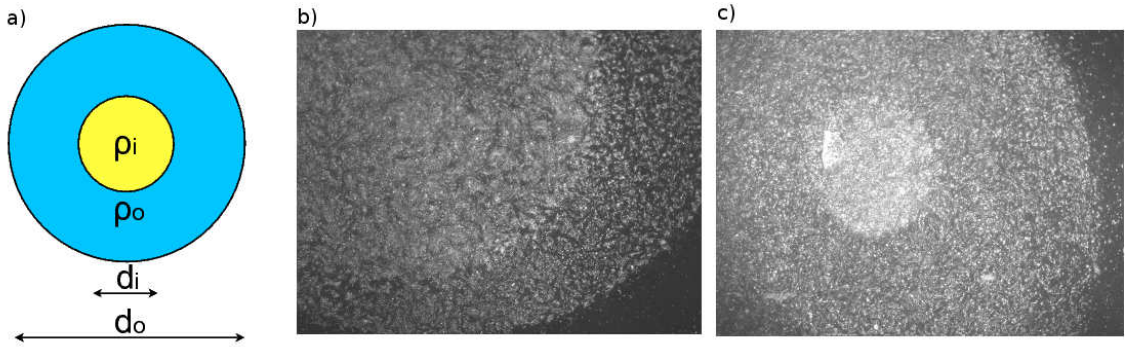

Figure 4–2: Illustration of the stacked disk geometry paradigm used to culture the tissue. (a) Schematic of engineered pacemakers plated as a disc of diameter (d_i), at variable inner density (ρ_i), and embedded in a layer of external tissue of outer density ρ_o=10^4 cells/cm^2 and outer diameter d_o=8.9 mm. Examples in (b) where (ρ_i=2×10^4 cells/cm^2, d_i=5.5 mm) and in (c) where (ρ_i=4×10^4 cells/cm^2, d_i=1.8 mm). Images in (b) and (c) are taken using phase contrast imaging with a field of view of ≈4 mm.

Table 4–1: Summary of spontaneous activity in dishes with the 1.8 mm diameter dense central mound. The interbeat intervals (at the central pacemaker) are averaged over a two minute period. Variability of the interbeat interval is lower in dishes with a dominant pacemaker.

Dish	Spontaneous Dynamics	Interbeat Interval (±SD)
1	dominant central pacemaker	0.91 ± 0.03 s
2	dominant central pacemaker	1.68 ± 0.02 s
3	dominant central pacemaker	1.41 ± 0.05 s
4	dominant central pacemaker	1.32 ± 0.04 s
5	dominant central pacemaker	1.65 ± 0.07 s
6	dominant central pacemaker	1.55 ± 0.06 s
7	dominant central pacemaker	1.60 ± 0.05 s
8	central pacemaker with wavebreak	2.13 ± 0.09 s
9	dominant side pacemaker	1.06 ± 0.02 s
10	spiral wave with central pacemaker	0.73 ± 0.10 s
11	spiral wave with central pacemaker	0.96 ± 0.09 s
12	spiral wave with central pacemaker	1.11 ± 0.08 s

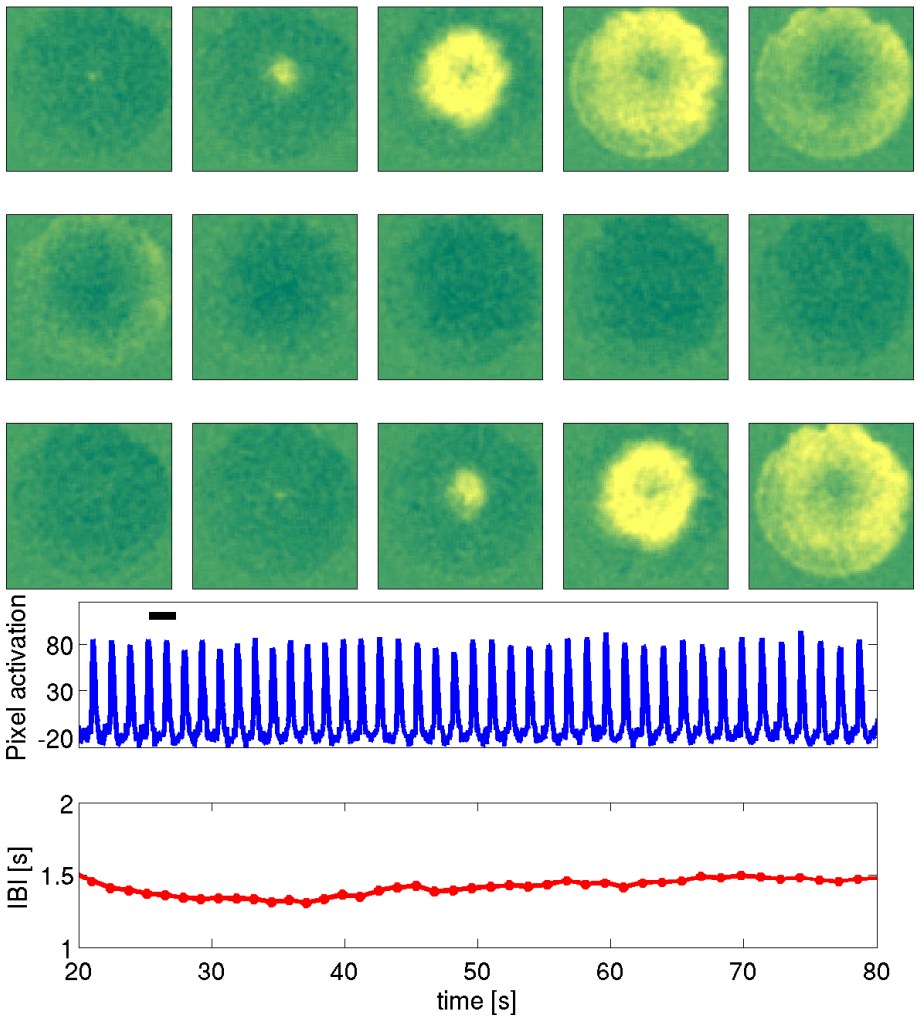

Figure 4–3: Central pacemaker periodically emits calcium waves which propagate outward and entrain surrounding tissue. Top panels: activation maps of intracellular calcium activity taken every 125 ms. Bottom panels: upper trace shows a time series of light intensity at pixel (50,50). The black bar shows the time range considered in the upper activation snapshots. The bottom trace shows that the interbeat intervals of activation times are relatively constant over many beats.

which the emerging side pacemaker has a period ≈57% shorter than the original period of the central pacemaker.

In nine cases more than one side pacemaker emerged, resulting in a complex sequence of switching between pacemaker foci. In this chapter I restrict my attention to the two cases in which waves from a single side pacemaker reset the central pacemaker leading to formation of reentrant waves. A representative sequence of dynamics is shown in Figure 4–5. A wave emitted from an pacemaker on the left edge of the preparation breaks up over the central pacemaker, and reenters back into the central pacemaker. An analysis of the scenario is presented Figure 4–5. The time series and periods of pixels at the side pacemaker site, central pacemaker site, and a site behind the central pacemaker show a lengthening of period at the central pacemaker corresponding to the wave emitted from the side pacemaker breaking up around it, but then reentering into it retrogradely. This causes a short-lived reentrant wave formed behind the central pacemaker. The rotating wave has a period lower than that seen before the wave breakup incident. With the side pacemaker still active the reentrant wave meanders and breaks across the central pacemaker resulting in the interbeat interval increasing again.

4.4.3 Effect of Side Pacemaker Period on Entrainment of the Excitable Medium in the Model

Using FitzHugh-Naguno model I first investigate how one pacemaker drives the surrounding excitable medium as the pacemaker beat rate is varied. To do this I vary the recovery parameter, w_L, at the side pacemaker site to see effect on the intrinsic period of the side pacemaker (T_{SP}) in the excitable medium with no central pacemaker. The parameter w_L prolongs T_{SP} by increasing the the amount of time

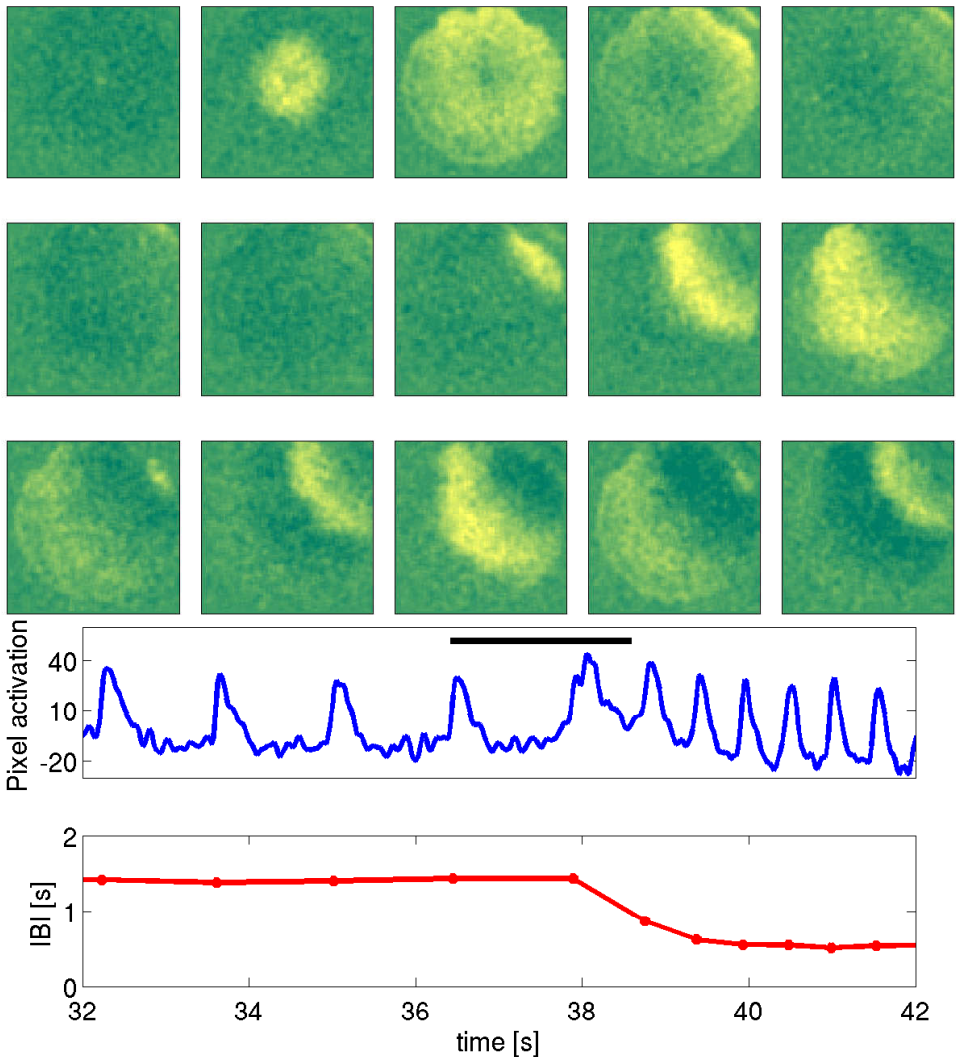

Figure 4–4: Application of E-4031 induces a side pacemaker with a shortened period to take over the central pacemaker. Top panels: activation snapshots showing a wave emitted from a central pacemaker followed by the emergence of a side pacemaker whose wave entrains the central pacemaker. Bottom figures show the timeseries and interbeat interval at pixel (63,66) during the pacemaker switch (represented by the black bar in time series panel below).

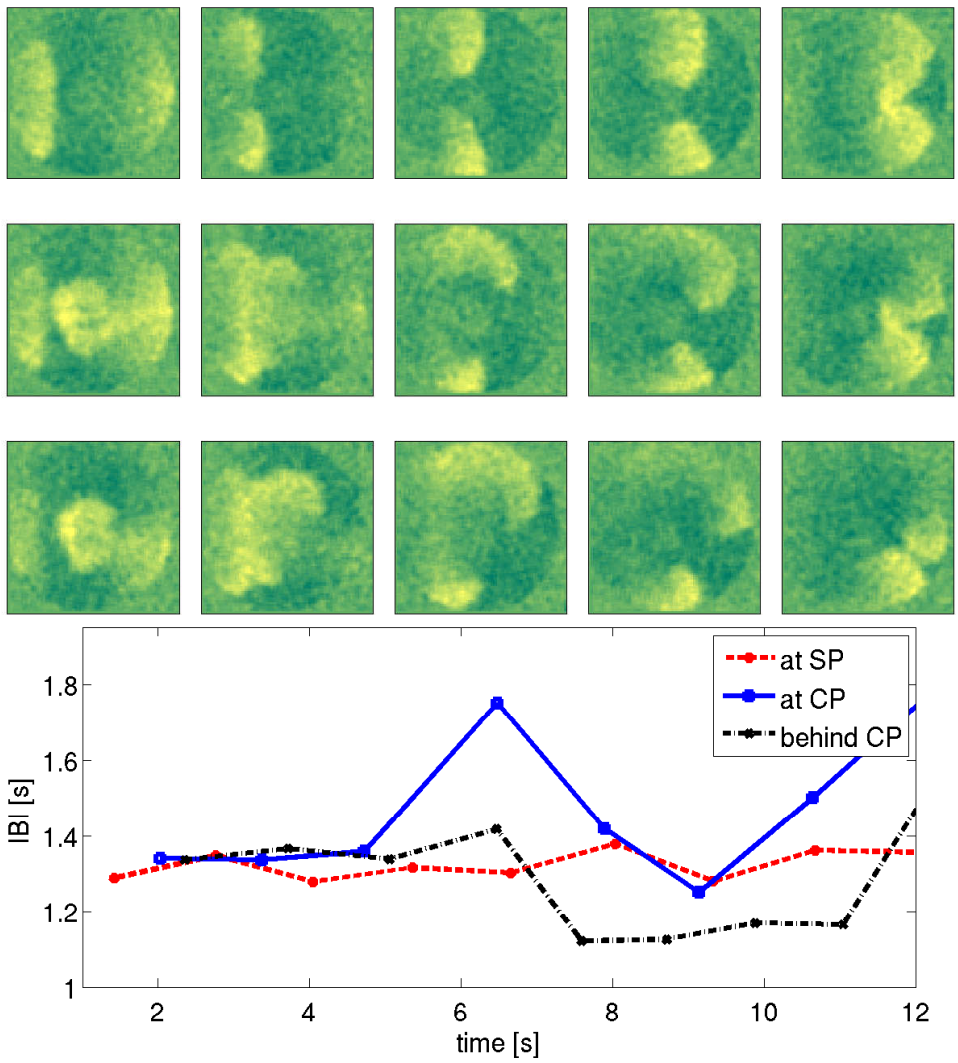

Figure 4–5: Reentrant waves formed through the interaction of two pacemakers in our cardiac tissue cultures. Top panels: snapshots of calcium activity taken every 150 ms show a wave emitted from the left side pacemaker breaking around the central pacemaker site and then reentering into it. Bottom trace: Interbeat intervals at three locations in the medium. The central pacemaker site has the largest change in its interbeat interval during the wavebreak incident.

spent in recovery (Figure 4–6, top panel). The bottom panel of Figure 4–6 shows the effect that changing w_L at the side pacemaker has on beat rates seen at the side pacemaker site and in the surrounding excitable medium. The medium is driven 1:1 (one beat of pacemaker for one wave through the medium) by the side pacemaker up to $w_L = 0.22$ beyond which the pacemaker is unable to drive the medium at every beat. The intervals at $0.225 < w_L < 0.245$ and $0.265 < w_L < 0.300$ are parameter regions of 2:3 and 2:1 entrainment between pacemaker and medium, respectively.

4.4.4 Wave Entrainment Between Two Pacemakers in the Model

To study the wave dynamics resulting from the interaction betwen side and central pacemakers, a central pacemaker with intrinsic period $T_{CP} = 1.55$ s is added to the medium and the rate of the side pacemaker is varied with w_L as in the previous section. The initial conditions were set such that the central pacemaker fires one beat at which point the side pacemaker begins emitting waves with varying intrinsic periods T_{SP}. The results are summarized in Figure 4–7. For $T_{SP} > T_{CP} = 1.55$ s, the entire medium is driven by the faster central pacemaker (Figure 4–7(a)). For $T_{CP} > T_{SP} > 0.67$ s the faster side pacemaker entrains the central pacemaker and the rest of the medium (Figure 4–7(b)). For $T_{SP} < 0.67$ s, waves from the side pacemaker begin to break up over the central pacemaker (Figure 4–7(c)). As was observed in the experiments, the wave break incidents in the model cause more variability in the interbeat intervals (Figure 4–7(d)). The cases leading to wave break over the central pacemaker are investigated further in the next two sections.

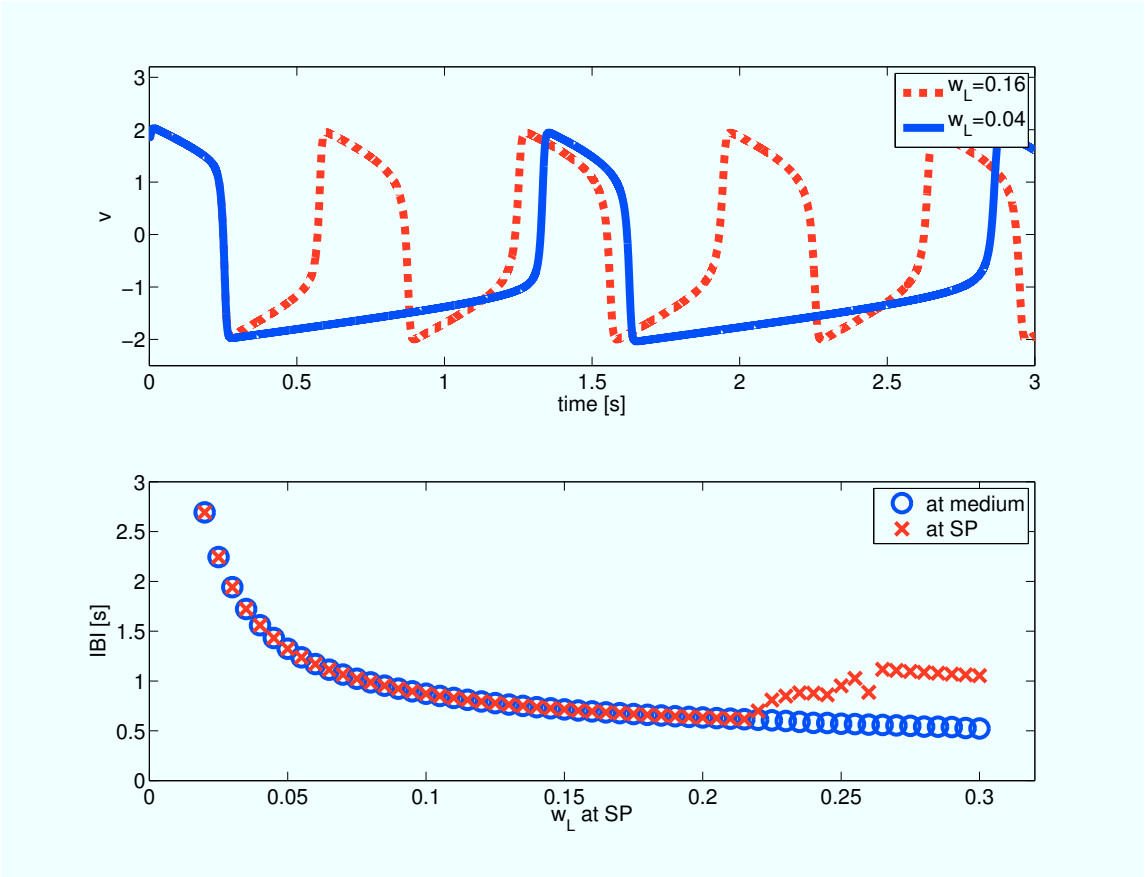

Figure 4–6: The effect of w_L on recovery and pacemaker rate. Top panel: increasing w_L of the side pacemaker decreases the oscillation period of the side pacemaker and the remaining excitable medium. Top trace: time series of the activation variable v at the side pacemaker when for $w_L = 0.04$ and $w_L = 0.016$ showing that the lower w_L decreases the period of oscillation by decreasing the amount of time the pacemaker takes to reach firing threshold. Bottom trace: the effect of w_L on interbeat interval at the pacemaker site and in the surrounding medium shows that the pacemaker can pace the medium up to $w_L = 0.022$ beyond which some beats fail to propagate from the side pacemaker.

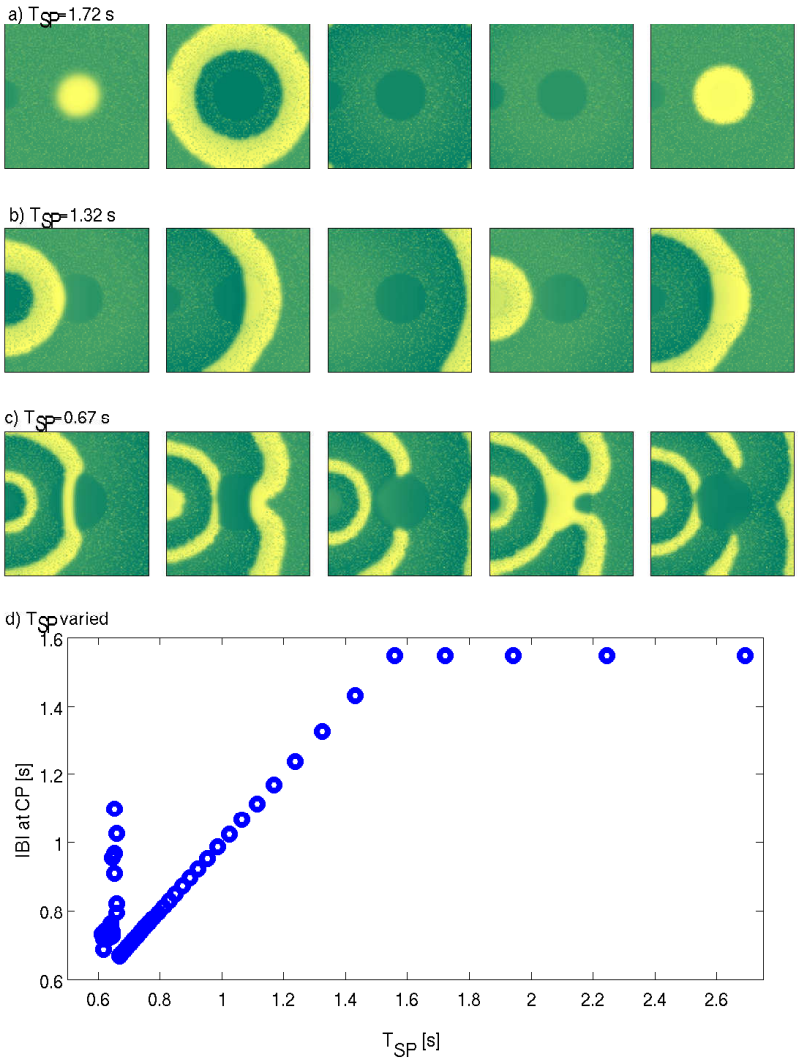

Figure 4–7: Varying side pacemaker period gives rise to three types of wave dynamics. Each row of panels shows snapshots of activity at for each type of dynamics. (a) For T_{SP}=1.72 s the central pacemaker entrains the medium. (b) When T_{SP}=1.32 s the side pacemaker begins to entrain the medium. (c) For T_{SP}=0.67 s the side pacemaker waves break around the central pacemaker site. (d) Side pacemaker period is varied and the last three interbeat intervals at the central pacemaker are shown for each.

4.4.5 Wave Breakup Over Central Pacemaker in the Model

Waves break when the central pacemaker is unable to propagate waves from the side pacemaker in a one-to-one fashion. Figure 4–7(a) shows that this 1:1 entrainment limit, $T_{CP}^{1:1}$, occurs when T_{SP} is 43% of the intrinsic period of the central pacemaker.

Phase resetting the central pacemaker can predict the effect of periodic forcing by the side pacemaker. To eliminate the effects of wave collisions between the two pacemakers (see [94]) we compute the phase resetting curve of the central pacemaker ordinary differential equation (Equation 4.1 at the central pacemaker with $D = 0$, and stimulus current, I_s). The shape of the stimulus current is taken from the current, $\frac{\partial v}{\partial t}$, at central pacemaker pixel (101,101) in the partial diferential equation simulation. The simulation is run with T_{SP} just below $T_{CP}^{1:1}$ and the wave profile chosen is from the last wave before breakup (see Figure 4–8(a), left trace). The resultant phase transition curve (Figure 4–8(a), right panel) shows the largest period shortening T_i/T_0=0.37 at φ =0.41. Other reasonable stimuli waveforms exhibit similar maximal shorteninings in period (for example, $I_s = 2.5(\tanh(10t) - \tanh(10(t - 0.2)))/2)$ s^{-1} induces a maximal shortening of the period to $0.38T_{CP}$). The resetting experiments that the pacemaker cannot be driven 1:1 for $T_{SP}/T_{CP} < 0.37 = T_{CP}^{1:1}/T_{CP}$, which is smaller but comparable to the factor of 0.43 found in the spatially-distributed model.

System properties which cause the discrepancy in $T_{CP}^{1:1}/T_{CP}$ between the spatial model and ordinary differential equation phase resetting estimate, include the size of the central pacemaker region and the proportion of breaks in the medium. Decreasing the diameter of the central pacemaker to 1.5 mm indeed lowers $T_{CP}^{1:1}/T_{CP}$ to 0.40 as shown in Figure 4–8(b), where the interbeat intervals measured at the center of the

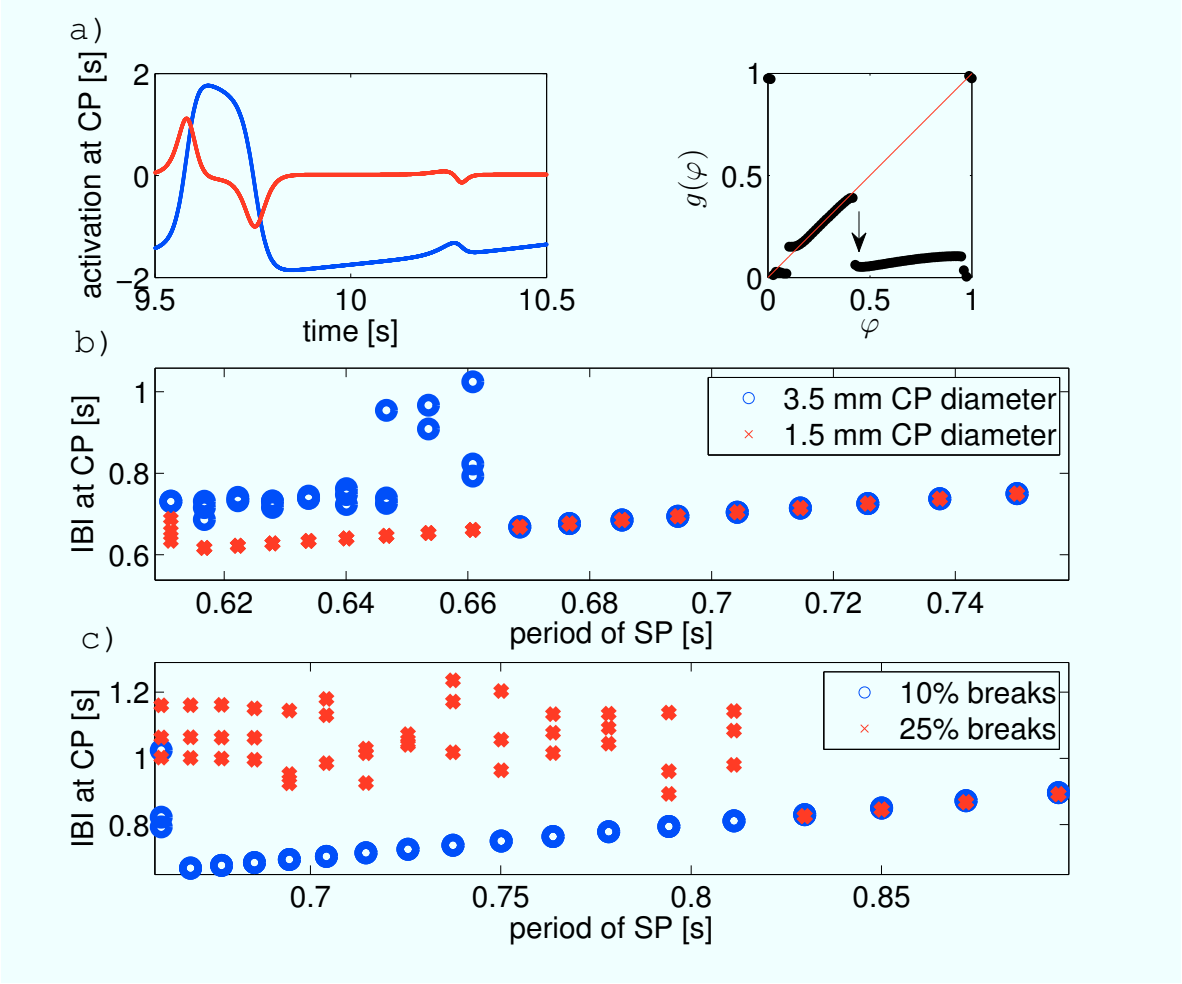

Figure 4–8: Loss of 1:1 entrainment leads to wave breakup around central pacemaker. (a) The left panel shows times series of voltage, v, (blue dots) and current, $\frac{dv}{dt}$, (red dots) measured at the central pacemaker during a passing wave followed by the first wave break. On the right, the phase transition curve shows the largest phase shift at φ =0.41 (arrow). (b) The effect of side pacemaker period on the interbeat intervals at the pacemaker site for two central pacemaker diameters. (c) Increasing the proportion of breaks causes wave breakup at longer side pacemaker periods.

central pacemaker for $T_{SP} = 0.66$ s are constant for the smaller central pacemaker diameter, but variable from beat to beat (due to wave breakup and reentry) for the larger diameter. Inasmuch as break heterogeneities decrease the wavelength of activation (see Figure 2–2) one would expect the density of heterogeneities to also have an effect on $T_{CP}^{1:1}/T_{CP}$ in addition to the effect of pacemaker diameter. This is confirmed in Figure 4–8(c), where increasing the proportion of break heterogeneities from 10% to 25% raises $T_{CP}^{1:1}/T_{CP}$ from 0.41 to 0.55. These two findings demonstrate that the limits of pacemaker entrainment are sensitive to the spatial distribution of both the wave and the reset pacemaker.

4.4.6 Reentrant Wave Patterns in the Model

The medium parameters β and ϵ were tuned to ensure the excitable medium sustained spiral waves with a rotation period $T_{SW} = 0.72$ s. This allows for the formation of reentry whenever the wave breaks over the central pacemaker, but does not guarantee sustained spiral waves with one dominant period in the system. The top panels of Figure 4–9 show that when $T_{SP} = 0.67$ s reentrant waves kept forming and breaking which lead to significantly fluctuating interbeat intervals behind the central pacemaker.

On the other hand, sustained reentrant waves are observed for some T_{SP}, like those leading to the unscattered interbeat intervals in the bottom trace of Figure 4–8. Top panels of Figure 4–10 show that when $T_{SP} = 0.64$ s, a spiral wave is formed on the side of the central pacemaker across from the side pacemaker. The bottom trace of Figure 4–10 shows that the spiral wave entrains the central area of the central pacemaker to $T_{SW} \simeq 0.72$ s over a long period of time. It is interesting that the

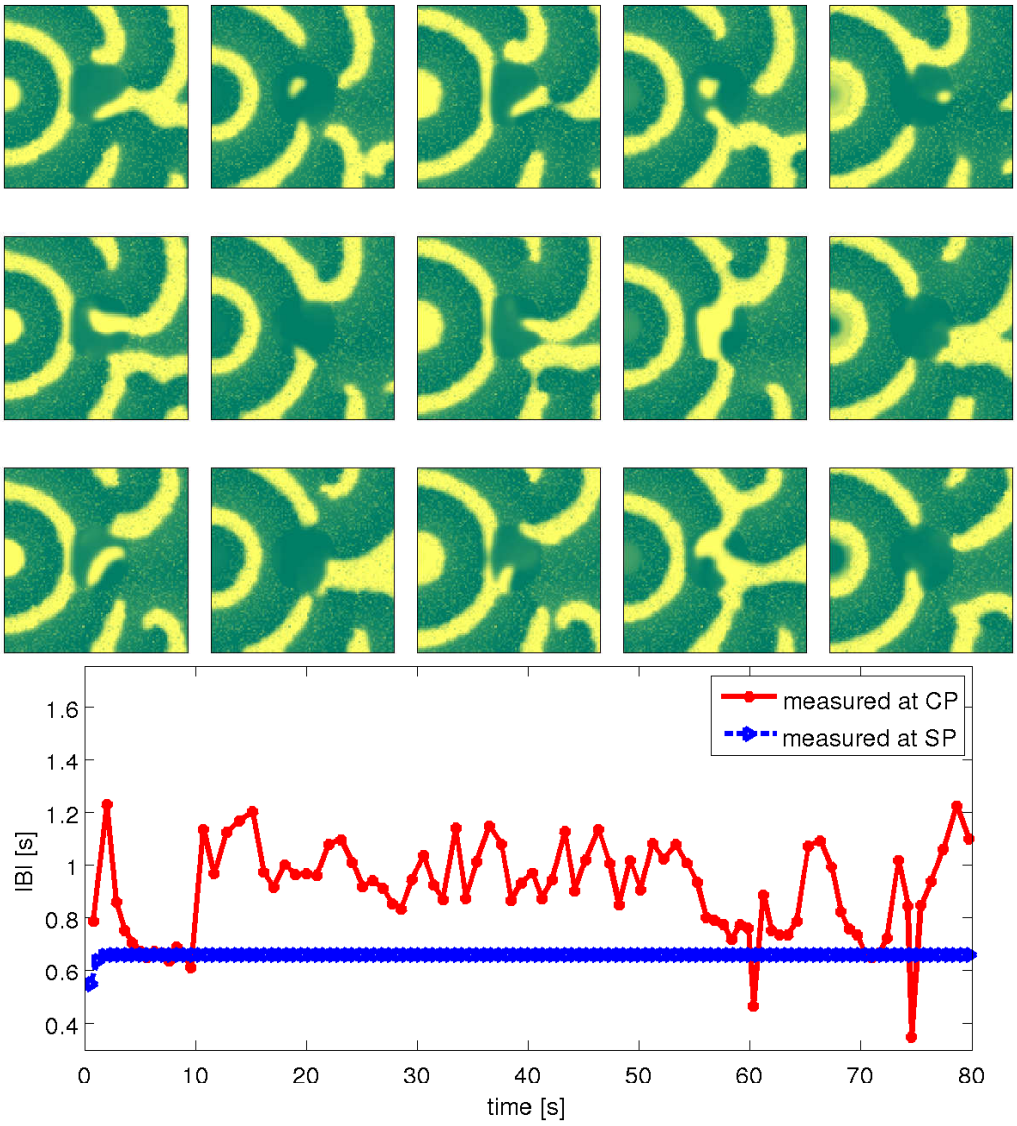

Figure 4–9: An example of reentrant waves which keep forming and breaking for T_{SP}=0.67 s. Top panels are snaphots of activity taken every 0.4 s starting at 24.2 s. The bottom figure shows irregularity of beat to beat intervals at the central pacemaker site despite the regularity observed near the side pacemaker.

spiral wave can sustain itself despite the fact that $T_{SP} < T_{SW}$. This seems possible due to the central pacemaker acting as a shield which blocks waves from the side pacemaker that should otherwise reset the spiral wave. Despite this observation the particular determinants which facilitate the maintenance of a spiral wave have yet to be determined in this system.

4.5 Discussion

The FitzHugh-Nagumo model has the property that when the two pacemaker rates are similar, the faster pacemaker entrains the other pacemaker and the rest of the medium. This occurs because the site at which waves from either pacemaker annihilate each other incrementally moves towards the slower pacemaker - known as "peeling back" of the slower wave train [1, 118, 113, 140, 190, 207, 251, 256].

Once waves from the faster pacemaker reach the slower pacemaker, there is the possibility of them either passing through it, or breaking up around it. Wave break occurs for waves coming at time intervals shorter than the one-to-one entrainment limit of the central pacemaker. This entrainment limit is approximated by the phase transition curve of the pacemaker ordinary differential equation.

The discrepancy between maximal beat rate for 1:1 pacing in the ordinary differential and partial differential equation models include pacemaker size and proportion of heterogeneities in the excitable medium. Increasing the number of breaks in the excitable medium raised $T_{CP}^{1:1}$ in the FitzHugh-Nagumo propagation model (Figure 4–8). For solitary waves, raising the proportion of breaks in the medium causes the wavelength to decrease (Figure 2–2). Once the waves are generated in trains, the wavelength of each wave further decreases because the excitable medium is not as

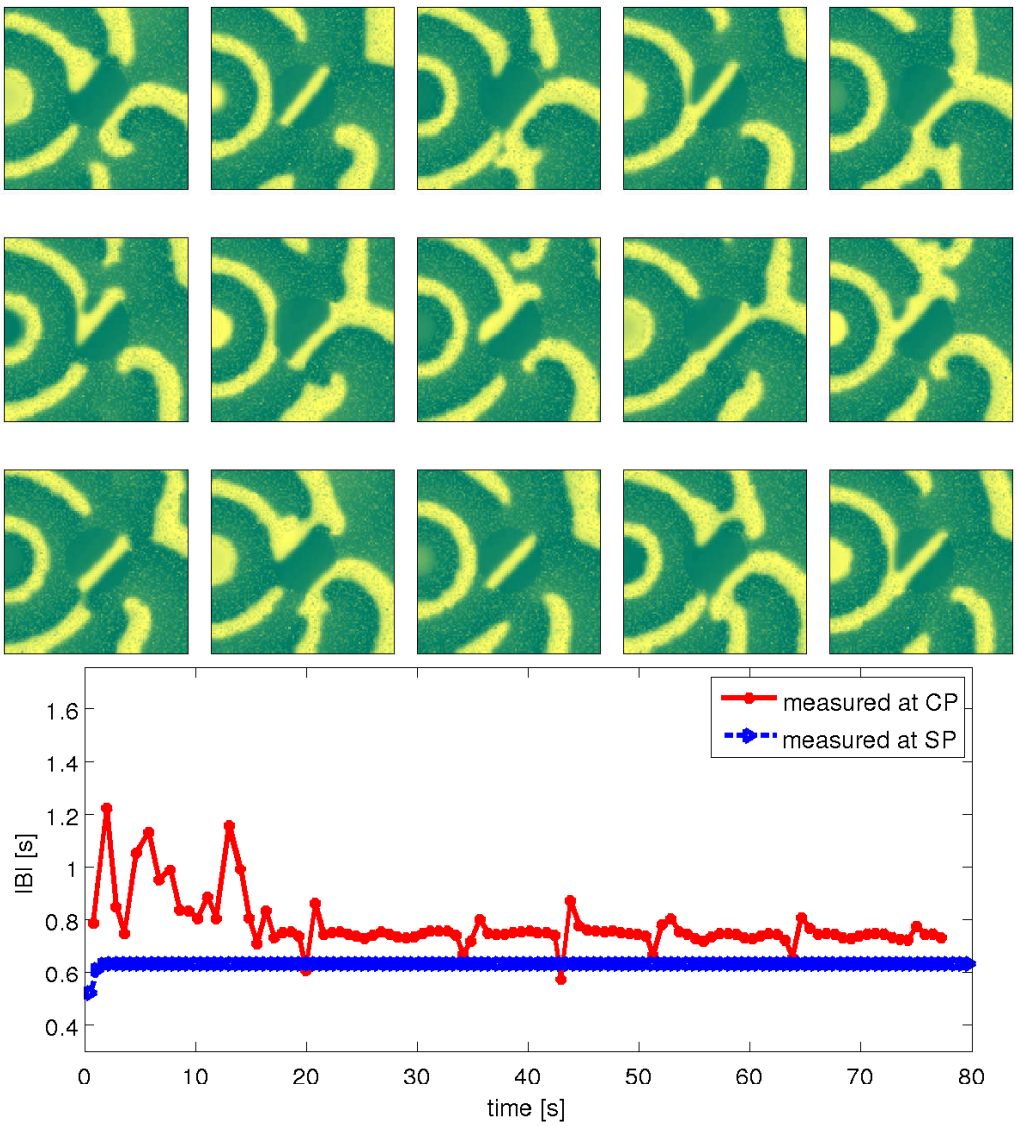

Figure 4–10: An example of a reentrant waves which keeps rotating at a constant period for $T_{SP} = 0.64$ s. Top panels are snapshots of activation patterns taken every 0.4 s starting at 40.2 s showing a spiral wave at bottom right of the central pacemaker. The bottom figure shows the calculated IBIs at the side and central pacemaker site showing the spiral waves mostly entraining the central pacemaker site.

recovered when the next wave arrives. Thus it is to be expected that increasing break proportion causes wave break at wave trains with shorter interbeat intervals, which was indeed been observed in the diffuse fibrosis simulations of Tusscher and Panfilov [221].

Decreasing the diameter of the central pacemaker decreased $T_{CP}^{1:1}$ (Figure 4–8), in line with previous findings which demonstrate that for circular inexcitable obstacles, pacing a large enough obstacle will cause wave break which does not reseal once the wave clears the obstacle [217]. Winfree described the behaviour of spiral waves in FitzHugh-Nagumo equations similar to the ones used here [245]. He found that the parameters β and γ control the existence of stable spiral wave reentry and the meander of the reentrant core. I used this to tune the excitable media to sustain non-meandering spirals, with relatively constant spiral wave period, T_{SW} =0.72 s. The fact that this period persists on one side of the central pacemaker while other side is driven faster by T_{SP} =0.64 s is an interesting finding. A similar results was obtained by Xie *et al.* [250], who found that a spatial heterogeneity (of the ϵ parameter) allows for the coexistence of two spiral waves with distinct periods. This occurs because of the formation of an insulating region (of broken waves) between the spirals, so that the faster one does not reset the slower. In the FitzHugh-Nagumo pacemaker model the insulating region is the central pacemaker, but the criteria for the formation of a sustained spiral wave is still not well understood. A more careful analysis of the role of central pacemaker diameter is needed to:

1. elucidate the detailed relationship between central pacemaker diameter (d_i) and $T_{CP}^{1:1}/T_{CP}$,

2. find the smallest d_i that causes the wave to break, and study the bifurcation which occurs there,
3. study the role of d_i as insulating regions. I hypothesize that:
    - larger d_i would be ameliorate the insulating effect (i.e.: lead to more cases of sustained reentry behind the central pacemaker),
    - a small enough d_i could not act as an insulator.

In addition to the computational modeling, I have documented my efforts to engineer a a dominant central pacemaker tissue culture. Many questions remain about the determinants of this dynamic. For example, it is not clear why large mounds are not successfully dominant pacemakers. Regardless of these considerations, the robust and stable dynamics of the preparation are well-suited for use as a reference (control) for many experimental manipulations. I have focused on the effect of E-4031, but am also interested in the role of central disk diameter, varying the proportion and properties of fibroblasts, stimulating the central disk from a distance, and the role of temperature and perfusion flow in determining the wave dynamics.

The observable effects of E-4031 on the dominant pacemaker preparations were the emergence of side pacemakers with a period shorter than the central pacemaker, and the induction of reentrant waves caused by wavebreak over the central pacemaker. The rate increasing effect of E-4031 on pacemakers is in accord with other experiments with chick cardiac tissue [126]. Kim and colleagues [126] also observed the induction of complicated interbeat interval patterns in chick aggregates, and modeled these using an ionic model. In the spatially-extended cardiac tissue preparation, I have demonstrated that complex sequences of interbeat intervals induced

by E-4031 can occur as a result of breakup of waves at the central pacemaker and the formation of reentrant propagation patterns. Asano *et al.* [10] also observed initiation of reentry due to E-4031, but found it to be caused by the firing of single ectopic escape beats caused by early afterdepolarization of the excitable tissue. This result points to a weakness in the present FitzHugh-Nagumo formulation, as it does not consider the biophysical effect of E-4031, in decreasing rapidly-rectifying potassium channel conductance. Developement of a biophysical monolayer model with this potassium current for chick ventricular monolayer would be useful to compare with the present results. One could modify two different ionic models used by Kim *et al.* [126] and Krogh-Madsen *et al.* [138] for these purposes.

4.6 Conclusions

In this chapter I have discussed conditions leading to wave breakup and formation of reentrant waves in a heterogeneous excitable medium with two sites of pacemaking. Experimental induction of faster pacemakers in the engineered cardiac tissue causes wave break and reentry around the slower pacemaker site. The FitzHugh-Nagumo model confirms that this scenario is consistent with a rate increase of a previously entrained slower pacemaker. The mathematical model further allows for predictions of breakup based on the phase transition curve, and demonstrates that central pacemaker size and density of breaks can influence the breakup of waves. Furthermore, it demonstrates persistent reentrant waves sustained even in the presence of a faster driving pacemaker. These results can be extended to clarify the role that system properties play in the generation of wave break and reentry for

systems with more than one distinct pacemaker sites, including the right atrium of the heart.

CHAPTER 5
Conclusions

5.1 Overview of Main Findings

The studies presented in the last three chapters demonstrate possibile rules governing how certain design properties of heterogeneous excitable media with pacemakers control the dynamics of sustained propagation of solitary pulses and wave trains, wave break and the formation of reentrant wave patterns. The FitzHugh-Nagumo model allowed for explicit control over these properties, and the findings are compiled in Table 5–1. Some of these results were complemented by observations of wave propagation in chick cardiac tissue culture. In particular, the stacked disk cardiac culture (Section 4.4.1) does exhibit wave entrainment by waves from the faster beating pacemaker (Figure 4–4). Also, the speeding up of a peripheral pacemaker caused wave break and reentry around the central pacemaker in both the experiments (Figure 4–5) and mathematical model (Figure 4–7). The following sections discuss these results in the broader context of the thesis.

5.1.1 Randomly Distributed Heterogeneities Influence Wave Breakup and Reentry

The presence of either break or sink heterogeneities decreases plane wave propagation speed in two dimensional excitable media. For low proportions of randomly distributed heterogeneties, the conduction velocity decreased linearly with the proportion of heterogeneities, followed by a rapid decrease once the plane wave began

Table 5–1: Overview of how the properties investigated influenced the waved dynamics in the FitzHugh-Nagumo propagation models studied in each results chapter of the thesis. *Note: the effect of stimulus timing effect is modified with stimulus amplitude, duration, and stimulus position relative to the pacemaker.

Property	**Relevant Chapters**	**Wave Propagation and Breakup**	**Reentrant Waves**
proportion of sinks	2	propagation fails for a range of $\phi_c \in [0.06, 0.09]$ depending on D	sustained reentrant waves coincident with wave break
proportion of breaks	2,4	propagation fails at $\phi_c = 0.41$, the site percolation threshold of the square lattice	no sustained reentry during solitary wave breakup; persistent reentry in the presence of pacemaker
diffusional coupling	2	raising D increases ϕ_c for sinks	not studied; see [243]
stimulus timing*	3,4	stimulus propagates leading to resetting for $0.50 < \varphi < 0.82$	wave echo at $\varphi = 0.5032$; multiple wave reflections for $\Delta x = 0.04$ cm
periods of two pacemakers	4	wave breaks for $T_{SP} > T_{CP}^{1:1}$ with $\frac{T_{CP}^{1:1}}{T_{CP}} \in [0.40, 0.55]$ depending on d_i and ϕ of breaks in the excitable medium	reentrant waves coincident with breakup; sustained spiral waves form behind central pacemaker in some cases
pacemaker size	4	bigger central pacemaker increases T_{SP} at which waves break	not studied yet

to break (Figures 2–3 and 2–5). Sinks cause wave break at much smaller densities than breaks because of their strong coupling to the medium. Futhermore, greater diffusional coupling decreases the amount of sinks needed to achieve propagation failure (Figure 2–5). This is not true in the case of breaks, where propagation fails at the percolation threshold of the square lattice, irrespective of diffussional coupling (Figure 2–3). Solitary wave breakup with break heterogeneities does not lead to sustained reentry (Figure 2–2), but the presence of breaks ameliorates the induction of wave break (Figure 4–8(c)) and sustained reentrant waves (Figure 4–10) when a pacemaker is present. These computational results offer a potentially useful characterization of the effects of fibroblasts and collagen deposits in modulating wave break and reentry in several types of paced cardiac tissue.

5.1.2 Resetting of Pacemaker on a Cable Generates Reentrant Echo Waves

The phase resetting of a pacemaker from a distance shows a rapid jump in the phase transition curve during the initiation of the stimulating pulse (Figure 3–3). According to the *Continuity Lemma* (Section 3.3.1), the phase transition curve will be continuous as long as the stimulus does not put the trajectory outside of the basin of attraction of the limit cycle. In the one dimenstional FitzHugh Nagumo model, the jump in the phase transition curve is shown to be continuous. This is achieved by using a slow wave solution that grows into an echo wave at the start of the resetting (Figure 3–5). For a coarser spatial discretization of the FitzHugh-Nagumo cable model multiple site of reflections occur (Figure 3–7). While these complex multi-echo solutions may be a numerical artifact of the discretization, there is evidence of similar multi-reflected waves in Moris-Lecar equations [20, 47] and in

Purkinje fibers [177]. The results raise important theoretical questions about the full spectrum of wave patterns possible, and their relation to one another in phase space. Overcoming the computational challenges in extending this analysis to two dimensional models would allow for tracking solutions leading to resetting and relate the effect of break and sink heterogeneities.

5.1.3 Loss of Entrainment Between Pacemakers Induces Reentrant Waves

To study the interactions between pacemakers in excitable media, a tissue stacked disk cardiac tissue culture preparation is developed to exhibit dominant central pacemaker dynamics (Figure 4–3). The determinants of this entrained state include central pacemaker diameter and density (Figure 4–2). The smallest and densest of the central disc diameters produced all of the regular central pacemaker dynamics, but more experiments need to be performed to understand why this is the case. The stacked disk culturing paradigm should indeed be developed further, for it opens the door to many other experiments which require regular spontaneous wave dynamics in chick cardiac monolayers.

In the dominant pacemaker cultures, side pacemakers are induced to beat faster than the central pacemaker by the application of E-4031 (Figure 4–4). The wavetrain from the side pacemaker breaks up into reentrant waves (Figure 4–5). This is another demonstration of the pro-arrhythmic effects of E-4031 in cardiac tissue [10, 126], but is also novel in that it highlights the role of reset pacemakers in the generation of complex reentrant wave dynamics.

The pacemaker switching scenario observed in the experiments is modeled using the FitzHugh-Nagumo equations with two sites of pacemaking. The model demonstrates that the pacemaker with faster beat rate entrains the slower pacemaker, up to a point where it cannot be entrained in a one-to-one fashion (Figure 4–7). The entrainment limit is approximated by the phase transition curve of the pacemaker ordinary differential equation, but is also modulated by spatial factors such as pacemaker diameter and proportion of breaks in the excitable tissue (Figure 4–8). An extension of these approaches using atrial computational models and experimental preparations, would be interesting to compare with the present results, and would be potentially useful in characterizing pacemaker mediated arrhythmias in the heart.

5.2 Other Important Dynamical Determinants

Table 5–1 lists the factors studied and their effects on wave dynamics. One can think of numerous other properties which could be investigated using the FitzHugh-Nagumo equations and *in vitro* cardiac tissue culture to complement the results presented in this thesis. These include: geometry of tissue or pacemaker(s), the distribution of cell types (cardiomyocytes, fibroblasts, blood vessel cells, and other specialized cell types), the anisotropic orientation of myocytes, the intercellular variation in coupling and electrophysiological parameters, as well as properties of the extracellular matrix, responses to environmental inputs (such as electrical stimulation, ablation, hypoxic injury, temperature, drug application, stretch, or shear stress). Underlying these responses (and the responses to them) is a rich network of molecular and genetic factors [37, 46, 16]. These properties are relevant to wave

dynamics in particular instances, but together they are a patchwork of results using different experimental and mathematical models. Compiling a complete picture of the structure-dynamics relation for simple models would allow one to see which relations are created, conserved, or lost as more biophysical constraints are added.

5.3 Closing Remarks

Thinking of excitation waves in the heart as a dynamical system, the structure-dynamics relations associate parameter values to certain types of dynamics, represented by sets of the state variables in function space. The typical dynamics of the heart (the sinus rhythm) is a periodic wave train emitted from the sinoatrial node and propagating through the atria and ventricles. The fact that the sinus rhythm persists under environmental perturbations leads to the description of this dynamical type as a stable limit cycle with a basin of attraction. Alongside this basin of the sinus rhythm are other basins containing trajectories representing certain types of reentrant wave patterns (associated with cardiac arrhythmias) and the rest state (death). Cardiac arrhythmias are dynamical diseases [75] in which parameters affect the distribution of basins representing dynamical types in the function space. This thesis provides a sketch of some structure-dynamics relations in simplified mathematical and experimental models of cardiac tissue. Attempting to complete our understanding of these relationships in increasingly detailed models will inform risk stratification and treatment strategies for pathophysiological conditions of the heart.

References

[1] K. Agladze, M. W. Kay, V. Krinsky, and N. Sarvazyan. Interaction between spiral and paced waves in cardiac tissue. *American Journal of Physiology - Heart and Circulatory Physiology*, 293(1):H503–H513, 2007.

[2] R. R. Aliev and A. V. Panfilov. A simple two-variable model of cardiac excitation. *Chaos, Solitons and Fractals*, 7(3):293301, 1996.

[3] M. A. Allessie and F. I. Bonke. Direct demonstration of sinus node reentry in the rabbit heart. *Circulation Research*, 44(4):557–568, 1979.

[4] M. A. Allessie, F. I. M. Bonke, and F. J. G. Schopman. Circus movement in rabbit atrial muscle as a mechanism of tachycardia. *Circulation Research*, 33(1):54–62, 1973.

[5] S. Alonso, M. Bär, and R. Kapral. Effective medium approach for heterogeneous reaction-diffusion media. *Journal of Chemical Physics*, 131(21):214102, 2009.

[6] S. Alonso, R. Kapral, and M. Bär. Effective medium theory for reaction rates and diffusion coefficients of heterogeneous systems. *Physical Review Letters*, 102(23):238302, 2009.

[7] C. Antzelevitch, J. Jalife, and G. K. Moe. Characteristics of reflection as a mechanism of reentrant arrhythmias and its relationship to parasystole. *Circulation*, 61(1):182–191, 1980.

[8] J. M. B. Anumonwo, M. Delmar, A. Vinet, D. C. Michaels, and J. Jalife. Phase resetting and entrainment of pacemaker activity in single sinus nodal cells. *Circulation Research*, 68(4):1138–1153, 1991.

[9] H. Arce, A. Lopez, and M. R. Guevara. Triggered alternans in an ionic model of ischemic cardiac ventricular muscle. *Chaos*, 12(3):807–818, 2002.

[10] Y. Asano, J. M. Davidenko, W. T. Baxter, R. A. Gray, and J. Jalife. Optical mapping of drug-induced polymorphic arrhythmias and torsade de pointes

in the isolated rabbit heart. *Journal of the American College of Cardiology*, 29(4):831 – 842, 1997.

[11] O. V. Aslanidi and O. A Mornev. Soliton-like regimes and excitation pulse reflection (echo) in homogeneous cardiac Purkinje fibers: Results of numerical simulations. *Journal of Biological Physics*, 25:149–164, 1999.

[12] D. S. Auerbach, K. R. Grzda, P. B. Furspan, P. Y. Sato, S. Mironov, and J. Jalife. Structural heterogeneity promotes triggered activity, reflection and arrhythmogenesis in cardiomyocyte monolayers. *The Journal of Physiology*, 589(9):2363–2381, 2011.

[13] K. Banach, M. D. Halbach, P. Hu, J. Hescheler, and U. Egert. Development of electrical activity in cardiac myocyte aggregates derived from mouse embryonic stem cells. *American Journal of Physiology - Heart and Circulatory Physiology*, 284(6):H2114–H2123, 2003.

[14] M. Bar, E. Meron, and C. Utzny. Pattern formation on anisotropic and heterogeneous catalytic surfaces. *Chaos.*, 204:204–214, 2002.

[15] L. Barr, W. Berger, and M. M. Dewey. Electrical transmission at the nexus between smooth muscle cells. *The Journal of General Physiology*, 51(3):347–368, 1968.

[16] E. Barth, G. Stämmler, B. Speiser, and J. Schaper. Ultrastructural quantitation of mitochondria and myofilaments in cardiac muscle from 10 different animal species including man. *Journal of Molecular and Cellular Cardiology*, 24(7):669 – 681, 1992.

[17] O. Bernus, C. W. Zemlin, R. M. Zaritsky, S. F. Mironov, and A. M. Pertsov. Alternating conduction in the ischaemic border zone as precursor of reentrant arrhythmias: A simulation study. *Europace*, 7(s2):S93–S104, 2005.

[18] A. Beuter, L. Glass, M. C. Mackey, and M. S. Titcombe (Eds.). *Nonlinear Dynamics in Physiology and Medicine*, volume 25. Springer-Verlag, New York, 2003.

[19] N. Bocarra and K. Cheong. Automata network SIR models for the spread of infectious diseases in populations of moving individuals. *Journal of Physics A*, 25(1255):2447–2461, 1992.

[20] B. Borek, L. Glass, and B. E. Oldeman. Continuity of resetting a pacemaker in an excitable medium. *SIAM Journal on Applied Dynamical Systems*, (in press).

[21] L. N. Bouman and H. J. Jongsma. Structure and function of the sino-atrial node: A review. *European Heart Journal*, 7(2):94–104, 1986.

[22] M. R. Boyett, H. Honjo, and I. Kodama. The sinoatrial node, a heterogeneous pacemaker structure. *Cardiovascular Research*, 47(4):658–687, 2000.

[23] P. M. Boyle and E. J. Vigmond. An intuitive safety factor for cardiac propagation. *Biophysical Journal*, 98(12):L57 – L59, 2010.

[24] R. D. Brown, S. K. Ambler, M. D. Mitchell, and C. S. Long. The cardiac fibroblast: Therapeutic target in myocardial remodeling and failure. *Annual Review of Pharmacology and Toxicology*, 45(1):657–687, 2005.

[25] J. Brugada, L. Boersma, C. J. Kirchhof, V. V. Heynen, and M. A. Allessie. Reentrant excitation around a fixed obstacle in uniform anisotropic ventricular myocardium. *Circulation*, 84(3):1296–1306, 1991.

[26] G. Bub. *Optical Mapping of Pacemaker Interactions*. PhD thesis, McGill University, 1999.

[27] G. Bub and N. El-Sherif. Monolayer cell cultures as model systems for studying paroxysmal atrial fibrillation. *Journal of Electrocardiology*, 37(1):44–46, 2004.

[28] G. Bub, L. Glass, N. G. Publicover, and A. Shrier. Bursting calcium rotors in cultured cardiac myocytes monolayers. *Proceedings of the National Academy of Science*, 95:10283–10287, 1998.

[29] G. Bub and A. Shrier. Propagation through heterogeneous substrates in simple excitable media. *Chaos*, 12(3):747–753, 2002.

[30] G. Bub, A. Shrier, and L. Glass. Global organization of dynamics in oscillatory heterogeneous excitable media. *Physical Review Letters*, 94(2):028105, 2005.

[31] D. Burke, M. C. Kiernan, and Bostock H. Excitability of human axons. *Clinical Neurophysiology*, 112(9):1575 – 1585, 2001.

[32] N. Bursac, R. D. Kirkton, L. C. McSpadden, and B. Liau. Characterizing functional stem cell-cardiomyocyte interactions. *Regenerative Medicine*, 5(1):87–105, 2010.

[33] N. Bursac, M. Papadaki, R. J. Cohen, F. J. Schoen, S. R. Eisenberg, R. Carrier, G. Vunjak-Novakovic, and L. E. Freed. Cardiac muscle tissue engineering: toward an in vitro model for electrophysiological studies. *American Journal of Physiology - Heart and Circulatory Physiology*, 277(2):433–444, 1999.

[34] N. Bursac, S. Parker, S. Iravanian, and L. Tung. Cardiomyocyte cultures with controlled macroscopic anisotropy: A model for functional electrophysiological studies of cardiac muscle. *Circulation Research*, 91(12):45–54, 2002.

[35] B. Burstein, P. Comtois, G. Michael, K. Nishida, L. Villeneuve, Y. Yeh, and S. Nattel. Changes in connexin expression and the atrial fibrillation substrate in congestive heart failure. *Circulation Research*, 105:1213–1222, 2009.

[36] C. Cabo and R. C. Barr. Reflection after delayed excitation in a computer model of a single fiber. *Circulation Research*, 71(2):260–270, 1992.

[37] S. Cardin, E. Libby, P. Pelletier, S. Le Bouter, A. Shiroshita-Takeshita, N. Le Meur, J. Léger, S. Demolombe, A. Ponton, L. Glass, and S. Nattel. Contrasting gene expression profiles in two canine models of atrial fibrillation. *Circulation Research*, 100(3):425–433, 2007.

[38] Y.-J. Chen and S.-A. Chen. Electrophysiology of pulmonary veins. *Journal of Cardiovascular Electrophysiology*, 17(2):220–224, 2006.

[39] J. Cheng, K. Kamiya, I. Kodama, and J. Toyama. Differential effects of MS-551 and E-4031 on action potentials and the delayed rectifier K^+ current in rabbit ventricular myocytes. *Cardiovascular Research*, 31(6):963–974, 1996.

[40] R. B. Clark, M. E. Mangoni, A. Lueger, B. Couette, J. Nargeot, and W. R. Giles. A rapidly activating delayed rectifier K^+ current regulates pacemaker activity in adult mouse sinoatrial node cells. *American Journal of Physiology - Heart and Circulatory Physiology*, 286(5):H1757–H1766, 2004.

[41] J. R. Clay, R. M. Brochu, and A. Shrier. Phase resetting of embryonic chick atrial heart cell aggregates. experiment and theory. *Biophysical Journal*, 58(3):609–621, 1990.

[42] W. C. Claycomb, N. A. Lanson, B. S. Stallworth, D .B. Egeland, J. B. Delcarpio, A. Bahinski, and N. J. Izzo. HL-1 cells: A cardiac muscle cell line that contracts and retains phenotypic characteristics of the adult cardiomyocyte. *Proceedings of the National Academy of Sciences*, 95(6):2979–2984, 1998.

[43] L. Collatz. *The Numerical Treatment of Differential Equations*. Springer-Verlag, New York, 1966.

[44] M. Courtemanche, L. Glass, M. D. Rosengarten, and A. L. Goldberger. Beyond pure parasystole: promises and problems in modeling complex arrhythmias. *American Journal of Physiology - Heart and Circulatory Physiology*, 257(2):H693–H706, 1989.

[45] H. Croisier, M. R. Guevara, and P. C. Dauby. Bifurcation analysis of a periodically forced relaxation oscillator: Differential model versus phase-resetting map. *Physical Review E*, 79(1):016209–016229, 2009.

[46] M. E. Curran, I. Splawski, K. W. Timothy, G. M. Vincent, E. D. Green, and M. T. Keating. A molecular basis for cardiac arrhythmia: HERG mutations cause long QT syndrome. *Cell*, 80(5):795 – 803, 1995.

[47] E. N. Cytrynbaum and T. J. Lewis. Global bifurcations and the appearance of a one-dimensional spiral wave in excitable media. *SIAM Journal on Applied Dynamical Systems*, 8:348–370, 2009.

[48] M. A. Dahlem and S. C. Müller. Self-induced splitting of spiral-shaped spreading depression waves in chicken retina. *Experimental Brain Research*, 115:319–324, 1997.

[49] J. M. T. De Bakker and H. M. V. Van Rijen. Continuous and discontinuous propagation in heart muscle. *Journal of Cardiovascular Electrophysiology*, 17(5):567–573, 2006.

[50] R. L. DeHaan and S. H. Gottlieb. The electrical activity of embryonic chick heart cells isolated in tissue culture singly or in interconnected cell sheets. *The Journal of General Physiology*, 52(4):643–665, 1968.

[51] R. L. DeHaan and R. Hirakow. Synchronization of pulsation rates in isolated cardiac myocytes. *Cell Research*, 70(1):214–220, 1972.

[52] E. J. Doedel and B. E. Oldeman. *AUTO-07P: continuation and bifurcation software for ordinary differential equations.* `http://cmvl.cs.concordia.ca/auto/`.

[53] J. R. Dormand and P. J. Prince. A family of embedded Runge-Kutta formulae. *Journal Computational Applied Mathematics*, 6:19–26, 1980.

[54] R. Dumollard, J. Carroll, G. Dupont, and C. Sardet. Calcium wave pacemakers in eggs. *Journal of Cell Science*, 115(18):3557–3564, 2002.

[55] A. J. Durston. Dictyostelium discoideum aggregation fields as excitable media. *Journal of Theoretical Biology*, 42:483–504, 1973.

[56] U. Egert and T. Meyer. Heart on a chip extracellular multielectrode recordings from cardiac myocytes in vitro. In S. Dhein, F. Mohr, and M. Delmar, editors, *Practical Methods in Cardiovascular Research*, pages 432–453. Springer Berlin Heidelberg, 2005.

[57] N. El-Sherif, R. A. Smith, and K Evans. Canine ventricular arrhythmias in the late myocardial infarction period: Epicardial mapping of reentrant circuits. *Circulation Research*, 49(1):255–265, 1981.

[58] E. Entcheva, Y. Kostov, E. Tchernev, and L. Tung. Fluorescence imaging of electrical activity in cardiac cells using an all-solid-state system. *IEEE Transactions on Biomedical Engineering*, 51(2):333–341, 2004.

[59] B. Ermentrout and J. Rinzel. Reflected waves in an inhomogeneous excitable medium. *SIAM Journal on Applied Mathematics*, 56:1107–1128, 1996.

[60] T. Eschenhagen, C. Fink, U. Remmers, H. Scholz, J. Wattchow, J. Weil, W. Zimmermann, H. H. Dohmen, H. Schafer, N. Bishopric, T. Wakatsuki, and E. L. Elson. Three-dimensional reconstitution of embryonic cardiomyocytes in a collagen matrix: a new heart muscle model system. *The FASEB Journal*, 11(8):683–694, 1997.

[61] T. Eschenhagen and W. H. Zimmermann. Engineering myocardial tissue. *Circulation Research*, 97(12):1220–1231, 2005.

[62] J. P. Fahrenbach, R. Mejia-Alvarez, and K. Banach. The relevance of non-excitable cells for cardiac pacemaker function. *The Journal of Physiology*, 585(2):565–578, 2007.

[63] V. G. Fast, B. J. Darrow, J. E. Saffitz, and A. G. Kléber. Anisotropic activation spread in heart cell monolayers assessed by high-resolution optical mapping: Role of tissue discontinuities. *Circulation Research*, 79(1):115–127, 1996.

[64] V. G. Fast and A. Pertsov. Shift and termination of functional reentry in isolated ventricular preparations with quinidine-induced inhomogeneity in refractory period. *Journal of Cardiovascular Electrophysiology*, 3(3):255–265, 1992.

[65] D. Fedida and M. R. Boyett. Activity-dependent changes in the electrical behaviour of sheep cardiac Purkinje fibres. *Proceedings of the Royal Society of London. Series B*, 225(1241):457–479, 1985.

[66] J. Feng, L. Yue, Z. Wang, and S. Nattel. Ionic mechanisms of regional action potential heterogeneity in the canine right atrium. *Circulation Research*, 83(5):541–551, 1998.

[67] F. Fenton and A. Karma. Vortex dynamics in three-dimensional continuous myocardium with fiber rotation: filament instability and fibrillation. *Chaos*, 8:20–47, 1998.

[68] F. H. Fenton, E. M. Cherry, H. M. Hastings, and S. J. Evans. Multiple mechanisms of spiral wave breakup in a model of cardiac electrical activity. *Chaos*, 12:852–892, 2002.

[69] R. FitzHugh. Impulses and physiological states in theoretical models of nerve membrane. *Biophysical Journal*, 1(6):445–466, 1961.

[70] L. H. Frame, R. L. Page, and B. F. Hoffman. Atrial reentry around an anatomic barrier with a partially refractory excitable gap. a canine model of atrial flutter. *Circulation Research*, 58(4):495–511, 1986.

[71] P. A. Friedman. Novel mapping techniques for cardiac electrophysiology. *Heart*, 87(6):575582, 2002.

[72] G. Gaudesius, M. Miragoli, S. P. Thomas, and S. Rohr. Coupling of cardiac electrical activity over extended distances by fibroblasts of cardiac origin. *Circulation Research*, 93(5):421–428, 2003.

[73] T. Gedeon and L. Glass. Continuity of resetting curves for FitzHugh-Nagumo equations on the circle. *Fields Institute Communications*, 21:225–236, 1999.

[74] L. Glass and M. E. Josephson. Resetting and anihilation of rentrant abnormally rapid hearbeat. *Physical Review Letters*, 75(10):2059–2062, 1995.

[75] L. Glass and M. C. Mackey. Pathological conditions resulting from instabilities in physiological control systems. *Annals of the New York Academy of Sciences*, 316(1):214–235, 1979.

[76] L. Glass, Y. Nagai, K. Hall, M. Talajic, and S. Nattel. Predicting the entrainment of reentrant cardiac waves using phase resetting curves. *Physical Review E*, 65:021908, 2002.

[77] L. Glass and A. T. Winfree. Discontinuities in phase resetting experiments. *American Journal of Physiology: Regulatory, Integrative, and Compuational Physiology*, 15:R251–R258, 1984.

[78] Multichannel Systems GmbH. Multichannel systems website. `http://www.multichannelsystems.com/`, June 2011.

[79] M. Golubitsky, V. G. LeBlanc, and I. Melbourne. Meandering of the spiral tip: An alternative approach. *Journal of Nonlinear Science*, 7:557–586, 1997.

[80] J. A. Gomes, D. Mehta, and M. N. Langan. Sinus node reentrant tachycardia. *Pacing and Clinical Electrophysiology*, 18(5):1045–1057, 1995.

[81] H. González, Y. Nagai, Bub G., L. Glass, and A. Shrier. Reentrant waves in a ring of embryonic chick ventricular cells imaged with a Ca^{2+} sensitive dye. *Biosystems*, 71(1-2):71–80, 2003.

[82] N. A. Gorelova and Bures J. Spiral waves of spreading depression in the isolated chicken retina. *Journal of Neurobiology*, 14:353 – 363, 1983.

[83] M. D. Graham, M. Bär, I. G. Kevrekidis, K. Asakura, J. Lauterbach, H.-H. Rotermund, and G. Ertl. Catalysis on microstructured surfaces: Pattern formation during CO oxidation in complex Pt domains. *Physical Review E*, 52(1):76–93, 1995.

[84] M. D. Graham, I. G. Kevrekidis, K. Asakura, J. Lauterbach, K. Krischer, H. H. Rotermund, and G. Ertl. Effects of boundaries on pattern formation: Catalytic oxidation of CO on platinum. *Science*, 264(5155):80 – 82, 1994.

[85] E. B. Griepp, J. H. Peacock, M. R. Bernfield, and J.-P. Revel. Morphological and functional correlates of synchronous beating between embryonic heart cell aggregates and layers. *Experimental Cell Research*, 113(2):273 – 282, 1978.

[86] J. Guckenheimer. Isochrons and phaseless sets. *Journal of Mathematical Biology*, 1:259–273, 1975.

[87] M. R. Guevara and L. Glass. Phase locking, period doubling bifurcations and chaos in a mathematical model of a periodically driven oscillator: a theory for the entrainment of biological oscillators and the generation of cardiac dysrhythmias. *Journal of Mathematical Biology*, 14(1):1–23, 1982.

[88] M. R. Guevara, L. Glass, and A. Shrier. Phase locking, period-doubling bifurcations, and irregular dynamics in periodically stimulated cardiac cells. *Science*, 214(4527):1350–1353, 1981.

[89] M. R. Guevara and H. J Jongsma. Phase resetting in a model of sinoatrial nodal membrane: ionic and topological aspects. *American Journal of Physiology-Heart and Circulatory Physiology*, 258(3-2):734–747, 1990.

[90] M. R. Guevara and A. Shrier. Phase resetting in a model of cardiac Purkinje fiber. *Biophysical Journal*, 52(2):165–175, 1987.

[91] M. R. Guevara, A. Shrier, and L. Glass. Phase resetting of spontaneously beating embryonic ventricular heart cell aggregates. *Journal of General Physiology*, 83(6-2):613–629, 1984.

[92] M. R. Guevara, A. Shrier, and L. Glass. Phase resetting of spontaneously beating embryonic ventricular heart cell aggregates. *American Journal of Physiology- Heart and Circulatory Physiology*, 251(6):1298–1305, 1986.

[93] M. D. Halbach, U. Egert, Hescheler J., and K. Banach. Estimation of action potential changes from field potential recordings in multicellular mouse cardiac myocyte cultures. *Cellular Physiology and Biochemistry*, 13(5):271–284, 2003.

[94] K. Hall and L. Glass. How to tell a target from a spiral: the two probe problem. *Physical Review Letters*, 82:5164–5167, 1999.

[95] H. Hashitani, H. Fukuta, H. Takano, M. F. Klemm, and H. Suzuki. Origin and propagation of spontaneous excitation in smooth muscle of the guinea-pig urinary bladder. *The Journal of Physiology*, 530(2):273–286, 2001.

[96] E. A. Heidenreich, J. F. Rodriguez, M. Doblare, B. Trenor, and J. M. Ferrero. Electrical propagation patterns in a 3D regionally ischemic human heart: A simulation study. In *Computers in Cardiology, 2009*, pages 665 –668, sept. 2009.

[97] A. L. Hodgkin and A. F. Huxley. A quantitative description of membrane current and its application to conduction and excitation in nerve. *Journal of Physiology*, 117(4):500 – 544, 1952.

[98] J.-H. Hong, J.-H. Choi, T.-Y. Kim, and K.-J. Lee. Spiral reentry waves in confluent layer of HL-1 cardiomyocyte cell lines. *Biochemical and Biophysical Research Communications*, 377(4):1269 – 1273, 2008.

[99] R. E. Horton, J. R. Millman, C. K. Colton, and Auguste D. T. Engineering microenvironments for embryonic stem cell differentiation to cardiomyocytes. *Regenerative Medicine*, 4(5):721–732, 2004.

[100] S. M. Hwang, K. H Yea, and K. J. Lee. Regular and alternant spiral waves of contractile motion on rat ventricle cell cultures. *Physical Review Letters*, 92(19):198103, May 2004.

[101] Alpha MED Scientific Incorporated. Med64 website. `http://www.med64.com/`, June 2011.

[102] The Mathworks Incorporated. Matlab website. `http://www.mathworks.com/products/matlab/`, June 2011.

[103] H. Inoue, T. Yamashita, A. Nozaki, and Sugimoto. T. Effects of antiarrhythmic drugs on canine atrial flutter due to reentry: Role of prolongation of refractory period and depression of conduction to excitable gap. *Journal of the American College of Cardiology*, 18(4):1098 – 1104, 1991.

[104] S. Iravanian, Y. Nabutovsky, C. Kong, S. Saha, N. Bursac, and L. Tung. Functional reentry in cultured monolayers of neonatal rat cardiac cells. *American Journal of Physiology - Heart and Circulatory Physiology*, 285(1):H449–H456, 2003.

[105] A. Ishimaru. *Wave Propagation in Random Media*. John Wiley and Sons, 1997.

[106] D. A. Israel, W. H. Barry, D. J. Edell, and R. G. Mark. An array of microelectrodes to stimulate and record from cardiac cells in culture. *American Journal of Physiology - Heart and Circulatory Physiology*, 247(4):669674, 1984.

[107] H. Ito and L. Glass. Theory of reentrant excitation in a ring of cardiac tissue. *Physica D*, 56(1):84–106, 1992.

[108] V. Iyer, R. Mazhari, and R. L. Winslow. A computational model of the human left-ventricular epicardial myocyte. *Biophysical Journal*, 87:1507–1525, 2004.

[109] E. M. Izhikevich. *Dynamical Systems in Neuroscience: The Geometry of Excitability and Bursting*. The MIT Press, Massachusetts, 1 edition, 2006.

[110] J. J. B. Jack, D. Noble, and R. W. Tsien. *Electric Current Flow in Excitable Cells*. Clarendon Press, Oxford, 1975.

[111] J. Jalife and C. Antzelevitch. Phase resetting and annihilation of pacemaker activity in cardiac tissue. *Science*, 206(4419):695–697, 1979.

[112] J. Jalife, C. Antzelevitch, V. Lamanna, and G. K. Moe. Rate-dependent changes in excitability of depressed cardiac Purkinje fibers as a mechanism of intermittent bundle branch block. *Circulation*, 67(4):912–922, 1983.

[113] J. Jalife, M. Delmar, J. Anumonwo, O. Berenfeld, and J. Kalifa. *Basic Cardiac Electrophysiology for the Clinician*. Blackwell Publishing, 2009.

[114] J. Jalife and G. K. Moe. Effect of electrotonic potentials on pacemaker activity of canine Purkinje fibers in relation to parasystole. *Circulation Research*, 39(6):801–808, 1976.

[115] M. J. Janse, T. Opthof, and A. G. Kléber. Animal models of cardiac arrhythmias. *Cardiovascular Research*, 39(1):165–177, 1998.

[116] S. B. Jones, D. E. Euler, W. C. Randall, G. Brynjolfsson, and E. L. Hardie. Atrial ectopic foci in the canine heart: hierarchy of pacemaker automaticity. *American Journal of Physiology: Heart Circulation Physiology*, 238(6):788–793, 1980.

[117] H. J. Jongsma and H. E. van Rijn. Electrotonic spread of current in monolayer cultures of neonatal rat heart cells. *Journal of Membrane Biology*, 9(1):341–360, 1972.

[118] M. E. Josephson. *Clinical Cardiac Electrophysiology: Techniques and Interpretations*. Lipincott Williams and Wilkins, 2002.

[119] R. W. Joyner. Effects of the discrete pattern of electrical coupling on propagation through an electrical syncytium. *Circulation Research*, 50(2):192–200, 1982.

[120] R. W. Joyner and F. J. van Capelle. Propagation through electrically coupled cells. how a small sa node drives a large atrium. *Biophysical Journal*, 50(6):11571164, 1986.

[121] O. I. Kanakov, G. V. Osipov, C.-K. Chan, and J. Kurths. Cluster synchronization and spatio-temporal dynamics in networks of oscillatory and excitable Luo-Rudy cells. *Chaos*, 17(1):0151111, 2007.

[122] D. Kaplan and L. Glass. *Nonlinear Dynamics in Physiology and Medicine*. Springer-Verlag, New York, 1995.

[123] H. Katoh, S. Ogawa, I. Furuno, Y. Sato, S. Yoh, K. Saeki, and Y. Nakamura. Electrophysiologic effects of E-4031, a class III antiarrhythmic agent, on reentrant ventricular arrhythmias in a canine 7-day-old myocardial infarction model. *Journal of Pharmacology and Experimental Therapeutics*, 253(3):1077–1082, 1990.

[124] J. P. Keener. The effects of gap junctions on propagation in myocardium: A modified cable theory. *Annals of the New York Academy of Sciences*, 591(1):257—277, 1990.

[125] I. Kehat, D. Karsenti, M. Amit, M. Druckmann, Y. Feld, J. Itskovitz-Eldor, and L. Gepstein. Long term high-resolution electrophysiological assessment of human embryonic stem cell derived cardiomyocytes: a novel in vitro model for the human heart. *Circulation Research*, 18(8):659661, 2001.

[126] M.-Y. Kim, M. Aguilar, A. Hodge, E. Vigmond, A. Shrier, and L. Glass. Stochastic and spatial influences on drug-induced bifurcations in cardiac tissue culture. *Physical Review Letters*, 103(5):058101, 2009.

[127] A. G. Kléber and Y. Rudy. Basic mechanisms of cardiac impulse propagation and associated arrhythmias. *Physiological Review*, 84(2):659–661, 2004.

[128] M. Klos, L. Hou, G. Lei, S. Morgenstern, J. Jalife, and T. Herron. Action potential propagation in monolayers of cardiac myocytes derived from embryonic stem cells. *Circulation*, 122(21):A16039, 2010.

[129] I. Kodama, M. R. Boyett, M. R. Nikmaram, M. Yamamoto, H. Honjo, and R. Niwa. Regional differences in effects of E-4031 within the sinoatrial node. *American Journal of Physiology - Heart and Circulatory Physiology*, 276(3):H793–H802, 1999.

[130] I. Kodama, M. R. Nikmaram, M. R. Boyett, R. Suzuki, H. Honjo, and J. M. Owen. Regional differences in the role of the Ca^{2+} and Na^{+} currents in pacemaker activity in the sinoatrial node. *American Journal of Physiology- Heart and Circulatory Physiology*, 272(6):2793–2806, 1997.

[131] T. Kofidis, P. Akhyari, B. Wachsmann, J. Boublik, K. Mueller-Stahl, R. Leyh, S. Fischer, and A. Haverich. A novel bioartificial myocardial tissue and its prospective use in cardiac surgery. *European Journal of Cardio-Thoracic Surgery*, 22(2):238–243, 2002.

[132] B. Y. Kogan. *Introduction to Computational Cardiology*. Springer, 2009.

[133] P. Kohl. Heterogeneous cell coupling in the heart: An electrophysiological role for fibroblasts. *Circulation Research*, 93(5):381–383, 2003.

[134] N. Kopell and L. N. Howard. Target patterns and horseshoes from a perturbed central force problem: Some temporally periodic solutions to reaction-diffusion equations. *Studies in Applied Mathematics*, 64:1–56, 1981.

[135] W. Krassowska, T. C. Pilkington, and R .E. Ideker. Potential distribution in three-dimensional periodic myocardium. *IEEE Transactions on Biomedical Engineering*, 37(3):252 –266, 1990.

[136] T. Krogh-Madsen and D. J. Christini. Resetting and termination of reentry in a loop-and-tail cardiac model. *Physical Review E*, 77:011916, 2008.

[137] T. Krogh-Madsen, L. Glass, E. J. Doedel, and M. R. Guevara. Apparent discontinuities in the phase-resetting reseponse of cardiac pacemakers. *Journal of Theoretical Biology*, 230:499–519, 2004.

[138] T. Krogh-Madsen, P. Schaffer, A. D. Skriver, L. K. Taylor, B. Pelzmann, B. Koidl, and M. R. Guevara. An ionic model for rhythmic activity in small

clusters of embryonic chick ventricular cells. *American Journal of Physiology - Heart and Circulatory Physiology*, 289(1):398–413, 2005.

[139] A. M. Kunysz, A. A. Munk, and A. Shrier. Phase resetting and dynamics in isolated atrioventrieular nodal cell clusters. *Chaos*, 5(1):184–192, 1995.

[140] K.-J. Lee. Wave pattern selection in an excitable system. *Physical Review Letters*, 79(15):2907–2910, 1997.

[141] M. J. Lee. Pseudo-random-number generators and the square site percolation threshold. *Physical Review E*, 78(3):031131, 2008.

[142] M. F. Leite, A. D. Burgstahler, and M. H. Nathansow. Ca^{2+} waves require sequential activation of inositol trisphosphate receptors and ryanodine receptors in pancreatic acini. *Gastroenterology*, 122(2):415 – 427, 2002.

[143] L. Leon, F. Roberge, and A. Vinet. Simulation of two-dimensional anisotropic cardiac reentry: Effects of the wavelength on the reentry characteristics. *Annals of Biomedical Engineering*, 22:592–609, 1994.

[144] L. J. Leon and F. A. Roberge. Directional characteristics of action potential propagation in cardiac muscle. a model study. *Circulation Research*, 69:378–395, 1991.

[145] D. Li, S. Fareh, T. K. Leung, and S. Nattel. Promotion of atrial fibrillation by heart failure in dogs: atrial remodeling of a different sort. *Circulation*, 100(1):87, 1999.

[146] Z.-Y. Lim, B. Maskara, F. Aguel, R. Emokpae, and L. Tung. Spiral wave attachment to millimeter-sized obstacles. *Circulation*, 114(20):2113–2121, 2006.

[147] C. Luo and Y. Rudy. A dynamic model of the cardiac ventricular action potential - simulations of ionic currents and concentration changes. *Circulation Research*, 74:1071–1097, 1994.

[148] E. C. Martinez and T. Kofidis. Adult stem cells for cardiac tissue engineering. *Journal of Molecular and Cellular Cardiology*, 50(2):312 – 319, 2011.

[149] A. G. Mayer. Rhythmical pulsations in scyphomedusae. *Publication of the Carnegie Institute*, 47:1–62, 1906.

[150] L.C. McSpadden, R.D. Kirkton, and N. Bursac. Electrotonic loading of anisotropic cardiac monolayers by unexcitable cells depends on connexin type and expression level. *American Journal of Physiology - Cell Physiology*, 297(2):339–351, 2009.

[151] G. Meiry, Y. Reisner, Y. Feld, S. Goldberg, M. Rosen, N. Ziv, and O. Binah. Evolution of action potential propagation and repolarization in cultured neonatal rat ventricular myocytes. *Journal of Cardiovascular Electrophysiology*, 12(11):12691277, 2001.

[152] D. C. Michaels, E. P. Matyas, and J. Jalife. Mechanisms of sinoatrial pacemaker synchronization: a new hypothesis. *Circulation Research*, 61:704–714, 1987.

[153] G. R. Mines. On circulating excitations in heart muscles and their possible relation to tachycardia and fibrillation. *Transactions of the Royal Society of Canada*, 9:43–52, 1914.

[154] G.R. Mines. On circulating excitation on heart muscles and their possible relation to tachycardia and fibrillation. *Transactions of the Royal Society of Canada*, 4(4419):43–53, 1914.

[155] G. K. Moe, J. Jalife, W. J. Mueller, and B. Moe. A mathematical model of parasystole and its application to clinical arrhythmias. *Circulation*, 56(6):968–979, 1977.

[156] O. Monfredi, H. Dobrzynski, T. Mondal, M. R. Boyett, and G. M. Morris. The anatomy and physiology of the sinoatrial node - a contemporary review. *Pacing and Clinical Electrophysiology*, 33(11):1392 – 1406, 2010.

[157] M. W. Mueller and W. D. Arnett. Propagating star formation and irregular structure in spiral galaxies. *Astrophysical Journal*, 210:670–678, 1976.

[158] J. D. Murray. *Mathematical Biology: An Introduction.* Number 1. Springer, New York, 2002.

[159] J. D. Murray, E. A. Stanley, and D. L. Brown. On the spread of rabies among foxes. *Proceedings of the Royal Society of London. Series B, Biological Sciences*, 229:111–150, 1946.

[160] O. S. Narula. Sinus node re-entry: A mechanism for supraventricular tachycardia. *Circulation*, 50(6):1114–1128, 1974.

[161] M. P. Nash and A. V. Panfilov. Electromechanical model of excitable tissue to study reentrant cardiac arrhythmias. *Progress in Biophysics and Molecular Biology*, 85(2-3):501522, 2004.

[162] S. Nattel, A. Shiroshita-Takeshita, B.J.J.M. Brundel, and L. Rivard. Mechanisms of atrial fibrillation: Lessons from animal models. *Progress in Cardiovascular Diseases*, 48(1):9 – 28, 2005.

[163] M. E. J. Newman and R. M. Ziff. Efficient Monte-Carlo algorithm and high-precision results for percolation. *Physical Review Letters*, 85(19):4104–4107, 2000.

[164] D. Noble. The relation of Rushton's 'liminal length' for excitation to the resting and active conductances of excitable cells. *Journal of Physiology*, 226(2):573–591, 1972.

[165] T. Nomura and L. Glass. Entrainment and termination of reentrant wave propagation in a periodically stimulated ring of excitable media. *Physical Review E*, 53(6):6353–6360, 1996.

[166] T. Opthof, A. C. G. Van Ginneken, L. N. Bouman, and H. J. Jongsma. The intrinsic cycle length of small pieces isolated from the rabbit sinoatrial node. *Journal of Molecular and Cellular Cardiology*, 19:923934, 1987.

[167] G. Oreto, F. Luzza, G. Satullo, M. P. Calabrò, and S. Carerj. Ventricular extrasystole of re-entry originating in the myocardium surrounding a parasystolic focus: a mechanism responsible for the irregularity of the interectopic intervals during parasystole. *Giornale Italiano di Cardiologia*, 14(9):702 – 706, 1984.

[168] H. M. Osinga and J. Moehlis. Continuation-based computation of global isochrons. *SIAM Journal on Applied Dynamical Systems*, 9(4):1201–1228, 2010.

[169] G. Osipov, O. Kanakov, C.-K. Chan, J. Kurths, S. Dana, L. Averyanova, and V. Petrov. Synchronization phenomena in networks of oscillatory and excitable Luo-Rudy cells. In S. Dana, P. Roy, and J. Kurths, editors, *Complex Dynamics in Physiological Systems: From Heart to Brain*, volume 41 of *Understanding Complex Systems*, pages 107–126. Springer Berlin / Heidelberg, 2009.

[170] A. Panfilov and J. P. Keener. Re-entry in an anatomical model of the heart. *Chaos, Solitons and Fractals*, 5(3-4):681 – 689, 1995.

[171] A. V. Panfilov. Spiral breakup as a model of ventricular fibrillation. *Chaos*, 8:57–64, 1998.

[172] R. Plonsey. Capability and limitations of electrocardiography and magnetocardiography. *IEEE Transactions on Biomedical Engineering*, 19(3):239 –244, may 1972.

[173] R. Plonsey and R. C. Barr. Mathematical modeling of electrical activity of the heart. *Journal of Electrocardiology*, 20(3):219–226, 1987.

[174] J. C. Polking and D. Arnold. *ODE Software in MATLAB*. `http://math.rice.edu/~dfield/`.

[175] A. Pumir, V. Nikolski, M. Hörning, A. Isomura, K. Agladze, K. Yoshikawa, R. Gilmour, E. Bodenschatz, and V. Krinsky. Wave emission from heterogeneities opens a way to controlling chaos in the heart. *Physical Review Letters*, 99:208101, 2007.

[176] V. S. Reiner and C. Antzelevitch. Phase resetting in a mathematical model of sinus node. *American Journal of Physiology- Heart and Circulatory Physiology*, 249(6-2):1143–1153, 1985.

[177] S. Richter and P. Brugada. Bidirectional ventricular tachycardia. *Journal of the American College of Cardiology*, 54(13):1189, 2009.

[178] F. A. Roberge, A. Vinet, and B. Victorri. Reconstruction of propagated electrical activity with a two-dimensional model of anisotropic heart muscle. *Circulation Research*, 58(4):461–475, 1986.

[179] M. A. Rossi. Connective tissue skeleton in the normal left ventricle and in hypertensive left ventricular hypertrophy and chronic chagasic myocarditis. *Medical Science Monitor*, 7(4):830–832, 2001.

[180] G. J. Rozanski. Atrial ectopic pacemaker escape mediated by phasic vagal nerve activity. *American Journal of Physiology: Heart Circulation Physiology*, 260(5-2):1507–1514, 1991.

[181] G. J. Rozanski, S. L. Lipsius, and W. C. Randall. Functional characteristics of sinoatrial and subsidiary pacemaker activity in the canine right atrium. *Circulation*, 67(6):1378–1387, 1983.

[182] D. S. Rubenstein and S. L. Lipsius. Mechanisms of automaticity in subsidiary pacemakers from cat right atrium. *Circulation Research*, 64(4):648–657, 1989.

[183] W. A. H. Rushton. Initiation of the propagated disturbance. *Proceedings of the Royal Society of London. Series B, Biological Sciences*, 124:210–243, 1937.

[184] F. Sachs. Electrophysiological properties of tissue cultured heart cells grown in a linear array. *Journal of Membrane Biology*, 4(6):348360, 1976.

[185] T. Sakai. Optical mapping analysis of the spatiotemporal pattern of experimental tachyarrhythmia in improved isolated rat atrium preparation. *The Journal of Physiological Sciences*, 58(2):87–97, 2008.

[186] B. Sandstede and A. Scheel. Defects in oscillatory media: toward a classification. *SIAM Journal on Applied Dynamical Systems*, 3(1):1–68, 2004.

[187] M. C. Sanguinetti and M. Perry. hERG1 channel blockers and cardiac arrhythmia. In O. N. Tripathi, U. Ravens, and M. C. Sanguinetti, editors, *Heart Rate and Rhythm*, pages 611–625. Springer Berlin Heidelberg, 2011.

[188] G. Schram, M. Pourrier, P. Melnyk, and S. Nattel. Differential distribution of cardiac ion channel expression as a basis for regional specialization in electrical function. *Circulation Research*, 90(9):939–950, 2002.

[189] G. Schram, M. Pourrier, P. Melnyk, and S. Nattel. Differential distribution of cardiac ion channel expression as a basis for regional specialization in electrical function. *Circulation Research*, 90(9):939–950, 2002.

[190] R. B. Schuessler, J. P. Boineau, and B. I. Bromberg. Origin of the sinus impulse. *Journal of Cardiovascular Electrophysiology*, 7(3):263–274, 1996.

[191] L. S. Schulman and P. E. Seiden. Percolation and galaxies. *Science*, 233(4672):425–431, 1986.

[192] T. K. Shajahan, B. Borek, A. Shrier, and L. Glass. Scaling properties of conduction velocity in heterogeneous excitable media. *Physical Review E*, 84:046208, 2011.

[193] T. K. Shajahan, A. R. Naik, and R. Pandit. Spiral-wave turbulence and its control in the presence of inhomogeneities in four models of cardiac tissue. *PLoS ONE*, 4(3):e4738, 2009.

[194] T. K. Shajahan, S. Sinha, and R. Pandit. Spiral-wave dynamics depend sensitively on inhomogeneities in mathematical models of ventricular tissue. *Physical Review E*, 75(1):0119291–8, 2007.

[195] T. K. Shajahan, S. Sinha, and R. Pandit. Spiral-wave dynamics depends sensitively on inhomogeneities in mathematical models of ventricular tissue. *Physical Review E*, 75:011929, 2007.

[196] R. M. Shaw and Y. Rudy. Ionic mechanisms of propagation in cardiac tissue. roles of the sodium and L-type calcium currents during reduced excitability and decreased gap junction coupling. *Circulation Research*, 81(5):727–741, 1997.

[197] A. Shimizu, M. Fukatani, A. Konoe, S. Isomoto, O. A. Centurion, and K. Yano. Electrophysiological effects of a new class III antiarrhythmic agent (E-4031) on the conduction and refractoriness of the in vivo human atrium. *Cardiovascular Research*, 27(7):1333–1338, 1993.

[198] T. Shimizu, M. Yamato, Y. Isoi, T. Akutsu, T. Setomaru, K. Abe, A. Kikuchi, M. Umezu, and T. Okano. Fabrication of pulsatile cardiac tissue grafts using a novel 3-dimensional cell sheet manipulation technique and temperature-responsive cell culture surfaces. *Circulation Research*, 90(3):40–48, 2002.

[199] T. Shimizu, M. Yamato, A. Kikuchi, and T. Okano. Cell sheet engineering for myocardial tissue reconstruction. *Biomaterials*, 24(13):2309–2316, 2003.

[200] K. Showalter and J. J. Tyson. Luther's 1906 discovery and analysis of chemical waves. *Journal of Chemical Education*, 64(9):742, 1987.

[201] T. A. Simmers and N. Sreeram. Sinoatrial reentry tachycardia: A review. *Herzschrittmachertherapie und Elektrophysiologie*, 14:156–161, 2003.

[202] S. Sinha, K. M. Stein, and D. J. Christini. Critical role of inhomogeneities in pacing termination of cardiac reentry. *Chaos*, 12(3):893–902, 2002.

[203] D. J. Snyders. Structure and function of cardiac potassium channels. *Cardiovascular Research*, 42(2):377–390, 1999.

[204] M. Spach. The discontinuous nature of electrical propagation in cardiac muscle. *Annals of Biomedical Engineering*, 11:208–261, 1983.

[205] M. Spach and J. M. Kootsey. The nature of electrical propagation in cardiac muscle. *American Journal of Physiology- Heart and Circulatory Physiology*, 244(1):3–22, 1983.

[206] N. Sperelakis. Cultured heart cell reaggregate model for studying cardiac toxicology. *Environmental Health Perspectives*, 26:234–267, 1978.

[207] A. T. Stamp, G. V. Osipov, and J. J. Collins. Suppressing arrhythmias in cardiac models using overdrive pacing and calcium channel blockers. *Chaos*, 12(3):931–940, 2002.

[208] C. F. Starmer, V. N. Biktashev, D. N. Romashko, M. R. Stepanov, O. N. Makarova, and V. I. Krinsky. Vulnerability in an excitable medium: analytical and numerical studies of initiating unidirectional propagation. *Biophysical Journal*, 65(5):1775–1787, 1993.

[209] J. M. Starobin and C. F. Starmer. Boundary-layer analysis of waves propagating in an excitable medium: Medium conditions for wave-front obstacle separation. *Physical Review E*, 54(1):430–437, 1996.

[210] J. M. Starobin and C. F. Starmer. Common mechanism links spiral wave meandering and wave-front–obstacle separation. *Physical Review E*, 55(1):1193–1196, 1997.

[211] D. Stauffer and A. Aharony. *Introduction to Percolation Theory*. Taylor & Francis, London, 1992.

[212] B. E. Steinberg, L. Glass, A. Shrier, and G. Bub. The role of heterogeneities and intracellular coupling in wave propagation in cardiac tissue. *Philosopical Transactions of the Royal Society A*, 364:1299–1311, 2006.

[213] O. Steinbock, P. Kettunen, and K. Showalter. Anisotropy and spiral organizing centers in patterned excitable media. *Science*, 269:1857, 1995.

[214] S. V. Straub, D. R. Giovannucci, and D. I. Yule. calcium wave propagation in pancreatic acinar cells. *The Journal of General Physiology*, 116(4):547–560, 2000.

[215] B. Surawicz, C. S. Kuo, and C. P. Reddy. Re-entry near the site of the ventricular parasystolic focus: an ecg study of patients with artificial ventricular pacemakers. *Journal of Electrocardiology*, 13(2):103 – 107, 1980.

[216] K. Tanaka, S. Zlochiver, K.L. Vikstrom, M. Yamazaki, J. Moreno, M. Klos, A.V. Zaitsev, R. Vaidyanathan, D.S. Auerbach, S. Landas, G. Guiraudon, J. Jalife, O. Berenfeld, and J. Kalifa. Spatial distribution of fibrosis governs fibrillation wave dynamics in the posterior left atrium during heart failure. *Circulation Research*, 101:839–847, 2007.

[217] M. Tanaka, A. Isomura, M. Horning, H. Kitahata, K. Agladze, and K. Yoshikawa. Unpinning of a spiral wave anchored around a circular obstacle by an external wave train: Common aspects of a chemical reaction and cardiomyocyte tissue. *Chaos*, 19(4):043114, 2009.

[218] K. H. W. J. ten Tusscher and A. V. Panfilov. Reentry in heterogeneous cardiac tissue described by the Luo-Rudy ventricular action potential model. *American Journal of Physiology -Heart and Circulartory Physiology*, 284(2):542–548, 2002.

[219] K. H. W. J. ten Tusscher and A. V. Panfilov. Influence of nonexcitable cells on spiral breakup in two-dimensional and three-dimensional excitable media. *Physical Review E*, 68(6-1):062902, 2003.

[220] K. H. W. J. ten Tusscher and A. V. Panfilov. Wave propagation in excitable media with randomly distributed obstacles. *Multiscale Modeling and Simulation*, 3(2):265–282, 2005.

[221] K. H. W. J. ten Tusscher and A. V. Panfilov. Influence of diffuse fibrosis on wave propagation in human ventricular tissue. *Europace*, 9(6):38–45, 2007.

[222] W. Thomson. On the theory of the electric telegraph. *Proceedings of the Royal Society*, 7:382–399, 1855.

[223] B. Trénor, L. Romero, J. Ferrero, J. Sàiz, G. Moltó, and J. Alonso. Vulnerability to reentry in a regionally ischemic tissue: A simulation study. *Annals of Biomedical Engineering*, 35(7):1756–1770, 2007.

[224] R. C. Truex and M. Q. Smythe. Comparative morphology of the cardiac conduction tissue in animals. *Annals of the New York Academy of Sciences*, 127:19–33, 1965.

[225] C.-F. Tsai, C.-T. Tai, M.-H. Hsieh, W.-S. Lin, W.-C. Yu, K.-C. Ueng, Y.-A. Ding, M.-S. Chang, and S.-A. Chen. Initiation of atrial fibrillation by ectopic

beats originating from the superior vena cava. *American Journal of Physiology-Heart Circulatory Physiology*, 102(1):67–74, 2000.

[226] L. Tung and A. G. Kléber. Virtual sources associated with linear and curved strands of cardiac cells. *American Journal of Physiology - Heart and Circulatory Physiology*, 279(4):H1579–H1590, 2000.

[227] J. J. Tyson. *Lecture Notes in Biomathematics: The Belousov-Zhabotinskii Reaction*, volume 10. Springer-Verlag, New York, 1976.

[228] J. J. Tyson, K. A. Alexander, V. S. Manoranjan, and J. D. Murray. Spiral waves of cyclic AMP in a model of slime mold aggregation. *Physica D*, 34(1-2):193–207, 1989.

[229] J. J. Tyson and J. P. Keener. Spiral waves in a model of myocardium. *Physica D*, 29:215–222, 1987.

[230] J. J. Tyson and J. P. Keener. Singular perturbation theory of traveling waves in excitable media (a review). *Physica D*, 32:327–361, 1988.

[231] K. Umapathy, S. Masse, K. Kolodziejska, G. D. Veenhuyzen, V. S. Chauhan, M. Husain, T. Farid, E. Downar, E. Sevaptsidis, and K. Nanthakumar. Electrogram fractionation in murine HL-1 atrial monolayer model. *Heart Rhythm*, 5(7):1029–1035, 2008.

[232] W. P. M. van Meerwijk, G. Debruin, A. C. G. van Ginneken, J. van Hartevelt, R. J. Jongsma, E. W. Kruyt, S. S. Scott, and D. L. Ypey. Phase resetting properties of cardiac pacemaker cells. *Journal of General Physiology*, 83(4):613–629, 1984.

[233] T. A. B. van Veen, H. V. M. van Rijen, and T. Opthof. Cardiac gap junction channels: modulation of expression and channel properties. *Cardiovascular Research*, 51(2):217–229, 2001.

[234] V. K. Vanag and I. R. Epstein. Inwardly rotating spiral waves in a reaction-diffusion system. *Science*, 294:835, 2001.

[235] V. K. Vanag and I. R. Epstein. Dash-waves in a reaction diffusion system. *Physical Review Letters*, 90:098301, 2003.

[236] E. Verheijck, R. Wilders, and L.N. Bouman. Atrio-sinus interaction demonstrated by blockade of the rapid delayed rectifier current. *Circulation*, 105(7):880–885, 2002.

[237] A. Vinet and F. Roberge. The dynamics of sustained reentry in a ring model of cardiac tissue. *Annals of Biomedical Engineering*, 22:568–591, 1994.

[238] S. Weidmann. The electrical constants of Purkinje fibres. *The Journal of Physiology*, 118(3):348360, 1952.

[239] S. Weinberg, E. A. Lipke, and L. Tung. In vitro electrophysiological mapping of stem cells. In John M. Walker and Randall J. Lee, editors, *Stem Cells for Myocardial Regeneration*, volume 660 of *Methods in Molecular Biology*, pages 215–237. Humana Press, 2010.

[240] N. Wiener and A. Rosenbluth. The mathematical formulation of the problem of conduction of impulses in a network of connected excitable elements, specifically in cardiac muscle. *Archives of the Institute of Cardiology in Mexico*, 16:205–265, 1946.

[241] A. T. Winfree. Spiral waves of chemical activity. *Science*, 175:634–636, 1972.

[242] A. T. Winfree. Patterns of phase compromise in biological cycles. *Journal of Mathematical Biology*, 1:73–95, 1974.

[243] A. T. Winfree. *The Geometry of Biological Time*, volume 8 of *Biomathematics*. Springer-Verlag, New York, 1980.

[244] A. T. Winfree. Electrical instability in cardiac muscle: phase singularities and rotors. *Journal of Theoretical Biology*, 138:353, 1989.

[245] A. T. Winfree. Varieties of spiral wave behavior: an experimentalists approach to the theory of excitable media. *Chaos*, 1:303–334, 1991.

[246] A. T. Winfree. 1992 lectures in complex systems. volume 5, chapter The Geometry of Excitability, pages 207–298. Addison-Wesley, Massachusetts, 1993.

[247] S. J. Woo, J. H. Hong, T. Y. Kim, B. W. Bae, and K. J. Lee. Spiral wave drift and complex-oscillatory spiral waves caused by heterogeneities in two-dimensional in vitro cardiac tissues. *New Journal of Physics*, 10(1):015005, 2008.

[248] K.-H. Wu, Y.-L. Liu, B. Zhou, and Z.-C. Han. Cellular therapy and myocardial tissue engineering: the role of adult stem and progenitor cells. *European Journal of Cardiothoracic Surgery*, 30(5):770–781, 2006.

[249] F. Xie, Z. Qu, and A. Garfinkel. Dynamics of reentry around a circular obstacle in cardiac tissue. *Physical Review E*, 58:6355, 1998.

[250] F. Xie, Z. Qu, A. Garfinkel, and J. N. Weiss. Electrophysiological heterogeneity and stability of reentry in simulated cardiac tissue. *American Journal of Physiology-Heart Circulation Physiology*, 280:H535, 2001.

[251] F. Xie, Z. Qu, J. N. Weiss, and A. Garfinkel. Interactions between stable spiral waves with different frequencies in cardiac tissue. *Physical Review E*, 59(2):2203–2205, Feb 1999.

[252] F. Xie, Z. Qu, J. N. Weiss, and A. Garfinkel. Coexistence of multiple spiral waves with independent frequencies in a heterogeneous excitable medium. *Physical Review E*, 63:031905, 2001.

[253] J. Xin. *An Introduction to Fronts in Random Media*. Springer New York, 2009.

[254] A. Xu and M. R. Guevara. Two forms of spiral-wave reentry in an ionic model of ischemic ventricular myocardium. *Chaos*, 8:157–174, 1998.

[255] L. Yin, H. Bien, and E. Entcheva. Scaffold topography alters intracellular calcium dynamics in cultured cardiomyocyte networks. *American Journal of Physiology - Heart and Circulatory Physiology*, 287(3):1276–1285, 2004.

[256] G.-Y. Yuan, G.-C. Zhang, G.-R. Wang, S.-G. Chen, and P. Sun. Elimination of spiral waves and competition between travelling wave impulses and spiral waves. *Chinese Physics Letters*, 22(2):291, 2005.

[257] D. P. Zipes. Mechanisms of clinical arrhythmias. *Journal of Cardiovascular Electrophysiology*, 14(8):902 – 912, 2003.

[258] D. P. Zipes and H. J. J. Wellens. Sudden cardiac death. *Circulation*, 98(21):2334–2351, 1998.

[259] S. Zlochiver, V. Muoz, K. L. Vikstromm, S. M. Taffet, O. Berenfeld, and J. Jalife. Electrotonic myofibroblast-to-myocyte coupling increases propensity to reentrant arrhythmias in two-dimensional cardiac monolayers. *Biophysical Journal*, 95(9):4469–4480, 2008.